VPS501, A NOVEL SNX-BAR PROTEIN INVOLVED IN AUTOPHAGY

by

Shreya Goyal

A dissertation submitted to the faculty of
The University of North Carolina at Charlotte
in partial fulfillment of the requirements
for the degree of Doctor of Philosophy in
Biological Sciences

Charlotte

2021

Approved by:

_____
Dr. Richard Chi

_____
Dr. Adam Reitzel

_____
Dr. Andrew Truman

_____
Dr. Verónica Segarra

_____
Dr. Juan Vivero-Escoto

©2021

Shreya Goyal

ALL RIGHTS RESERVED

ABSTRACT
SHREYA GOYAL. Vps501, A Novel SNX-BAR Protein Involved In Autophagy
(Under the direction of DR. RICHARD CHI)

Careful control of intracellular signaling pathways plays an important role in a cell's ability to maintain stable internal conditions in the face of an ever-changing extracellular environment. This is particularly true as it relates to the process of cellular self-eating or autophagy. Macroautophagy (herein referred to as autophagy) is a catabolic process by which unneeded or damaged cellular components are sequestered as cargo into unique double-membrane vesicles called autophagosomes which fuse to the vacuole (yeast lysosome) to be metabolized. The autophagy-related (Atg) proteins that mediate and regulate the process are evolutionarily conserved across all autophagy pathways, including starvation-induced bulk autophagy and cargo-selective autophagy pathways. The central theme of this thesis is to understand how autophagy is affected by lipids and regulatory proteins in yeast. In this thesis, we have summarized the field's understanding of lipid homeostasis and trafficking during autophagy and autophagosome formation. Furthermore, we have extended this knowledge by discovering a clear interplay between autophagy and the SNX-BAR protein subfamily. In recent years, the SNX-BARs have been reported to have emerging roles in autophagy, however, such mechanisms of action have been primarily indirect. In this thesis, we have characterized a novel SNX-BAR protein, we have termed Vps501 and have found it directly affects autophagy which brings to light a new role of SNX-BAR proteins in autophagy regulation.

DEDICATION

This work is dedicated to my parents, my brother Aditya and my partner Christian

Your love and support are the reason I am here today!

Droit au but!

ACKNOWLEDGEMENTS

First and foremost, I would like to thank my mentor, Dr. Richard Chi for giving me the opportunity to work in his lab and for taking a chance on me. I owe everything I know about research to him. He has been extremely patient with me while I struggled with experiments or results, and I know that he's always got my back. I have learned so much from him not just about research but also about teaching, mentorship, outreach and for that I am forever grateful. I would also like to thank him for all the times he invited the us over to his house and making me feel welcomed on holidays when I was feeling the most homesick. I will forever cherish all the moments I spent in the Chi lab, every time we would get excited over new results, all the fun and crazy talks we had in the lab, how Dr. Chi would pull my leg on the smallest of things (sushi at Mr. Tokyo!), for pushing me to do my best and guiding me at every step of the way.

Next, I would like to thank my committee members Dr. Andrew Truman, Dr. Adam Reitzel, Dr. Veronica Segarra and Dr. Juan.Vivero-Escoto for agreeing to serve on my committee and their feedback throughout my graduate research. I am thankful to Dr. Andrew Truman for giving me the title of "honorary member of the Truman lab", for all the great discussions, help and support. Thank you also for inviting me to your lab meals and for letting me borrow reagents from your lab!

I would like to thank Dr. Reitzel for helping me with the phylogenetics part of my project and for being a great graduate program director. I appreciate how you are always happy to answer all questions offer your help with a great smile. I would like to thank Dr. Veronica for being a great asset to me all through my PhD years. You have not only helped me with

experiments and writing, but also with your words of wisdom. Thank you for encouragement and cheering! I would like to thank Dr. Vivero for giving me the opportunity to collaborate with him and his valuable input during my committee meetings. Next, I would like to thank all the past and present members of the Chi lab, without whom, my PhD life would be incomplete. Starting off with the current members, Trey Grissom, who has been an amazing lab mate. I will miss our talks ranging from research to universe and beyond! Thank you for never complaining about dishes in the sink or me always using your pipettes. I would like to point out that you have amazing organizational skills and which I hope to have someday! I would like to thank the other current members of the lab, Jacob, Sarah, Mildred, Marjan and Dr. Rahman for making the lab such a fun place to work at and helping me out with everything.

I would like to thank my undergrads, Carrie Rapier, Alyssa Lucero, Aaron Stecher and Daria Al-khalidi for helping me out with my experiments, being great friends and for all the fun stuff that we shared in the lab and outside.

I would like to thank the past members of the Chi lab, Devin Clegg, Jonathan Taylor, Rachel Bare, Sydney Garell, Elvira An, Henry Weaver, Laura Phipps and Kate Bulauitan for being like second family to me. I would like to extend my thanks especially to Devin, Elle, Henry, Laura P and Isaac for welcoming me to the lab when I first joined in. I will never forget our late-night experiments, chess tournaments, Halloween and everything in between. Thank you, guys, for teaching me the ropes when I first joined, and I really miss you all! I would like to thank all my friends over to the Truman lab as well. Thank you, guys, for your great discussions and friendly banters!

Thank you to all my professors and faculty of the Biology Department. Dr. Christine Richardson for being very helpful and answering my questions regarding the graduate program, Dr. Shan Yan for his helpful discussions and letting us use his size exclusion column, Dr. Valery for letting us borrow regents from his lab, Dr. Tomida for being very helpful and letting us use his lab equipment and all other faculty for their thoughtful advice throughout the years and their infectious love for science.

I would like to thank my seniors, Dr. Sebastien Felt, Dr. Abhishek Dey, Dr. Austin Jefferies, Dr. Ru, and post docs over at the Dr. Yan's lab for their help with experiments and their valuable troubleshooting advice.

Thank you to Dr. Dreau for his banter, advice, help and humor that makes me laugh especially on tough days. Thank you for sparing a few minutes of your busy schedule to humor us, I hope you can make your dream come true of buying an island one day!

Thanks to all my friends in department over the years, Katherine Holtzman, who has been an honorary member of the Chi lab, thank you for your talks and laughter! Thank you also for taking the unforgettable NY trip with us and all the Thanksgiving dinners! Dr. Priyanka Grover who is always there offering the best advice and being the big sister, I never knew I needed.

Thanks to Nitika for keeping me sane through the last few years of this crazy journey. I have learnt so much for you and your ambition and drive is infectious. If I am even half the person you are, I would consider that a success! Thanks for saying yes to all and every crazy idea I have and being by my side during all situations! Your moral support means a lot to me.

Also, thanks to Austin, Laura, Sara, Gaith, Kiran, Khahn, Arundhati, Jade and all my other friends who have shared the PhD journey with me. You guys have been great!

Thank you to David Gray for helping with any issues with the equipment, especially the autoclave and the centrifuges.

Thank you to all the faculty and staff here in the Department of Biological Sciences specially Ruthie Moser, Brendan Bishop, Andrea Strong and the Graduate school and the team at the International Student Scholars Office.

Thanks to my friends back home, Sunidhi, Titin, Gaurav, Sonali, Karthik, Abhishek, Govind, Shivani and everyone else if I am missing. Thank you for all the calls, zooms meetings, virtual birthdays and celebrations. Your friendship means the world to me, and I would not be here without the support of you guys!

Last but not the least, thank you to my family who have been by my side through thick and thin. I would like to thank my dad who has been a great idol throughout my life. My mom who never misses to call me and check on my every single day. My grandparents who are cheering for me from far away, chacha, mama-mami, my cousins and all the extended relatives who support me and make me feel loved every single day!

I would like to thank my brother Aditya, who somehow has become wise beyond his years! Thank you for your great advice, reality checks, rational solutions and daily dose of laughter! Its amazing to have you!

This acknowledgement would be incomplete without mentioning Dr. Bressy, who has been like a ray of sunshine in my life! I would not have made it without his support. Thank you for being my biggest cheerleader, for all your advice, help, love and for always always

being there for me. Thanks for making my dream, your dream, and never letting me give up.

Again, from the bottom of my heart, thank you to each and every one!

Shreya

TABLE OF CONTENTS

LIST OF TABLES

CHAPTER 2

CHAPTER 4

LIST OF FIGURES

CHAPTER 1

CHAPTER 2

CHAPTER 3

LIST OF ABBREVIATIONS

Acronyms and Abbreviations

Atg/ATG proteins - Autophagy-related proteins

PAS - Pre-autophagosomal structure

PA - Phosphatidic acid

PG - Phosphatidylglycerol

PE- Phosphatidylethanolamine

PC - Phosphatidylcholine

PS - Phosphatidylserine

PI - Phosphatidylinositol (PI)

PI3P - Phosphatidylinositol-3-phosphate (PI3P)

PI(3,5)P2 - Phosphatidylinositol-3, 5-biphosphate (PI (3,5) P2)

PI4P2 - Phosphatidylinositol-3-phosphate (PI4P)

PI(4,5)P2 - Phosphatidylinositol-4, 5-biphosphate (PI(4,5)P2)

PI3K - Phosphatidylinositol-3-kinase (PI3K)

S1P - Sphingosine-1-phosphate (S1P)

BAR - Bin-Amphiphysin-Rvs161 (BAR) homology

CBB - Coomassie brilliant blue

GFP - Green Fluorescent Protein

ORF - Open reading frame

PGK - Phosphoglycerate kinase

PX: Phox homology domain

ROI - Region of interest

SNX - Sorting nexin

SNX-BAR - Sorting nexin containing a BAR domain

WT - Wild-type

TEN - Tubular endosomal network

VL - Vacuolar lumen

VM - Vacuolar membrane

FPLC- Fast protein liquid chromatography

CHAPTER 1: INTRODUCTION

Maintaining cellular health is the most essential biological activity for all living things. From yeast to humans, this is achieved by a dynamic transport of receptors and nutrients in and out of the cell, or within various organelles via interconnected membrane trafficking pathways. Collectively, this is referred to as the endomembrane system and consists of organelles such as the cell membrane, endosome, Golgi apparatus, and lysosome. The endosome is the main hub that accepts proteins, lipids and other molecules collectively called "cargo" that are received via endocytosis from the plasma membrane or via trafficking from the secretory pathway (1). From the endosome, the cargo is either destined towards the lysosome (yeast vacuole) or exported out towards the Golgi via retrograde trafficking or the plasma membrane via the recycling pathway (Figure 1). The endosome is an integral sorting station of the endomembrane system that coordinates sorting, export and degradation of cargo and facilitates nutrient sensing, quality control check and cellular homeostasis (1, 2)

The outstanding question in the field is how the endosome coordinates sorting and export of cargo to various destinations. Substantial research using *Saccharomyces cerevisiae*, have provided some insight into endosomal sorting machineries, however the exact mechanism is still not known. We now know, transport carriers out of the endosome do not carry bulk protein and lipid independently of any signal, rather sorting machineries recognizing sorting signals fine tune the export of cargo to various and precise destinations (3). The major sorting machineries working at the endosome include the retromer complex,

sorting nexins, and the ESCRT machinery. Amongst these, the sorting nexins are one of the largest and extensively studied family of proteins. The SNX-BAR are a subfamily of sorting nexins and are of particular interest to researchers because of their role in endosome transport carrier (ETC) formation.

Role of SNX-BAR proteins in the endomembrane system

Endosomal transport is achieved by recognition of cargo, endosomal membrane remodeling into tubules and finally the scission of tubules to form cargo-carrying transport vesicles. These events are orchestrated by the assembly of coat proteins at the endosome and one of the major family of proteins facilitating this is the sorting nexins(SNX) (4). SNX are an evolutionary conserved class of proteins that are characterized by their ability to bind PtdIns(3)P, the major lipid species of the endosome. The sorting nexins are important to maintain homeostasis within the cell and defects can severely compromise cellular health and the ability to survive during starvation conditions. Sorting nexins have also been implicated in numerous neurodegenerative disorders such as Parkinson's, Alzheimer's, cardiovascular myopathies and even cancers (5, 6).

A subfamily of SNX proteins contains an additional BAR (Bin/Amphiphysin/Rvs) domain that has the capability to deform high curvature membranes such as that of the endosome into tubules (7). Twelve SNX-BAR proteins have been identified in humans, while seven have been identified in yeast (7) (Figure 2). Yeast SNX-BAR proteins have been well studied because of their association with the retromer complex and their role in mediating

the transport of cargo from endosome to the trans Golgi network (TGN) via the retrograde pathway. The retromer consists of cargo selection complex (CSC), Vps26, Vps29 and Vps35, however this complex does not have intrinsic membrane binding ability and thus associate with SNX BAR proteins for their endosomal recruitment (8). SNX-BAR proteins, Vps5 and Vps17 have been extensively studied for their association with the retromer complex and for mediating the retrograde transport of Vps10. Defects in the retromer results in the accumulation of Vps10 in the vacuole membrane and the secretion of vacuolar hydrolases thus disrupting vacuole biogenesis and homeostasis. Overexpressed Vps10 has also been shown to be retrieved back to the Golgi with the help of the Vps5-Vps17 retromer assembling at the vacuole (9)

Other SNX-BAR proteins in yeast have also been implicated in retrograde trafficking, however, these are known to function independent of the retromer complex (10). The Snx4 protein family consisting of Snx4, Snx41 and Atg20/Snx42 were shown to be involved in the plasma membrane recycling of various cargos such as SNARE Snc1, and ABC transporter Ste6 independent of the retromer. Mvp1 is another SNX-BAR protein in yeast and studies have shown that Mvp1 can directly interact with dynamin-like protein Vps1 and facilitate the fission of Vps5-Vp17 decorated tubules to form transport carrier (11). A recent study showed Mvp1 forms an autoinhibitory tetrameric structure, shedding some insight into the possible regulation of SNX-BAR proteins (12). Moreover, recent reports have suggested a dynamic interplay between SNX-BAR proteins at the pre-vacuolar endosome (PVE) and autophagy(13).

Autophagy and its upstream regulators

Autophagy is a catabolic process by which unneeded or damaged cellular components are sequestered as cargo into unique double-membrane vesicles called autophagosomes (14, 15) . Once made, autophagosomes deliver their contents for breakdown by docking and fusing with the cell's degradative organelle, the vacuole (in yeast) or the lysosome (in animals). These key steps and the autophagy-related (Atg) proteins that mediate and regulate them are evolutionarily conserved across all autophagy pathways, including starvation-induced bulk autophagy and cargo-selective autophagy pathways (14-16). While vacuoles and lysosomes can serve as storage and/or recycling depots for cells, their delimiting membranes host signaling events critical for autophagosome biogenesis.

Initiation of autophagy occurs with the inactivation of *target of rapamycin complex* (TORC1) when starvation conditions are sensed. TORC1 subunits (Kog1, Lst8, Tco89, Tor1) localizes to the yeast vacuole membrane, independent of nutrient availability. This complex functions by integrating signals from many intracellular and extracellular cues from a variety of kinases, GTPases and their effectors (17, 18)(Figure 3). TORC1 inactivation triggers the formation of the autophagosome generating machinery comprised of seventeen Atg gene products, including Atg13, a regulatory subunit of the Atg1 protein kinase complex. The initiation step is marked by the dephosphorylation of Atg13, stimulating all seventeen Atg proteins to interact. Recently, an upstream regulator of the TORC1 pathway, the yeast SEA complex, was identified to be part of this web of GTPase effectors (19, 20)(Figure 4). The SEA complex (GATOR complex in humans) is a conserved eight protein complex (Sea1, Sea2, Sea3, Sea4, Seh1, Sec143, Npr2, Npr3)

made up of proteins that are structurally similar to membrane coating complexes (20, 21) (Figure4A). The SEA complex is also dynamically associated to the vacuole membrane and can inactivate TORC1 to initiate autophagy; however, its complete function is not well understood (Figure 4B).

Role of the SNX4 family during autophagy

As mentioned above, the Snx4 family comprising of Snx4, Snx42/Atg20 and Snx41 have additional roles beyond retrograde trafficking. They have been shown to interact with the core autophagic machinery and have been found to play critical roles in several autophagy pathways, including the cytoplasm-to-vacuole targeting (CVT) pathway, pexophagy, mitophagy, and starvation-induced selective autophagy of fatty acid synthase and of the proteasome (22-26). To function, Snx4 forms distinct dimers with either Snx42 or Snx41 and facilitates the transport of distinct proteins. For example, Snx4-41 has been shown to traffic Atg27, an integral membrane autophagy protein, between Golgi and the endosome, while Snx4-Atg20 have been shown to traffic Atg9, another integral membrane autophagy, between the Golgi and endosome. Both exhibit modest autophagy defects when singly deleted (27). Atg11 a scaffold protein involved in the CVT pathway and selective autophagy, has also been shown to interact with Atg20 (28). The Snx4 family is also observed to be associated to Atg17 at the PAS(24, 29, 30). Upon autophagy induction, Atg17 forms a complex with Atg31 and Atg29 and recruits Atg13 to initiate autophagosome formation (31). Recently, the Snx4 family has also been found to be involved in starvation-induced bulk autophagy. Defects in Snx4 lead to the accumulation of autophagy intermediates and results in defective autophagosome maturation and fusion

with the vacuole. Additionally, phosphatidylserine (PS) trafficking by the Snx4 family was found to be critical for to maintaining lipid homeostasis to ensure that vacuole membrane is competent to fuse with the autophagosome (32).

Taken together, this brings to light the importance of understanding SNX-BAR proteins in not only endosome sorting but also lipid homeostasis during autophagy. Interestingly, only one of the seven annotated SNX-BARs in yeast, open reading frame (ORF) YKR078W, has not been studied. In this thesis, we provide the initial characterization of YKR078W, and find it directly affects autophagy regulation which extends the current field's understanding of SNX-BAR function during autophagy.

1.2. Figures

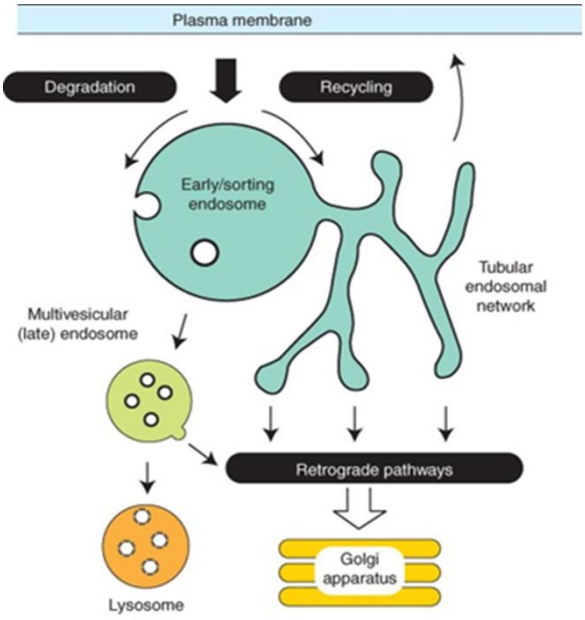

Figure 1. Endosomal sorting pathways. The endosome is the central cargo sorting hub, that receives cargo via endocytosis from the plasma membrane. At the endosome, cargo can be sorted into the degradative pathway resulting in the eventual degradation in the lysosome/vacuole, or into various export pathways resulting in cargo reuse. The recycling pathway delivers cargo back to the plasma membrane while the retrograde pathway delivers cargo to the trans-Golgi network. Endosomal transport carriers (ETC) carry cargo destined to the export pathways, bud off from the tubular endosomal network whereas vesicles that bud into the lumen of multivesicular endosomes carry cargo to degradation pathway. Careful sorting of cargo as well as remodeling of the endosomal membrane into tubules and vesicles is regulated by various proteins and complexes such as the sorting nexin protein family. Modified from (8)

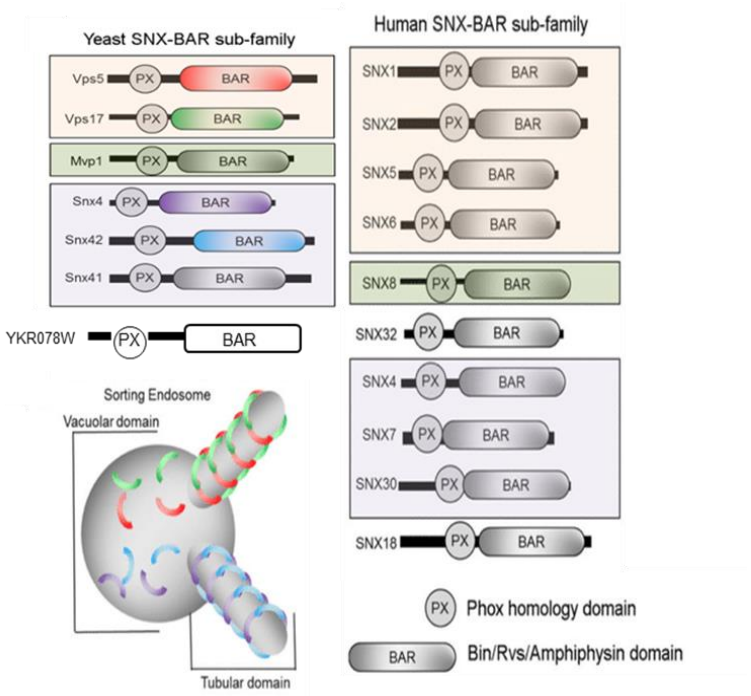

Figure 2. Conserved SNX-BAR protein family and their key features. Yeast contains seven SNX-BAR proteins while their number has expanded to twelve in humans. All SNX-BAR proteins contain an evolutionary conserved Phox-homology (PX) domain that recognizes phosphatidylinositol 3-phosphate (PI3P). An additional Bin-Amphiphysin-Rvs (BAR) dimerization domain is also present that recognizes curved surfaces such as the endosomal membrane. The BAR domain helps in forming SNX-BAR oligomers that coat the membrane of endosomes and eventually lead to the formation of endosomal-derived transport carrier. SNX-BAR proteins have been shown to homo- or heterodimerize (colored boxes). Distinct SNX-BAR dimers coat and tubulate the endosome resulting in specific cargo trafficking onto distinct export pathways. Modified from (33)

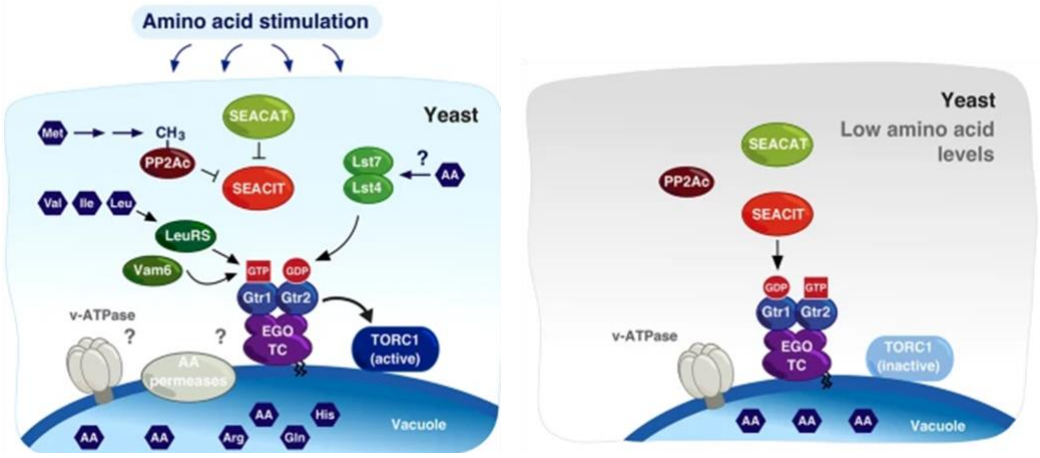

Figure 3. Regulation of target of rapamycin complex 1 (TORC1) during amino acid starvation. The activation of TORC1 is modulated by Rag GTPAses which can be found under 2 different confirmations depending on the availability of amino acids. In yeast, TORC1 is constitutively at the vacuolar membrane where the active confirmation of Rag GTPAses Gtr1-GTP/Gtr2-GDP, keep TORC1 active (left). Under amino acid starvation condition, Gtrs are inactivated by the GTPase activating protein (GAP) activity of the SEA complex (SEACIT) towards Gtr1 resulting in the inactivation of the TORC1 complex (right). Furthermore, upstream regulators such as LeuRS, Vam6 and Lst4-Lst7 promote in the activation/inactivation of TORC1 by sensing amino acid availability and mediating the conformation of Rag GTPases. Moreover, in yeast, methionine availability can be sensed by the catalytic PP2A subunit, PP2Ac which antagonizes SEACIT assembly, adding multiple layers of regulation to amino acid sensing and TORC1 activation.

AA, amino acids; Arg, arginine; Gln; glutamine; His, histidine; Ile, isoleucine; Leu, leucine; Met, methionine; Val, valine. Modified from (18)

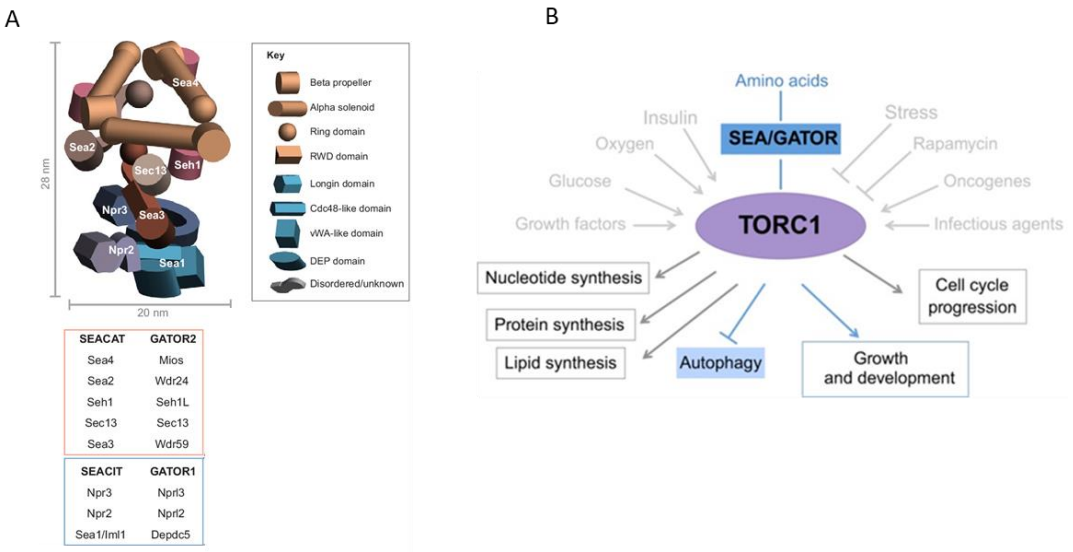

Figure 4. The molecular architecture of the SEA complex and TORC1 regulation. (A) The molecular architecture of the SEA complex obtained through integrative remodeling is depicted. The SEA complex can be divided into 2 subunits, SEACAT and SEACIT. The SEACAT subunit comprises of Sea2, Sea3, Sea4, Sec13 and Seh1. The SEACAT subunit comprises of Sea1, Npr2 and Npr3. The proteins of the SEA complex are conserved in mammalians and are called the GATOR complex. (B) TORC1 regulates diverse pathways in the cell such as the cell growth, protein synthesis, cell cycle etc. Inactivation of TORC1 results in autophagy initiation and can be regulated by the SEA complex. Modified from (21)

1.3. References

1. Ma M, Burd CG. Retrograde trafficking and plasma membrane recycling pathways of the budding yeast Saccharomyces cerevisiae. Traffic. 2020;21(1):45-59.
2. Scott CC, Vacca F, Gruenberg J. Endosome maturation, transport and functions. Semin Cell Dev Biol. 2014;31:2-10.
3. Nothwehr SF, Ha SA, Bruinsma P. Sorting of yeast membrane proteins into an endosome-to-Golgi pathway involves direct interaction of their cytosolic domains with Vps35p. J Cell Biol. 2000;151(2):297-310.
4. Cullen PJ, Korswagen HC. Sorting nexins provide diversity for retromer-dependent trafficking events. Nat Cell Biol. 2011;14(1):29-37.
5. Hu YB, Dammer EB, Ren RJ, Wang G. The endosomal-lysosomal system: from acidification and cargo sorting to neurodegeneration. Transl Neurodegener. 2015;4:18.
6. Yang J, Villar VAM, Rozyyev S, Jose PA, Zeng C. The emerging role of sorting nexins in cardiovascular diseases. Clin Sci (Lond). 2019;133(5):723-37.
7. van Weering JR, Verkade P, Cullen PJ. SNX-BAR proteins in phosphoinositide-mediated, tubular-based endosomal sorting. Semin Cell Dev Biol. 2010;21(4):371-80.
8. Burd C, Cullen PJ. Retromer: a master conductor of endosome sorting. Cold Spring Harb Perspect Biol. 2014;6(2).
9. Arlt H, Reggiori F, Ungermann C. Retromer and the dynamin Vps1 cooperate in the retrieval of transmembrane proteins from vacuoles. J Cell Sci. 2015;128(4):645-55.
10. Hettema EH, Lewis MJ, Black MW, Pelham HR. Retromer and the sorting nexins Snx4/41/42 mediate distinct retrieval pathways from yeast endosomes. EMBO J. 2003;22(3):548-57.
11. Chi RJ, Liu J, West M, Wang J, Odorizzi G, Burd CG. Fission of SNX-BAR-coated endosomal retrograde transport carriers is promoted by the dynamin-related protein Vps1. J Cell Biol. 2014;204(5):793-806.
12. Sun D, Varlakhanova NV, Tornabene BA, Ramachandran R, Zhang P, Ford MGJ. The cryo-EM structure of the SNX-BAR Mvp1 tetramer. Nat Commun. 2020;11(1):1506.
13. Suzuki SW, Emr SD. Membrane protein recycling from the vacuole/lysosome membrane. J Cell Biol. 2018;217(5):1623-32.
14. Yang Z, Klionsky DJ. Eaten alive: a history of macroautophagy. Nat Cell Biol. 2010;12(9):814-22.
15. Nakatogawa H. Mechanisms governing autophagosome biogenesis. Nat Rev Mol Cell Biol. 2020.
16. Su MY, Peng WH, Ho MR, Su SC, Chang YC, Chen GC, et al. Structure of yeast Ape1 and its role in autophagic vesicle formation. Autophagy. 2015;11(9):1580-93.
17. Binda M, Peli-Gulli MP, Bonfils G, Panchaud N, Urban J, Sturgill TW, et al. The Vam6 GEF controls TORC1 by activating the EGO complex. Mol Cell. 2009;35(5):563-73.
18. Powis K, De Virgilio C. Conserved regulators of Rag GTPases orchestrate amino acid-dependent TORC1 signaling. Cell Discov. 2016;2:15049.
19. Algret R, Fernandez-Martinez J, Shi Y, Kim SJ, Pellarin R, Cimermancic P, et al. Molecular architecture and function of the SEA complex, a modulator of the TORC1 pathway. Mol Cell Proteomics. 2014;13(11):2855-70.

20. Panchaud N, Peli-Gulli MP, De Virgilio C. SEACing the GAP that nEGOCiates TORC1 activation: evolutionary conservation of Rag GTPase regulation. Cell Cycle. 2013;12(18):2948-52.
21. Dokudovskaya S, Rout MP. SEA you later alli-GATOR--a dynamic regulator of the TORC1 stress response pathway. J Cell Sci. 2015;128(12):2219-28.
22. Kanki T, Wang K, Baba M, Bartholomew CR, Lynch-Day MA, Du Z, et al. A genomic screen for yeast mutants defective in selective mitochondria autophagy. Molecular biology of the cell. 2009;20(22):4730-8.
23. Nemec AA, Howell LA, Peterson AK, Murray MA, Tomko RJ, Jr. Autophagic clearance of proteasomes in yeast requires the conserved sorting nexin Snx4. The Journal of biological chemistry. 2017;292(52):21466-80.
24. Nice DC, Sato TK, Stromhaug PE, Emr SD, Klionsky DJ. Cooperative binding of the cytoplasm to vacuole targeting pathway proteins, Cvt13 and Cvt20, to phosphatidylinositol 3-phosphate at the pre-autophagosomal structure is required for selective autophagy. The Journal of biological chemistry. 2002;277(33):30198-207.
25. Okamoto K, Kondo-Okamoto N, Ohsumi Y. Mitochondria-anchored receptor Atg32 mediates degradation of mitochondria via selective autophagy. Developmental cell. 2009;17(1):87-97.
26. Shpilka T, Welter E, Borovsky N, Amar N, Shimron F, Peleg Y, et al. Fatty acid synthase is preferentially degraded by autophagy upon nitrogen starvation in yeast. Proceedings of the National Academy of Sciences of the United States of America. 2015;112(5):1434-9.
27. Ma M, Burd CG, Chi RJ. Distinct complexes of yeast Snx4 family SNX-BARs mediate retrograde trafficking of Snc1 and Atg27. Traffic. 2017;18(2):134-44.
28. Popelka H, Klionsky DJ, Ragusa MJ. An atypical BAR domain protein in autophagy. Autophagy. 2018;14(7):1155-6.
29. Hanley SE, Willis SD, Cooper KF. Snx4-assisted vacuolar targeting of transcription factors defines a new autophagy pathway for controlling ATG expression. Autophagy. 2021:1-19.
30. Uetz P, Giot L, Cagney G, Mansfield TA, Judson RS, Knight JR, et al. A comprehensive analysis of protein-protein interactions in Saccharomyces cerevisiae. Nature. 2000;403(6770):623-7.
31. Kabeya Y, Kamada Y, Baba M, Takikawa H, Sasaki M, Ohsumi Y. Atg17 functions in cooperation with Atg1 and Atg13 in yeast autophagy. Molecular biology of the cell. 2005;16(5):2544-53.
32. Ma M, Kumar S, Purushothaman L, Babst M, Ungermann C, Chi RJ, et al. Lipid trafficking by yeast Snx4 family SNX-BAR proteins promotes autophagy and vacuole membrane fusion. Molecular biology of the cell. 2018;29(18):2190-200.
33. Chi RJ, Harrison MS, Burd CG. Biogenesis of endosome-derived transport carriers. Cell Mol Life Sci. 2015;72(18):3441-55.

CHAPTER 2: INTRACELLULAR LIPID HOMEOSTASIS AND TRAFFICKING IN AUTOPHAGY

Abstract

In eukaryotes, lipids are not only an important constituent of the plasma membrane but are also used to generate specialized membrane-bound organelles, including temporary compartments with critical functions. As such, lipids play a key role in intracellular homeostasis—the ability of a cell to maintain stable internal conditions upon changes in its extracellular environment. Autophagy, one of the cellular processes through which eukaryotic cells strive for survival under stress, is heavily dependent on lipid and membrane trafficking through the de novo formation of autophagosomes—temporary, large, and double-bilayered organelles in which materials are encapsulated for recycling. This chapter discusses what we know about lipid homeostasis and trafficking during autophagy and autophagosome formation, and comments on future directions of the field.

2.1 Introduction

Careful control of cellular lipid pathways plays an important role in a cell's ability to maintain stable internal conditions in the face of an ever-changing extracellular environment. This is particularly true as it relates to cellular self-eating or autophagy, a process brought about by proteins collectively known as the Atg (in yeast) or ATG (in mammals, **A**u**T**opha**G**y) proteins (1). Macroautophagy (herein referred to as autophagy) is the catabolic process by which unneeded or damaged cellular components are sequestered as cargo into unique double-membrane vesicles called autophagosomes (1). Once made, autophagosomes deliver their contents for breakdown by docking and fusing with the cell's degradative organelle, the lysosome in animal cells or the vacuole in plant and yeast cells. Following the breakdown of these materials, the components can undergo efflux to enable recycling and reuse by cells. Autophagy can be activated in many ways, including by starvation and cellular damage. When induced by starvation, autophagy allows for the recycling of nutrients to sustain metabolism in the absence of extracellular nutrients. Under other conditions, such as when specific cellular components are damaged, autophagy can take more specific forms, targeting the damaged components for sequestration into autophagosomes and delivery to lysosomes/vacuoles for destruction and recycling of the generated materials. The damaged components sequestered by more targeted forms of autophagy include mitochondria (mitophagy), ribosomes (ribophagy), and peroxisomes (pexophagy) (2-4). Dysregulation of autophagy has been linked to a variety of human disease states, including cancer, neurodegenerative disease, and heart disease (5). Mutations in ATG genes can result in autosomal recessive human genetic conditions including diseases like Niemann-Pick Type C1, a progressive lipid storage disorder

associated with impaired autophagosome maturation and characterized by neurodegeneration (6), Gaucher disease, a disorder related to the inability to breakdown specific cargo once autophagosomes fuse with the lysosome and characterized by hematologic symptoms (7), and Pompe disease, commonly coupled with glycogen accumulation in autophagic compartments and lysosomes, often resulting in myopathies (8, 9). These relationships between autophagy and human disease have generated much interest in attaining a better understanding of autophagic processes, especially its hallmark—autophagosome formation (1, 5).

Autophagosomes differ from smaller, more traditional types of transport vesicles in that they form de novo (anew) rather than budding off of a pre-existing donor organelle, range from 600-900 nm rather than 60-100 nm in diameter, and are delimited by two bilayer membranes rather than by a single bilayer (1). Autophagosome formation takes place at distinct cellular locations called pre-autophagosomal structures (PAS). Anew, membrane materials from different intracellular lipid sources are brought to the PAS to ultimately nucleate, form, and complete autophagosome biogenesis—highlighting the important role of lipid homeostasis in autophagy. Much effort has been dedicated to understanding the lipid trafficking events leading to autophagosome formation, the unique hallmark of autophagy. In this review, we discuss the progress that has been made in understanding this relationship between autophagosome formation and lipid homeostasis.

We begin this discussion by surveying the diversity of lipids present inside cells, including evidence on the role of each lipid type in autophagy. We discuss how membrane

composition helps establish organelle identity, in order to place autophagosome formation within a larger context of lipid homeostasis. After considering how these lipids relate to autophagy, we discuss the membrane trafficking events leading to autophagosome formation. We conclude by commenting on the questions that remain unanswered at the intersection of autophagy and lipid trafficking.

2.2. Structure/Function Diversity of Lipids and Membranes in Eukaryotes

Lipids are the only biologically relevant macromolecules that cannot be categorized as a polymer—their diversity is not dependent on monomer sequence like that of complex carbohydrates, proteins, or nucleic acids. The diversity of lipids is instead dependent on their chemical structure and the unique properties that are attained by combining different lipid molecules in the context of biological membrane bilayers (10-12). The structural diversity of lipids in biological membranes can be divided into three different groups: glycerophospholipids (also often referred to as phospholipids), sphingolipids, and sterols (Figure 1). These three types of amphipathic lipids, when combined in different ratios and leaflet asymmetries, give rise to a variety of biological membrane bilayer properties such as fluidity and curvature. Lipids in biological membranes can be covalently modified through the attachment of carbohydrate or phosphate moieties through glycosylation or phosphorylation, respectively. These modified lipids also contribute to the functional diversity of biological membranes. The properties of a membrane bilayer are also influenced by the proteins embedded within it. Some transmembrane proteins can be post-translationally modified to contain chemical groups like carbohydrates (glycoproteins) and phosphate groups (phosphoproteins) that also inform membrane function. Some membrane

and peripheral membrane proteins can be modified by covalent attachment to lipid groups as well.

Glycerophospholipids

Glycerophospholipids or phospholipids are the major component of biological membranes and their name evokes the building blocks used for their synthesis, including a three-carbon glycerol backbone (Figure 1A). This glycerol molecule is modified so that two of its hydroxyl groups (the ones attached to carbons 1 and 2) are esterified to covalently attach long-chain fatty acids to its backbone (10-12). The fatty acid esterified to carbon 1 is often saturated (no carbon to carbon double-bonds) and the fatty acid esterified to carbon 2 is often unsaturated (with carbon to carbon double bonds present) (10-12). Carbon to carbon double bonds in fatty acids have bends associated with them, which modify interactions with adjacent molecules and contribute to the fluidity of the bilayer (10-12). The hydroxyl group on the third carbon of the glycerol backbone is covalently attached or esterified to phosphoric acid, adding a highly polar head group to the phospholipid and contributing to its amphipathic nature (10-12).

Glycerophospholipid diversity is determined by the specific fatty acids and potentially alcohol-modified phosphoric acid groups attached to the glycerol backbone. A cell can generate a large variety of more than 100 glycerophospholipids, each with a different combination of fatty acids on carbons 1 and 2 and a head group on carbon 3 (10-12). Glycerophospholipids are named depending on the head group attached to carbon 3. Common glycerophospholipids in cells include: phosphatidic acid (PA),

phosphatidylglycerol (PG), phosphatidylethanolamine (PE), phosphatidylcholine (PC), phosphatidylserine (PS), and phosphatidylinositol (PI) (10-12). PE is the simplest phospholipid, with just a phosphoric acid moiety as a head group, while the other common types have alcohol-modified phosphoric acid head groups (10-12). PI in particular is the kind of lipid that plays a major role in determination of organelle identity, as described later in this review (10-12).

Certain phospholipids and lipid-modifying enzymes are key for autophagy. For example, the PI3Kinase complex (Class III and potentially Class II) and its substrate PI are essential for autophagosome formation (13-14). Moreover, soluble autophagy-related proteins known to be required for the induction of autophagosome formation like Atg1 are known to be recruited to membrane enriched with PI and PI3P (13-14).

Another lipid component essential for autophagosome formation is PE (13-14). PE lipids present in the autophagosome are important for the ability of this structure to associate with Atg8, another essential autophagy protein. This is because successful recruitment of Atg8 to autophagosomes involves Atg8 lipidation to the head group of PE, ultimately yielding a mature autophagosome that is decorated by lipidated Atg8 (13-14). In fact, PE is the lipid that contributes the most to autophagosome expansion (13-14).

Sphingolipids

The backbone of sphingolipids is not glycerol but sphingosine, an amino alcohol synthesized from palmitoyl-CoA and serine (10-12). The covalent attachment of the

sphingosine backbone to a fatty acid through an amide linkage yields an amphipathic sphingolipid (Figure 1B) (10-12). Common examples of this type of lipid in cells include ceramides (the simplest form of sphingolipid), phosphosphingolipids (also known as sphingomyelins, the only phospholipids without a glycerol backbone), and glycosphingolipids (10-12). The differences and diversity between these sphingolipids is dependent on the type of fatty acid and additional head groups attached to the sphingosine backbone. Sphingolipids were discovered and can be predominantly found in nervous tissue. This type of lipid can also be found in lower eukaryotes such as budding yeast (10-12).

Sphingolipids such as sphingosine-1-phosphate (S1P) and ceramides have been found to have an effect on autophagy (13-14). S1P, as part of its well-known role in fostering proliferation and cell survival, can induce autophagy in a way that engages elements usually associated with apoptosis (13-14). Ceramides, in their well-known role in promoting cell cycle arrest, promote cell death while engaging elements associated with autophagy (13-14).

Sterols

Sterols are four-ringed steroid molecules that contain a hydroxyl functional group at position 3 and as well as a variety of potential side chains (Figure 1C) (10-12). These lipids can be present in plant, animal, and microbial cells such as budding yeast. The predominant form of sterol lipid in animal cells is cholesterol. In other organisms, the lipid forms most

similar to cholesterol in function are called by different names (Figure 1C). For example, the functional yeast equivalent of cholesterol is referred to as ergosterol (Figure 1C). Sterols in eukaryotes have been shown to influence specific forms of autophagy including chaperone-mediated autophagy (CMA), pexophagy (autophagy of peroxisomes) and lipophagy (autophagy of lipid droplets) (13-14). These types of specific autophagy are beyond the scope of this review and are therefore not discussed.

2.2.2 Lipid Contributions to Membrane Structure/Function

Membrane Curvature

The concept of membrane curvature refers to the lipid composition asymmetry between the two leaflets of a membrane bilayer (11,15-16). The membrane curvature of an area can be changed, not only by altering its lipid composition, but also through the function of specialized proteins that can bind and remodel membranes. Early autophagosomes, often referred to as phagophores, have a high degree of curvature and are enriched for PI and PI3P (13-14). This combination of curvature and lipid composition is thought to help recruit a collective of autophagy-related proteins such as Atg1 and Atg3 to the site of autophagosome formation (13-14).

Membrane fluidity

Membrane fluidity refers to the ability of a membrane to sustain diffusion-driven movement of molecules within it (11, 17). In membranes, diffusion takes place laterally (11, 15, 17). The presence of unsaturated and sterol lipid structures enhances membrane

fluidity, ultimately allowing for more lateral diffusion of molecules and rendering it easier to bend and deform (11, 17).

This relationship between membrane fluidity and bending is highly relevant to autophagosome membranes (13-14). Early autophagosomal structures are characterized by high levels of curvature, suggesting that fluidity is key for autophagosome formation (13-14). In fact, autophagosomes are enriched for unsaturated lipids, and abrogation of enzyme functions that mediate desaturation can have inhibitory effects on autophagy (13-14).

Lipid Microdomains

Membranes are not even in composition throughout. Instead, they can have areas of differential lipid composition such as lipid rafts. Lipid rafts are generally more tightly packed (less fluid) than neighboring membrane material and their edges are usually rich in sphingolipids and cholesterol (11, 15, 17-18). Lipid rafts, because of their differential lipid composition, can act as scaffolds for non-clathrin-mediated internalization dynamics (11, 15, 17-18).

While no specific lipid microdomains have been identified as characteristic of autophagosome membranes, it is known that lipid rafts associated with the endoplasmic reticulum and mitochondria can contribute to autophagosome formation from these lipid sources (13-14).

2.3. Organelle Lipid Identity

Each membrane-bound organelle in the cell is characterized by a membrane bilayer with a particular lipid composition, leading to unique physical properties and the ability to recruit a specific set of interacting partners (Table 1). For this reason, organelle identity is not only defined by the collection of lipids displayed by the membrane of a particular organelle, but also by the set of proteins and molecules that are able to associate and interact with it. It is also important to recognize that these membranes can be remodeled and change their properties over time as cells strive to respond to stimuli.

The two main molecular determinants of organelle membrane identity in cells are lipid content, specifically PIs, and association with activated small GTPases (such as the Rab family of proteins) (19-20). These membrane elements can easily be remodeled and changed, in contrast to transmembrane proteins and other integral membrane elements, allowing for the dynamic regulation and sculpting of membranes. Small GTPases exhibit diversity that correlates with specific subcellular locations, such that Rab 1 (ER and Golgi), Rab 2 (cis Golgi), Rab 4/11 (Recycling endosomes), and Rab 5 (Early endosomes, plasma membrane, clathrin coated vesicles) each localize to the membranes of different organelles (19-20).

Small GTPases like Rabs exist in two forms: a GTP-bound active and membrane associated form, and a GDP-bound inactive cytosolic form. While Rabs can be lipidated (prenylated) at their C-terminus, facilitating their anchoring to the membrane, what is thought to

determine Rab-membrane interaction specificity are the proteins that facilitate their GDP/GTP exchange (19-20).

Organelle identity is also determined by specific forms of PI, with phosphate groups covalently linked to positions 3, 4, or 5 of their inositol ring (11-12, 15, 19-22). The plasma membrane contains predominantly PI4P and PI(4,5)P2, with the latter synthesized from the former (19-22). These two can be phosphorylated by PI3-kinases (PI3K) to generate signaling lipids (19-22). PI(4,5)P2 can also be cleaved to generate diacylglycerol (DAG; which can activate autophagic response) and I(1,4,5)P3 second messengers (19-22). PI4P can also be found in the Golgi (19-20). Early endosomes are characterized by the presence of PI(3)P through the function of PI3-OH kinases like Vps34, which require small GTPases like Rab5 to function at the proper location (13-14, 19-22). This requirement for a Rab GTPase to produce the corresponding PI species characteristic of the compartment highlights the close functional relationship between the two key determinants of organelle identity (19-22). The presence of PI(3,5)P (synthesized from PI3P) is characteristic of late endosomes (19-22).

The lipid composition of organelles is influenced by exchange of materials between them. There are different ways in which such exchanges can take place, including vesicle-mediated membrane trafficking between organelles, lipid droplet function, and direct exchange of lipid species via membrane contact sites between organelles such as the ER and Golgi. While the ER is the central site for intracellular lipid synthesis, lipid trafficking is essential for lipids to move from the ER to different organelles in order to maintain

homeostatic membrane composition required for morphology, signaling and cellular processes. Moreover, it is common for organelles like the Golgi and endosome to change their lipid and membrane compositions as they mature.

Much of what we know about the lipid content of intracellular organelles or compartments is due to lipidomics studies that have served as a tool to identify lipid species in these membranes (23-27). Biochemical fractionation and/or extraction techniques are used to isolate organellar membranes of interest and subject them to mass spectrometry for lipid identification and lipidome determination, similar to proteomics studies that have been used to catalog the protein content of many of these organelles (27). Different efficiencies and membrane targets can be obtained depending on how the samples are prepared and treated during extraction leading up to ionization and mass spectrometry analysis (27). Different types of data processing allow for a range of lipidomics applications, from species identification and quantification to pathway and network analysis (27). These techniques have been thoroughly reviewed elsewhere and outside of the scope of this review article (27).

While proteomic studies have shed light on the proteins that reside in autophagosomes (28-31), an autophagosome lipidome has yet to be experimentally determined. Through microscopy and biochemical methods, we know that the lipid identity of autophagosomes is defined largely by the presence of PE, PI and PI3P. In the following section of this review, we discuss in detail the molecular processes that bring about lipid homeostasis and trafficking during autophagy, particularly in autophagosome formation.

2.4. Understanding Autophagosomes: A non-traditional membrane vesicle

Current efforts to better understand autophagy are focused on the molecular details leading to the formation of autophagosomes, a double-membraned vesicle unlike any other in size and structure, that serves as the hallmark of autophagy. These approaches have mainly focused on understanding the intracellular trafficking of autophagy-related transmembrane proteins that are thought to help deliver lipids to the growing autophagosome via vesicle transport. Insights have also been obtained from assessing the influence of lipid-dependent enzymes as well as lipid-synthesis and transport pathways on autophagy. For example, mutation of PI3K enzymes severely impairs autophagy (32-33), pointing at the importance PI and some of its phosphorylated forms in autophagic processes. In these ways, we have identified that PE and PI lipids play an important role in autophagy (Table 2) (34-43). We discuss these findings below.

2.4.1 Membrane Dynamics during Autophagy

The process of autophagy is often thought about to happen in different stages—initiation or nucleation of phagophores (cup-shaped, double-membraned autophagosome precursors), expansion of phagophores, completion or closure of autophagosomes, fusion of autophagosomes with the lysosome/vacuole, and the efflux of materials from the lysosome/vacuole for reuse (Figure 2). Because our review aims to focus on the lipid homeostasis and trafficking during autophagy, we focus our discussion below on the first four stages of autophagy (initiation through fusion).

Initiation

During the initial stages of autophagy, essential Atg proteins are recruited to PAS structures to nucleate the gathering of membrane de novo and to generate autophagosome precursors called phagophores. In mammalian cells, phagophores can be formed at PAS sites proximal to ER, mitochondria, or plasma membrane (13-14). In yeast however, PAS structures are perivacuolar in nature, leading phagophores to originate at locations proximal to the vacuole with membrane contributions with other cellular locations like discussed below. While mammalian cells can display many PAS structures at steady state, yeast often display one of these structures at any given time.

Initially, activated or triggered by upstream inhibition of mTOR, core autophagy proteins collect at the PAS structure. These core factors include the ULK1 complex, ATG13, FIP200, ATG101, (yeast Atg1, Atg13, Atg17, Atg29 and Atg31) (13-14). The mobilization of these factors ultimately leads to the PAS recruitment and activation of the PI3K/Vps34 kinase complex which allows for the generation of PI3P at this site (from PI) (Figure 2A) (13-14, 30-31). This enzyme activity drives forward phagophore initiation/nucleation, allowing additional recruitment of other proteins like WIPI proteins (Atg18 in yeast). WIPI proteins are key PI3P effectors. PI3K regulator proteins like ATG14 (Atg14 in yeast) are also recruited to the PAS, allowing for the modulation of initiation/nucleation of phagophore formation (13-14). ATG14 is also able to mediate homotypic fusion of single-membrane vesicles at the PAS, allowing more traditional membrane vesicles delivered to the PAS to fuse and contribute to the nucleation and growth of the phagophore (13-14). In this way, the phagophore has been found to accept lipid inputs from the ER, ER exit sites

(ERES), the Golgi, the plasma membrane and recycling endosomes for its growth and expansion (Figure 2A) (13-14).

Generation of PI3P at PAS sites functions as a scaffold for ATG/Atg proteins to associate with the PAS, helping in the expansion, elongation and curvature generation needed for autophagosome formation to proceed successfully (13-14).

Expansion

The lipidation of Atg8 (LC3) onto PE lipid molecules in the growing phagophore membrane is key for autophagosome formation. Other Atg proteins like ATG16L1 (yeast Atg16) as well as ATG12-ATG5 are required for Atg8 lipidation with PE. Interestingly, some of these required Atg factors like ATG16L1 partly reside in the recycling endosome and have been found to localize to the PAS in a PX-BAR/SNX protein-dependent manner (for example, SNX18) (13-14). While not considered core Atg proteins, PX-BAR/SNX proteins are membrane remodeling proteins that have also been found to be required for autophagosome formation.

While the exact lipid composition of the phagophore/autophagosome is still under debate, because of the findings described above, PI3P is thought to be one of the most abundant lipid species present in these structures. In fact, recent findings identify the ATG protein ATG2A as a lipid shuttle factor that facilitates PI3P-dependent autophagosome growth (44-46). Other phosphoinositides such as PI4P, PI(4,5)P2 and PI(3,5)P2 have also been suggested to play a role in the expansion of the phagophore (13-14). Apart from these, as

mentioned above, sphingosine-1-phosphate (S1P) and ceramide, also contribute to autophagy. And while, Atg8/LC3 lipidation resulting in LC3-PE is important for the expansion and closure of the autophagosome, the intracellular membranes that are the source of this PE still remain to be identified. PE is produced from phosphatidylserine (PS) in mitochondria, which might be one of the sources of PE (Figure 2A). PE might also be shuttled from the ER, plasma membrane and recycling endosomes. It has been recently shown by Ma et al. (39), that PS trafficking by sorting nexin Snx4 in yeast is required for maintaining the correct lipid composition of the vacuole for autophagosome fusion in yeast (Figure 2C). Thus, maintenance of organelle lipid identity through proper trafficking and lipid homeostasis are crucial for autophagy as well.

ATG9 trafficking

ATG9 (Atg9 in yeast) is a six-transmembrane protein that is required for autophagosome formation (47-54). ATG9 trafficking is one of the most studied topics in the autophagy field, highlighting the important role it plays in autophagy—the autophagic phenotypes of null mutants are very penetrant. While this is the case, we still lack detailed information about the function of this protein during autophagy. Yeast studies have shown that Atg9 is localized to PAS as well as cytoplasmic vesicles of 30-60nm diameter that bud-off of the late Golgi. It is believed that Atg9 shuttles between the PAS and its cytoplasmic vesicle pool upon autophagy induction (Figure 2C). At the PAS, Atg9 associates with Atg1, Atg2 as well as Atg18. Since Atg9 is a transmembrane protein, its trafficking directly affects the funneling or channeling of membrane to the PAS and the growing autophagosome. The Atg9 vesicles are thought to originate at the Golgi and contain fusion factors such as

subunits of the TRAPIII (Trs85) complex that are responsible for fusion with the growing autophagosome (47-48, 54). Once Atg9 reaches the lysosome/vacuole as autophagosomes fuse, some studies suggest that the protein can be recycled out of the vacuolar membrane for reuse in new rounds of autophagosome formation. These studies are synergistic with findings that Atg9 traffics through endosomal compartments, as this might be a intermediary step important for recycling. This recycling model is supported by the observation that mutations in the retromer complex, when combined with mutations in tethering factor Trs85, can abrogate trafficking of Atg9 to the PAS. Similarly the combination mutations with GARP subunits, that are responsible for tethering vesicles to the Golgi from the endosome, with Trs85 result in defective autophagy. Atg9 trafficking is influenced by other autophagy proteins such as Atg27 and Atg23 (55-58). Atg23 is a peripheral membrane protein that facilitates the anterograde trafficking of Atg9 from the Golgi to the PAS. Atg27, another transmembrane protein that facilitates formation of Atg9 vesicles at the late Golgi, is itself observed to be present in early/late endosomes, PAS, Golgi and vacuolar membrane. Atg27 can be retrieved from the vacuole in a process that is Snx4-dependent. Furthermore, earlier studies identified a C terminal tyrosine (YSAV) motif in Atg27 that is important for the proper delivery of Atg27 to the vacuole as well as to maintain Atg9 pools at the endosome that can be mobilized to different compartments during autophagy (Figure 2C). Taken together, the complexity of Atg9 trafficking synergizes with the hypothesis that a collection of different membranes such as endosome and Golgi all contribute to the lipid identity of the autophagosome.

Autophagosomal fusion with the lysosome/vacuole

After the autophagosome is completed, the double membrane vesicle is ready for fusion with the lysosome/vacuole. The fusion of the autophagosome not only requires components of the fusion machinery as well as PI3P turnover, but it also requires the disassembly or retrieval of several ATG proteins from the autophagosome. In yeast, phosphoinositide phosphatases, including those from the myotubularin protein family, like Ymr1, along with Sjl2 and Sjl3 are important for removal of PI3P from completed autophagosomes, making autophagosomes fusion-competent (Figure 2D). In mammalian cells, PI3P phosphatase MYM-3 acts similarly to Ymr1 in promoting autophagosome maturation and fusion. Fusion of autophagosomes with the lysosome is mediated by RAB7-like protein Ypt7 along with the HOPS (Homotypic fusion and vacuole protein sorting) tethering complex and SNARE (Soluble Ethylmaleimide-Sensitive Factor Attachment Protein Receptor) proteins. Three Q–SNAREs: Vam3, Vti1 and Vam7 have been identified in yeast along with R-SNARE Ykt6 as key for this fusion step. Vamp7 is a sorting nexin family protein containing a PX domain that interacts with PI3P. Studies suggest that Vam7 interacts with Atg17-Atg29-Atg31 trimer complex via Atg17 interaction. In mammalian cells, SNAREs such as SYN12, SNAP29 and VAMP7/8 are responsible for autophagosome fusion with the lysosome. Interestingly, the PI3K VPS34 has also been linked with later stages of autophagy, including lysosomes returning to normal or regenerating once fusion with autophagosomes has taken place. Other phosphorylated lipid species like PI4P and PI(4,5)P2 can also facilitate lysosomal regeneration, allowing for new rounds of autophagy to occur. This might also trigger the formation of recycling vesicles packaging ATG protein cargo for recycling off the lysosomal membrane.

Another aspect that is key for late autophagy stages to proceed is intact lysosomal/vacuolar lipid homeostasis and lipid identity. For example, yeast vacuoles have unique lipid composition that is different from other membrane organelles within the cell. Vacuoles are enriched with lipids such as, myo-inositols, PI3P, and typically PI3,5P2, among other lipids such as ergosterol, diacylglycerol and some sphingolipids (Figure 2D). The specific lipid identity of vacuoles is important for the recruitment of fusion factors such as SNARES Ypt7 and HOPS that allow fusion of autophagosomes. Thus, the specific lipid identity of vacuole is important for its physiological function and its fusion with the late endosome and autophagosome.

2.5. Conclusion

While progress has been made in understanding the molecular underpinnings of autophagosome formation, our understanding has been primarily advanced by understanding the functions of proteins that lead and are required for this autophagic vesicle to form (28-31). Because the extensive level of membrane remodeling that takes place during autophagy formation, much will be gained by investigating the process using methods that focus on the membrane and lipid biology of the process (23-27). This new perspective has the potential of changing the way we have conventionally understood the remodeling of membranes for vesicle formation.

2.6 Figures and Tables

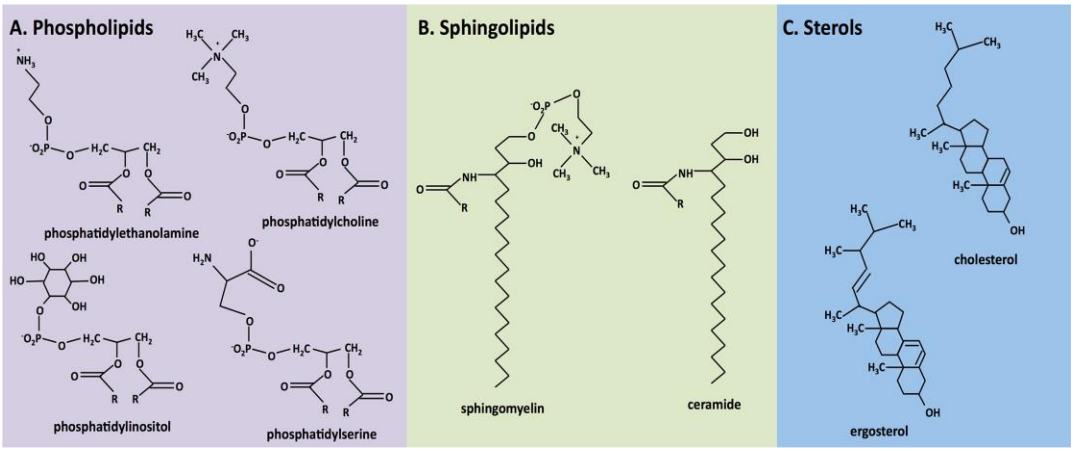

Figure 5. Chemical structures of selected cell membrane lipids. Examples of some of the different types of lipids that can be found in cell membranes, namely (A) phospholipids, (B) sphingolipids, and (C) sterols.

Table 1. Lipid Content of different Organelle Membranes.

Organelle Membrane	Lipid Content
Plasma membrane	ceramide, sphingosine, S1P, diglyceride (alsoknown as diacylglycerol), PI4P, PI(4,5)P2, PI(3,4)P2,PI(3,4,5)P3
Endoplasmic Reticulum	PC, PE, PI, PS, PA, ceramide, galactosylceramide, cholesterol and ergosterol.
Mitochondria	PE, PG, cardiolipin, PA
Golgi	PE, PS, PC, PI4P, sphingolipid
Late endosome	PI(3,5)P2, PI3P, PS
Lipid Droplets	triacylglycerol esters and steryl esters, PE

Table 2. Organellar lipid contributions to Autophagic Processes and Autophagosome Formation. The table below describes the lipid contributions of different intracellular organelles or donor membranes to the progression of autophagy and/or autophagosome formation along with the autophagy processes or steps benefiting from these contributions.

Donor Membrane	Lipid Contributions	Autophagic Process/Step Benefited	References
Endoplasmic Reticulum	PI3P	Autophagosome formation	34
Mitochondria	PE	Autophagosome formation	35
Plasma Membrane	PI3P	Autophagosome and ATG16 vesicle formation	36
Golgi	PI4P, PE, PS	ATG9 vesicles formation, autophagosome fusion with vacuole/lysosome	37-39
Late Endosome	PI3P, PI(3,5)P2, PS	Autophagosome formation, autophagosome fusion with vacuole/lysosome	39, 40
ER-Golgi Intermediate compartments	PE	LC3/Atg8 lipidation	41
ER-Mitochondria contactsites	PE	Autophagosome formation	42
ER-Plasma membrane contact site	PI3P	Autophagosome formation	43

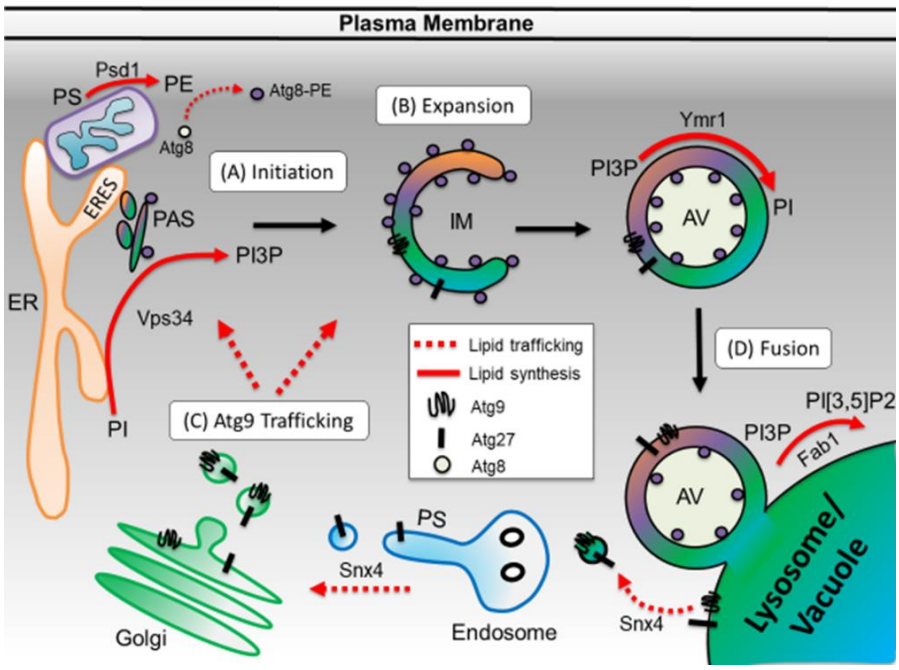

Figure 6. Lipid biosynthesis and trafficking during autophagosome biogenesis and fusion. The relative lipid contributions via lipid trafficking or lipid biosynthesis from each organelle are shown. (A) Upon autophagy induction, membrane is sequestered from pools of lipid donors such as the ER, mitochondria, Golgi, endosome and vacuole to form the pre-autophagosomal structure (PAS) or isolation membrane (IM). (B) PI in the PAS is converted to PI3P via Vps34 and Atg8-PE is enriched, allowing for IM expansion and closure. (C) Additional lipid membrane from Atg9-Atg27 vesicle trafficking allows for further expansion of the IM. (D) Autophagosome (AV) maturation is completed once PI3P is converted into PI by myotubularin phosphatases such as Ymr1. The mature AV can fuse to the vacuole which has converted PI3P into PI(3,5)P2 via Fab1 kinase. PI(3,5)P2 permits fusion of AV and endosomes. Vacuole lipid homeostasis is further aided by Snx4 trafficking of PS and Atg27 from the endosome and vacuole.

2.7. References

1. Yang Z, Klionsky DJ. Eaten alive: a history of macroautophagy. Nat Cell Biol. 2010 Sep;12(9):814.
2. Wang K, Klionsky DJ. Mitochondria removal by autophagy. Autophagy. 2011 Mar 1;7(3):297-300.
3. Cebollero E, Reggiori F, Kraft C. Reticulophagy and ribophagy: regulated degradation of protein production factories. Int J of Cell Biol. 2012 Feb 28;2012:182834.
4. Sakai Y, Oku M, van der Klei IJ, Kiel JA. Pexophagy: autophagic degradation of peroxisomes. Biochim Biophys Acta Mol Cell Res. 2006 Dec 1;1763(12):1767-75.
5. Choi AM, Ryter SW, Levine B. Autophagy in human health and disease. N Engl J of Med. 2013 Feb 14;368(7):651-62.
6. Sarkar S, Carroll B, Buganim Y, Maetzel D, Ng AH, Cassady JP, Cohen MA, Chakraborty S, Wang H, Spooner E, Ploegh H. Impaired autophagy in the lipid-storage disorder Niemann-Pick type C1 disease. Cell Rep. 2013 Dec 12;5(5):1302-15.
7. Ivanova MM, Changsila E, Iaonou C, Goker-Alpan O. Impaired autophagic and mitochondrial functions are partially restored by ERT in Gaucher and Fabry diseases. PloS One. 2019 Jan 11;14(1):e0210617.
8. Raben N, Roberts A, Plotz PH. Role of autophagy in the pathogenesis of Pompe disease. Acta Myol. 2007 Jul;26(1):45.
9. Lim JA, Sun B, Puertollano R, Raben N. Therapeutic benefit of autophagy modulation in Pompe disease. Mol Ther. 2018 Jul 5;26(7):1783-96.
10. Harayama T, Riezman H. Understanding the diversity of membrane lipid composition. Nat Rev Mol Cell Biol. 2018 May;19(5):281.
11. Voet D, Voet JG, Pratt CW. Fundamentals of biochemistry: life at the molecular level. 5th ed. New Jersey: Wiley; 2016.
12. Berg JM, Tymoczko JL, Stryer L. Biochemistry. 8th ed. New York: W H Freeman; 2015.
13. Knævelsrud H, Simonsen A. Lipids in autophagy: constituents, signaling molecules and cargo with relevance to disease. Biochim Biophys Acta Mol Cell Biol Lipids. 2012 Aug 1;1821(8):1133-45.
14. Dall'Armi C, Devereaux KA, Di Paolo G. The role of lipids in the control of autophagy. Curr Biol. 2013 Jan 7;23(1):R33-45.
15. Ridgway N, McLeod R, editors. Biochemistry of lipids, lipoproteins and membranes. 6th ed. Amsterdam: Elsevier; 2015.
16. McMahon HT, Boucrot E. Membrane curvature at a glance. J Cell Sci. 2015 Mar 15;128(6):1065-70.
17. Beney L, Gervais P. Influence of the fluidity of the membrane on the response of microorganisms to environmental stresses. Appl Microbiol Biotechnol. 2001 Oct 1;57(1-2):34-42.
18. Edidin M. Lipid microdomains in cell surface membranes. Curr Opin Struct Biol. 1997 Aug 1;7(4):528-32.
19. Behnia R, Munro S. Organelle identity and the signposts for membrane traffic. Nature. 2005 Dec 1;438(7068):597.

20. Alberts B, Bray D, Hopkin K, Johnson AD, Lewis J, Raff M, Roberts K, Walter P. Essential cell biology. 5th ed. New York: W W Norton; 2019.
21. van Meer G, Voelker DR, Feigenson GW. Membrane lipids: where they are and how they behave. Nat Rev Mol Cell Biol. 2008 Feb;9(2):112.
22. van Meer G, de Kroon AI. Lipid map of the mammalian cell. J Cell Sci. 2011 Jan 1;124(1):5-8.
23. Brügger B. Lipidomics: analysis of the lipid composition of cells and subcellular organelles by electrospray ionization mass spectrometry. Annu Rev Biochem. 2014 Jun 2;83:79-98.
24. Klose C, Surma MA, Simons K. Organellar lipidomics—background and perspectives. Curr Opin Cell Biol. 2013 Aug 1;25(4):406-13.
25. Loizides-Mangold U. On the future of mass-spectrometry-based lipidomics. FEBS J. 2013 Jun 1;280(12):2817-29.
26. Aviram R, Manella G, Kopelman N, Neufeld-Cohen A, Zwighaft Z, Elimelech M, Adamovich Y, Golik M, Wang C, Han X, Asher G. Lipidomics analyses reveal temporal and spatial lipid organization and uncover daily oscillations in intracellular organelles. Mol Cell. 2016 May 19;62(4):636-48.
27. Yang K, Han X. Lipidomics: techniques, applications, and outcomes related to biomedical sciences. Trends Biochem Sci. 2016 Nov 1;41(11):954-69.
28. Øverbye A, Brinchmann MF, Seglen PO. Proteomic analysis of membrane-associated proteins from rat liver autophagosomes. Autophagy. 2007 Jul 16;3(4):300-22.
29. Shui W, Sheu L, Liu J, Smart B, Petzold CJ, Hsieh TY, Pitcher A, Keasling JD, Bertozzi CR. Membrane proteomics of phagosomes suggests a connection to autophagy. Proc Natl Acad Sci. 2008 Nov 4;105(44):16952-7.
30. Dengjel J, Høyer-Hansen M, Nielsen MO, Eisenberg T, Harder LM, Schandorff S, Farkas T, Kirkegaard T, Becker AC, Schroeder S, Vanselow K. Identification of autophagosome-associated proteins and regulators by quantitative proteomic analysis and genetic screens. Mol Cell Proteomics. 2012 Mar 1;11(3):M111-014035.
31. Zimmermann AC, Zarei M, Eiselein S, Dengjel J. Quantitative proteomics for the analysis of spatio-temporal protein dynamics during autophagy. Autophagy. 2010 Nov 16;6(8):1009-16.
32. Diao J, Liu R, Rong Y, Zhao M, Zhang J, Lai Y, Zhou Q, Wilz LM, Li J, Vivona S, Pfuetzner RA. ATG14 promotes membrane tethering and fusion of autophagosomes to endolysosomes. Nature. 2015 Apr 23;520(7548):563.
33. Ma M, Burd CG, Chi RJ. Distinct complexes of yeast Snx4 family SNX-BARs mediate retrograde trafficking of Snc1 and Atg27. Traffic. 2017 Feb;18(2):134-44.
34. Axe EL, Walker SA, Manifava M, Chandra P, Roderick HL, Habermann A, Griffiths G, Ktistakis NT. Autophagosome formation from membrane compartments enriched in phosphatidylinositol 3-phosphate and dynamically connected to the endoplasmic reticulum. J Cell Biol. 2008 Aug 25;182(4):685-701.
35. Hailey DW, Rambold AS, Satpute-Krishnan P, Mitra K, Sougrat R, Kim PK, Lippincott-Schwartz J. Mitochondria supply membranes for autophagosome biogenesis during starvation. Cell. 2010 May 14;141(4):656-67.
36. Ravikumar B, Moreau K, Jahreiss L, Puri C, Rubinsztein DC. Plasma membrane contributes to the formation of pre-autophagosomal structures. Nat Cell Biol. 2010 Aug;12(8):747.

37. Mari M, Griffith J, Rieter E, Krishnappa L, Klionsky DJ, Reggiori F. An Atg9-containing compartment that functions in the early steps of autophagosome biogenesis. Journal Cell Biol. 2010 Sep 20;190(6):1005-22.
38. Judith D, Jefferies HB, Boeing S, Frith D, Snijders AP, Tooze SA. ATG9A shapes the forming autophagosome through Arfaptin 2 and phosphatidylinositol 4-kinase IIIβ. J Cell Biol. 2019 May 6;218(5):1634-52.
39. Ma M, Kumar S, Purushothaman L, Babst M, Ungermann C, Chi RJ, Burd CG. Lipid trafficking by yeast Snx4 family SNX-BAR proteins promotes autophagy and vacuole membrane fusion. Mol Biol Cell. 2018 Sep 1;29(18):2190-200.
40. Dall'Armi C, Devereaux KA, Di Paolo G. The role of lipids in the control of autophagy. Curr Biol. 2013 Jan 7;23(1):R33-45.
41. Ge L, Melville D, Zhang M, Schekman R. The ER–Golgi intermediate compartment is a key membrane source for the LC3 lipidation step of autophagosome biogenesis. Elife. 2013 Aug 6;2:e00947.
42. Hailey DW, Rambold AS, Satpute-Krishnan P, Mitra K, Sougrat R, Kim PK, Lippincott-Schwartz J. Mitochondria supply membranes for autophagosome biogenesis during starvation. Cell. 2010 May 14;141(4):656-67.
43. Nascimbeni AC, Giordano F, Dupont N, Grasso D, Vaccaro MI, Codogno P, Morel E. ER–plasma membrane contact sites contribute to autophagosome biogenesis by regulation of local PI3P synthesis. EMBO J. 2017 Jul 14;36(14):2018-33.
44. Osawa T, Noda NN. Atg2: A novel phospholipid transfer protein that mediates de novo autophagosome biogenesis. Protein Sci. 2019 Jun;28(6):1005-12.
45. Maeda S, Otomo C, Otomo T. The autophagic membrane tether ATG2A transfers lipids between membranes. Elife. 2019 Jul 4;8:e45777.
46. Valverde DP, Yu S, Boggavarapu V, Kumar N, Lees JA, Walz T, Reinisch KM, Melia TJ. ATG2 transports lipids to promote autophagosome biogenesis. J Cell Biol. 2019 Jun 3;218(6):1787-98.
47. Yamamoto H, Kakuta S, Watanabe TM, Kitamura A, Sekito T, Kondo-Kakuta C, Ichikawa R, Kinjo M, Ohsumi Y. Atg9 vesicles are an important membrane source during early steps of autophagosome formation. J Cell Biol. 2012 Jul 23;198(2):219-33.
48. Kakuta S, Yamamoto H, Negishi L, Kondo-Kakuta C, Hayashi N, Ohsumi Y. Atg9 vesicles recruit vesicle-tethering proteins Trs85 and Ypt1 to the autophagosome formation site. J Biol Chem. 2012 Dec 28;287(53):44261-9.
49. Suzuki SW, Yamamoto H, Oikawa Y, Kondo-Kakuta C, Kimura Y, Hirano H, Ohsumi Y. Atg13 HORMA domain recruits Atg9 vesicles during autophagosome formation. Proc Natl Acad Sci USA. 2015 Mar 17;112(11):3350-5.
50. Karanasios E, Walker SA, Okkenhaug H, Manifava M, Hummel E, Zimmermann H, Ahmed Q, Domart MC, Collinson L, Ktistakis NT. Autophagy initiation by ULK complex assembly on ER tubulovesicular regions marked by ATG9 vesicles. Nat Commun. 2016 Aug 11;7:12420.
51. Rao Y, Perna MG, Hofmann B, Beier V, Wollert T. The Atg1–kinase complex tethers Atg9-vesicles to initiate autophagy. Nat Comm. 2016 Jan 12;7:10338.
52. Reggiori F, Tooze SA. Autophagy regulation through Atg9 traffic. J Cell Biol. 2012 Jul 23;198(2):151-3.

53. Orsi A, Razi M, Dooley HC, Robinson D, Weston AE, Collinson LM, Tooze SA. Dynamic and transient interactions of Atg9 with autophagosomes, but not membrane integration, are required for autophagy. Mol Biol Cell. 2012 May 15;23(10):1860-73.
54. Shirahama-Noda K, Kira S, Yoshimori T, Noda T. TRAPPIII is responsible for vesicular transport from early endosomes to Golgi, facilitating Atg9 cycling in autophagy. J Cell Sci. 2013 Nov 1;126(21):4963-73.
55. Yen WL, Legakis JE, Nair U, Klionsky DJ. Atg27 is required for autophagy-dependent cycling of Atg9. Mol Biol Cell. 2007 Feb;18(2):581-93.
56. Yen WL, Klionsky DJ. Atg27 is a second transmembrane cycling protein. Autophagy. 2007 May 10;3(3):254-6.
57. Backues SK, Orban DP, Bernard A, Singh K, Cao Y, Klionsky DJ. Atg23 and Atg27 act at the early stages of Atg9 trafficking in S. cerevisiae. Traffic. 2015 Feb;16(2):172-90.
58. Segarra VA, Boettner DR, Lemmon SK. Atg27 tyrosine sorting motif is important for its trafficking and Atg9 localization. Traffic. 2015 Apr;16(4):365-78.

CHAPTER 3: VPS501, A NOVEL VACUOLAR SNX-BAR PROTEIN COOPERATES WITH THE SEA COMPLEX TO REGULATE TORC1 SIGNALING DURING AUTOPHAGY

Abstract

The sorting nexins (SNX), constitute a diverse family of molecules that play varied roles in membrane trafficking, cell signaling, membrane remodeling, organelle motility and autophagy. In particular, the SNX-BAR proteins, a SNX subfamily characterized by a dimeric Bin/Amphiphysin/Rvs (BAR) domain and a conserved Phox-homology domain, have well-characterized endosomal trafficking roles in budding yeast. Phylogenetic analyses allowed us to identify a novel SNX-BAR protein, Vps501. We report that Vps501 uniquely localizes to the vacuolar membrane and interacts with the SEA complex to regulate TORC1 inactivation. We found cells displayed a severe deficiency in starvation-induced/nonselective autophagy only when SEA complex subunits are ablated in combination with Vps501, indicating a cooperative role with the SEA complex. Additionally, we found the SEACIT complex becomes destabilized, which resulted in aberrant endosomal TORC1 activity and subsequent Atg13 hyperphosphorylation.

3.1 Introduction

The sorting nexin (SNX) family is an evolutionarily conserved class of cellular trafficking proteins that are most well-known for their ability to bind phospholipids to catalyze endosomal sorting reactions and other membrane trafficking pathways in the cell (1, 2). SNX proteins are structurally characterized by an evolutionarily conserved region known as the Phox (PX) homology domain, which allows them to recognize the lipid composition of the endosome, most notably phosphatidylinositol-3-phosphate (PI3P) (3). The SNX proteins are divided into subfamilies according to the presence of other characteristic domains such as a Bin-Amphiphysin-Rvs (BAR) domain (4). BAR domains allow members of the SNX-BAR subfamily to bind high positive curvature structures, driving the formation of endosomal tubules, while also conferring the ability to form sorting complexes that facilitate cargo selection (4-6). The *Saccharomyces cerevisiae* genome encodes seven annotated SNX-BAR proteins, while the human genome encodes twelve (3, 4, 7). In addition to working with complexes such as retromer to mediate retrograde and recycling trafficking of cargos at the tubular endosomal network (TEN) (3-6, 8), SNX-BAR proteins contribute to other important conserved cellular processes such as macroautophagy (herein referred to as autophagy) and selective autophagy (9-11).

Autophagy is a stress response in which eukaryotic cells recycle damaged or unneeded components by sequestering them in double-bilayered compartments called autophagosomes. Once made, autophagosomes deliver their contents for breakdown by docking and fusing with the cell's degradative organelle, the lysosome in animal cells or the vacuole in plant and yeast cells. These key steps and the core autophagy-related (Atg) proteins that mediate and regulate them are evolutionarily conserved across all autophagy

pathways, including starvation-induced bulk autophagy and cargo-selective autophagy pathways (12-15). While vacuoles and lysosomes can serve as storage and/or recycling depots for cells, their delimiting membranes host critical signaling events for autophagy induction such as the inactivation of *target of rapamycin* (TOR).

TORC1 has been shown to mediate multiple biological pathways that relay nutrient availability information to ensure cellular homeostasis in eukaryotic cells (16-18). The primary function of TORC1 is to control TOR kinase activity, linking changes in nutrient levels with transcriptomic reprogramming via its downstream effectors to promote cell proliferation (19). In yeast, TORC1 has been found to inhibit macro and microautophagy (20-22) and control the MVB pathway-driven degradation of plasma membrane proteins (23-26), through mechanisms that have not been yet characterized.

Multiprotein complexes such as TORC1 in yeast are tethered to the vacuolar membrane and function by integrating signals from many intracellular and extracellular cues from a variety of kinases, GTPases and their effectors (27). Recently, an upstream regulator of the TORC1, the yeast SEA complex (GATOR complex in humans), was identified and shown to be part of this web of GTPase effectors (28, 29). The SEA complex is a conserved eight protein complex (Sea1, Sea2, Sea3, Sea4, Seh1, Sec13, Npr2, Npr3) made up of proteins with structural characteristics similar to the membrane coating complexes such as the nuclear pore complex, the COPII vesicle coating complex and HOPS/CORVET tethering complexes (30). The SEA complex is also dynamically associated to the vacuolar membrane; however, its complete function is not well understood.

Substantial effort has gone into understanding the membrane trafficking events required to form autophagosomes and the contributions of SNX-BAR proteins to the autophagy pathway. In fact, SNX-BAR proteins have been shown to mediate an emerging number of autophagy-related processes. For example, the Snx4-Snx41 SNX-BAR heterodimer mediates the retrograde endosome-to-Golgi transport of the autophagy-related protein Atg27, an integral membrane protein that when deleted leads to decreased autophagosome number and autophagic flux in budding yeast (9, 31). Moreover, Snx4-mediated retrograde trafficking of proteins and lipids helps the cell maintain the phosphatidylserine (PS) and phosphatidylethanolamine (PE) homeostasis, which is required to allow autophagosome fusion with the vacuole, one of the final stages of autophagy (10). As we come to understand the full range of SNX-BAR protein functions, it is becoming clear that this group of proteins has a critical role in the network of cellular players that collectively regulate autophagy, including those associated with the TORC1 complex.

In this study, we report the identification of a novel yeast SNX-BAR protein, encoded by yeast open reading frame (ORF) YKR078W, that contributes to TORC1 regulation alongside the SEA complex. Our findings bring us to a more complete understanding of SNX-BAR family of proteins and the important role they play in TORC1 signaling during autophagy.

3.2 Materials and Methods

Phylogenetic Analysis

To determine the identity of *Saccharomyces cerevisiae* YKR078W in relation to other SNX-BAR sorting nexins, we conducted a phylogenetic analysis. We used a former analysis of SNX-BAR proteins in opisthokonts (e.g., fungi Vps5, and Vps17, animal and choanoflagellate SNX 5/6/32 and SNX 1/2) by Koumandou et al. (2011) as an initial seed alignment. We added additional Vps5 proteins from other fungal species from the family Saccharomycetaceae for better resolution of fungal Vps5 proteins, including YKR078W. Furthermore, to identify if other fungi have a protein similar to YKR078W, we used BLASTp to query protein models at FungalDB to identify additional SNX-BAR sorting nexins with similarity to YKR078W from *S. cerevisiae*. These searches only recovered the single Vps5 protein from the fungal species. No additional proteins were detected with an E-value less than 10 (search threshold). Full-length sequences for all taxa for each gene family were aligned with Muscle 3.6 (54) and edited manually in the case of clear errors. Maximum likelihood analyses were conducted with RAxML v.8.2.4 (55) using a LG+G matrix model determined by ProtTest v.3, (56) and a trimmed alignment containing the conserved PX +BAR and SNX-BAR domains. Support for particular nodes for maximum likelihood analyses was assessed with 1,000 bootstraps. Trees were visualized and illustrated with FigTree v1.4 (http://tree.bio.ed.ac.uk/software/figtree/).

Yeast Strains and Culture Conditions

Yeast strains were grown using standard media and conditions (Guthrie and Fink, 1991) unless indicated. Yeast strains were constructed in BY4742 (*MATα his3-1, leu2-0, met15-*

0, and *ura3-0)* by homologous recombination of gene-targeted, polymerase chain reaction (PCR)-generated DNAs using the method of (57) and/or derived from the EUROSCARF KANMX deletion collection (Open Biosystems/Thermo Scientific, Waltham, MA) or produced by replacement of the complete reading frame with the *HIS3MX6* or *URA3* cassette. Gene deletions were confirmed by PCR amplification of the deleted locus. Cells were grown in standard synthetic complete medium lacking nutrients required to maintain selection for auxotrophic markers and/or plasmid, unless indicated otherwise. To induce bulk or non-selective autophagy, cells were grown to log phase, harvested, and transferred to SD(-N) medium for nitrogen starvation (2% dextrose, 0.17% Yeast Nitrogen Base without amino acids and without ammonium sulfate) for 16 hours or resuspended in standard synthetic complete medium containing 0.2 μg/mL of rapamycin (R-5000, LC laboratories) for 2-4hrs at 30°C.

For the construction of an integrated N terminal GFP-Vps501 yeast strain under a GPD promoter, we PCR amplified pGFP-^{GPD}Vps501 (described below) using the following primers that included 50 bp flanking the *VPS501* locus; ATCAGAACTGCAACCCTACAGATTAGATATGGAGAACGACAAGGCGTCACGT GAGCAAGGGCGAGGAGCTGTTCA and GCTTTTTCAGTAGTAAATTATCTTCTTTAATTACGTTATTATGTACATATTTGG CTTATGTGCTCATCTGGTACA. PCR products were subsequently transformed into cells ablated for *VPS501* (by replacement with a URA marker) and allowed to homologously recombine into the *VPS501* locus. Resulting clones were selected on F.O.A 5-Fluoroorotic Acid (5-FOA) and confirmed by PCR.

Light Microscopy and Image Analysis

Yeast cells from cultures grown to $OD_{600} \approx 0.5$ were mounted in growth medium, and 3D image stacks were collected at 0.3-µm z increments on a DeltaVision elite workstation (Cytiva) based on an inverted microscope (IX-70; Olympus) using a 100×1.4NA oil immersion lens. Images were captured at 24°C with a 12-bit charge-coupled device camera (CoolSnap HQ; Photometrics) and deconvolved using the iterative-constrained algorithm and the measured point spread function. To visualize vacuole morphology, yeast cells were labeled with 7-Aminochloromethylcoumarin (CMAC; Life Technologies) at a concentration of 100 µM for 30 min in synthetic medium at room temperature. To visualize the vacuolar membrane, FM4-64 (32nM) was added to cell cultures for 20 min at 30°C. Cells were then washed, resuspended in fresh medium, and then incubated for 60 minutes to allow FM4-64 to accumulate in the vacuolar membrane (58). Image analysis and preparation was done using Softworx 6.5 (Cytiva) and ImageJ v1.50d (Rasband).

Vacuolar membrane localization analyses for GFP-Vps501, Atg27-2XGFP, YPT7-mCherry was determined using a manual method implemented using ImageJ v1.53c (Rasband). A region of interest (ROI) was selected to contain a single cell and the total sum of GFP fluorescence was calculated (TF). Next, we used the Mask macro to delineate the vacuole ROI defined by FM4-64 and overlayed onto the GFP channel to define the vacuole fluorescence (VF). To calculate cytosol fluorescence intensity (CF), the vacuole mask was inverted so that all pixels outside of the mask were assigned a maximum value and the regions corresponding the vacuole signal were assigned a value of zero. A ratio of the VF to TF is presented in the graphs. Vacuolar membrane localization for Seh1-GFP, Sec13-GFP and Atg27-2xGFP, were calculated by calculating the percent of cells with

GFP signal on the vacuole using FM4-64 and CMAC as visual guides to determine vacuole boundaries. To quantify vacuolar lumen localization, wildtype cells or mutants were visually scored for presence of GFP in the vacuolar lumen. Kog1-GFP puncta numbers were quantified from z stacks collected at 0.3-μm intervals. Total patches/cell were counted from maximum intensity projections from small budded cells. A minimum of 100 cells was used in all experimental conditions and performed in biological triplicate.

GFP-Atg8 Processing and Immunoblotting

For quantitative immunoblot analysis of GFP-Atg8, cells were grown under standard vegetative or autophagy inducing conditions to $OD_{600} \approx 0.5$, as described above. Typically, 3.0×10^7 cells were harvested by centrifugation and lysed by glass bead agitation in SDS-PAGE sample buffer. 10% polyacrylamide gels were loaded with 5.0×10^7 cell equivalents and transferred onto standard 0.45 μm nitrocellulose. Anti-GFP primary mouse monoclonal antibody (1814460, Roche) was diluted 1:2500 and Santa Cruz (sc-2055) goat anti-mouse HRP-conjugated antibody was used at 1:10000. Anti-Pgk1 at 1:5000 (Life Technologies) was used as loading controls. Centromeric GFP-Atg8 (59) plasmids were used in the processing assays.

Atg13 immunoblots were done as previously described (60) with the following modifications. 3.0×10^7 cells were harvested by centrifugation and precipitated by Trichloroacetic acid (TCA). 7.5% polyacrylamide gels were loaded with 0.75×10^7 cell equivalents. Anti-HA monoclonal (Invitrogen, 26183) and used at 1:5000 and goat anti-mouse HRP-conjugated antibody was used at 1:5000. p3xHA-Atg13 was purchased from Addgene (Plasmid #59544) and used in all indicated experiments. All enhanced

chemiluminescence *(ECL)* blots were development on a Chemidoc-MP (Bio-Rad) and band intensities were quantified using Quantity One 1D analysis software (Bio-Rad) and all statistical analysis done using GraphPad Prism 8.

Plasmids

pGFP-^{GPD}Vps501 was constructed using Gateway cloning. Plasmid insert was made using PCR amplified wild-type genomic *VPS501* locus with the following primers: GGGGACAAGTTTGTACAAAAAAGCAGGCTTAGAGAACGACAAGGCGTCACA T and GGGGACCACTTTGTACAAGAAAGCTGGGTTTCATTGGCTTATGTGCTCATCTG GT and cloned using a BP recombination reaction into pDONR221. Resulting DONOR vector was recombined with pAG425GPD-EGFP-ccDB (61) in a final LR recombination reaction to generate the pAG415GPD-eGFP-Vps501 expression clone (pGFP-^{GPD}Vps501).

Mass spectrometry

Yeast strains expressing GFP-Vps501 were grown to 0.5 X10^7 cell density in YPD media. GFP fusion proteins were purified as follows: 200mg of whole cell protein extract was incubated with GFP-Trap Magnetic Agarose (ChromoTek) at 4°C for 20 minutes with gentle agitation. GFP-Trap beads were collected and washed five times (50mM Tris-HCL pH 7.4, 150mM NaCl, Roche complete Protease Inhibitor Cocktail EDTA free). After the final wash, the buffer was aspirated and the GFP-Trap beads were incubated with 5x SDS-PAGE sample buffer and denatured for five minutes at 95°C. 20 µL of each sample was analyzed by SDS-PAGE, followed by an immunoblot. The experiment was performed in triplicate and normalized to the Nano-Trap magnetic beads alone.

Trypsin digestion of samples from SDS-PAGE gel plugs

The gel plugs for each sample were excised by a sterile razor blade, divided into 2 sections 1 cm each, and additionally chopped into 1 mm pieces. Each section was washed in distilled H_2O and destained using 100 mM NH_4HCO_3 pH 7.5 in 50% acetonitrile. A reduction step was performed by addition of 100 ml 50mM NH_4HCO_3 pH 7.5 and 10 ml of 200mMtris(2-carboxyethyl) phosphine HCl at 37°C for 30 min. The proteins were alkylated by addition of 100 ml of 50 mM iodoacetamide prepared fresh in 50 mM NH_4HCO_3 pH 7.5 buffer and allowed to react in the dark at 20°C for 30 min. Gel sections were washed in water, then acetonitrile, and vacuum dried. Trypsin digestion was carried out overnight at 37°C with 1:50-1:100 enzyme-protein ratio of sequencing grade-modified trypsin (Promega) in 50 mM NH_4HCO_3 pH 7.5, and 20mM $CaCl_2$. Peptides were extracted with 5% formic acid and vacuum dried and sent to the Mayo Clinic Proteomics Core facility for HPLC and LC-MS/MS data acquisition.

HPLC for mass spectrometry

All samples were re-suspended in Burdick & Jackson HPLC-grade water containing 0.2% formic acid (Fluka), 0.1% TFA (Pierce), and 0.002% Zwittergent 3-16 (Calbiochem), a sulfobetaine detergent that contributes the following distinct peaks at the end of chromatograms: MH^+ at 392, and in-source dimer (2 M+ H^+) at 783, and some minor impurities of Zwittergent 3-12 seen as MH^+ at 336. The peptide samples were loaded to a 0.25 ml C8 OptiPak trapping cartridge custom-packed with Michrom Magic (Optimize Technologies) C8, washed, then switched in-line with a 20 cm by 75 mmC18 packed spray

tip nano column packed with Michrom Magic C18AQ, for a 2-step gradient. Mobile phase A was water/acetonitrile/formic acid (98/2/0.2) and mobile phase B was acetonitrile/isopropanol/water/formic acid (80/10/10/0.2). Using a flow rate of 350 nL/min, a 90 min, 2-step LC gradient was run from 5% B to 50% B in 60 min, followed by 50%-95% B over the next 10 min, hold 10 min at 95% B, back to starting conditions and re-equilibrated.

LC-MS/MS analysis

Electrospray tandem mass spectrometry (LC-MS/MS) was performed at the Mayo Clinic Proteomics Core on a Thermo Q-Exactive Orbitrap mass spectrometer, using a 70,000 RP survey scan in profile mode, m/z 340-2000 Da, with lock masses, followed by 20 MSMS HCD fragmentation scans at 17,500 resolution on doubly and triply charged precursors. Single charged ions were excluded, and ions selected for MS/MS were placed on an exclusion list for 60 s.

LC-MS/MS data analysis, statistical analysis

All LC-MS/MS *.raw Data files were analyzed with MaxQuant version 1.5.2.8, searching against the SPROT *Saccharomyces cerevisiae* database downloaded 09.28.2017 and searched using the following criteria: LFQ quantification with a min of 1 high confidence peptide. Trypsin was selected as the protease with max miss cleavage set to 2. Carbamidomethyl (C) was selected as a fixed modification. Variable modifications were set to Deamidation (NQ), Oxidization (M), Formylation (n-term), and Phosphorylation (STY). Orbitrap mass spectrometer was selected using a MS error of 20 ppm and a MS/MS error of 0.5 Da. A 1% FDR cutoff was selected for peptide, protein, and site identifications.

LFQ Intensities were reported based on the MS level peak areas determined by MaxQuant and reported in the proteinGroups.txt file. Proteins were removed from the results file if they were flagged by MaxQuant as “Contaminants”, “Reverse” or “Only identified by site”. Complete three biological replicates were performed. The abundance data from each biological replicate were normalized to the ratio of Vps501 bait protein in that biological replicate. LFQ Peak intensities were analyzed in each run to determine protein hits that fell into the category of either Vps501 elution (VE) only hits or Bead elution (BE) only hits and retained if they confirmed to VE state across all 3 runs. LFQ Sig cutoffs are Sig Up > 1.2 ratio (Log2 0.26) and Sig Down < 0.8 ratio (Log2 -0.32). Any hits that were not observed in at least 2 replicates each were labeled ‘no quant’ (a normalized ratio was still calculated but not included in final data set analysis). A list of proteins identified and corresponding ratios can be found in the Appendix. The mass spectrometry proteomic data have been deposited to the ProteomeXchange Consortium (http://proteomecentral.proteomexchange.org) (62) via the PRIDE partner repository (63, 64).

3.3 Results

YKR078W/VPS501 and VPS5 are phylogenetically related but functionally distinct

Phylogenetic analysis of the SNX-BAR sorting nexins allowed us to identify ORF YKR078W from *Saccharomyces cerevisiae* as a SNX-BAR candidate that forms a well-supported clade (bootstrap = 99) with Vps5 proteins from *S. cerevisiae* and other closely related species from the family Saccharomycetaceae (Figure 1A, Figure 1). As previously shown by Koumandou et al. (2011), fungal Vps5 proteins are most closely related to SNX1/2 proteins from animals and choanoflagellates (32). The simplest explanation for the existence of two Vps5-like proteins in *S. cerevisiae* is a recent gene duplication event. To assess whether or not there is functional overlap between the Vps5 and YKR078W proteins, we used *YKR078W*Δ yeast cells to examine the localization of the vacuolar hydrolase receptor Vps10. This receptor is trafficked from the prevacuolar endosome to Golgi by the Vps5-dependent retromer-SNX-BAR complex and is mistrafficked to the vacuole in *vps5*Δ cells (33-35). We hypothesized that, if there is functional overlap between the Vps5 and YKR078W proteins, Vps10 mislocalization in *YKR078W*Δ would phenocopy the *vps5*Δ mutant. However, deletion of YKR078W did not affect Vps10 localization (Figure 1B), indicating that while Vps5 and YKR078W are phylogenetically related, they are functionally different. In light of these findings, we gave YKR078W the distinct, but Vps5-related name of Vps501. We will use the Vps501 annotation throughout the remainder of this paper.

N-terminally tagged Vps501 localizes to the vacuolar membrane

While Vps501 shares common evolutionary ancestors and lineage with Vps5, its function within the cell has so far remained uncharacterized. Multiple genome-wide localization screens using C-terminally fused GFP failed to detect expression and/or failed to localize Vps501 to any intracellular compartment (36). Interestingly, we have discovered that Vps501 appears to be nonfunctional as a C-terminal GFP fusion (data not shown). However, a fully integrated N-terminal GFP fusion appeared to preserve the functionality and localization of Vps501. Instead of an endosomal localization, which might be expected based on its homology to Vps5, we detect the protein predominantly on the limiting membrane of the vacuole, and in a few intracellular puncta (Figure 1C, upper panels). This localization pattern remains consistent when Vps501 is chromosomally tagged under the control of either its endogenous promoter (Figure 1C, upper panels) or a constitutive TDH3/GPD promoter (Figure 1C, lower panels), and when expressed from an extrachromosomal plasmid (Figure 1C, middle, panels).

Identification of Vps501 physical and genetic interactions

To gain insights into Vps501 function, we used a co-immunoprecipitation mass spectrometry approach to identify its interactors. We purified GFP-Vps501 complexes and characterized the Vps501 interactome using mass spectrometry (Figure 3A). The list of Vps501 interacting proteins was enriched for proteins involved in amino acid/carbohydrate metabolism, protein translation, protein folding, and endocytosis (Appendix Table 1). Our analysis of strong interactors of Vps501 identified subunits of the evolutionarily conserved eight-protein SEA complex (Sea1, Seh1) and the TORC1 subunit Kog1, each of which

resides on the vacuolar membrane and is linked with autophagy through TORC1 signaling regulation (Figure 3B). Moreover, we found that Vps501 and its vacuolar interactors identified through mass spectrometry (Sea1, Seh1 and Kog1), colocalize at the vacuolar membrane (Figure 3C).

We next performed a series of genetic and functional studies to interrogate the potential link between the *VPS501* gene and TORC1 signaling and to determine whether it is epistatic to any of the genes encoding the subunits of the SEA complex. Nitrogen starvation or rapamycin inhibits TORC1 triggering autophagy induction, and we initially used fluorescence microscopy to assess localization of the canonical autophagy marker GFP-Atg8 in strains deleted for *VPS501* singly or in combination with different SEA complex subunits upon the induction of autophagy (Figure 4A). GFP-Atg8 processing was also monitored by immunoblotting to detect increases in both total GFP-Atg8 signal and ratio of free GFP to total GFP signal over time (Figure 4B, C). Collectively, these assays allowed us to evaluate whether deletion of *VPS501* results in autophagic flux defects or exacerbates those caused by SEA complex mutants. We found that cells lacking *VPS501* display no defects in starvation-induced or rapamycin-induced autophagy, unless combined with deletions of SEACIT subunits. Interestingly, both fluorescence microscopy and immunoblot analysis of *sea1*Δ*vps501*Δ cells showed a striking loss of autophagic flux in GFP-Atg8, indicating that Vps501 and the SEA complex work synergistically during autophagy (Figure 4). Other groups have reported kinetic delays in autophagic flux following deletion of *SEA1*, either alone or in combination with deletion of other SEA complex subunits (28). We found that combined loss of *VPS501* and *SEA1* severely impairs autophagy, nearly approximating the complete loss observed in the *atg1*Δ control. It is also

worth noting that, as reported in previous studies, *NPR2* and *NPR3* deletions cause significant defects in both bulk and specific forms of autophagy, likely masking any synthetic defect present in *vps501*Δ mutant cells (37). *VPS501* deletion in combination with each of the SEACAT subunits resulted in only a partial reduction in autophagic flux as evidenced by GFP-Atg8 processing defects, with the most significant defect occurring in *seh1*Δ*vps501*Δ cells (Figure 5).

Vps501-Sea1 interaction stabilizes the SEA Complex

Given the strong autophagic defects associated with the combined loss of *Vps501* and the SEA complex, we set out to examine the role of Vps501 in the maintaining the SEA complex to the vacuolar membrane. Again, we found a clear cooperative role for Vps501 and Sea1 to maintain the SEA complex to the vacuolar membrane. Among the SEA complex, we found that the SEACIT subunits Npr2 and Npr3 were dramatically mislocalized to the vacuolar lumen (VL) in 85% of *vps501*Δ*sea1*Δ cells compared to 15-40% when Sea1 or Vps501 is ablated alone (Figure 7 A-B). While the SEACAT subunits Sea2, Sea3, Sea4 were also mislocalized to the VL in 100% of *vps501*Δ*sea1*Δ cells, this defect was masked by the 80-90% mislocalization observed in the *sea1*Δ single mutant (Figure 8). The remaining SEACAT subunits Seh1 and Sec13 were significantly mislocalized from the vacuolar membrane to non-vacuolar compartments in both *sea1*Δ and *vps501*Δ*sea1*Δ cells but were not found in the vacuole lumen. Seh1 and Sec13 have previously reported roles in the nucleus and ER, respectively, and likely become enriched at these locations when vacuolar membrane localization is compromised (Figure 8) (38). The enhancement of the phenotype observed in the *vps501*Δ*sea1*Δ cells suggests Sea1 and Vps501 have parallel or partially redundant roles to stabilize the localization of the SEA

complex to the vacuolar membrane and in particular the Npr2, Npr3 SEACIT subunits. These results suggested Vps501 is possibly a part of a larger mechanism that regulates TORC1 signaling.

The TORC1 complex and induction of autophagy are defective in vps501Δsea1Δ cells

While other sorting nexins have previously been found to contribute to autophagy indirectly by mobilizing lipid membranes for autophagosome biogenesis or potentiating vacuolar fusion, the role of Vps501 in autophagy appears to be more direct (10, 39-41). The clear physical and genetic interactions of Vps501 with the SEA complex indicate a potential role in regulating TORC1 signaling, possibly during the induction of autophagy. To test this hypothesis, we targeted subunits of TORC1 to determine whether they were defective in v*ps501Δsea1Δ* cells. We were particularly interested in the Kog1 subunit, as it was one of our most abundant hits in the proteomics screen for Vps501 interactors (Figure 3). Like what others have found, we localized Kog1-2XGFP to two independent TORC1 pools; one around the vacuolar membrane and a second in dot-like perivacuolar structures (Figure 9A) (42, 43). This dual localization is consistently present in wildtype, *vps501Δor sea1Δ* cells. Interestingly, the dot-like perivacuolar structures exhibit enhanced accumulation in *vps501Δsea1Δ* cells, with the average number of Kog1-2XGFP dots enriched 2-fold relative to the wildtype or single mutant controls. The vacuolar Kog1-2XGFP pool appears be reduced, either in the presence or absence of nitrogen (Figure 9A-B). Recently, these dot-like TORC1 structures have been referred to as signaling endosomes and have been shown to have unique phosphorylation targets (42, 43).

One such target is Atg13, a regulatory subunit of the Atg1 signaling complex that is required for induction of autophagy (44). When TORC1 is active, Atg13 is phosphorylated,

inhibiting induction of autophagy. Therefore, we hypothesized that Atg13 phosphorylation would be defective in *vps501*Δ*sea1*Δ cells if autophagy induction were impaired. We analyzed Atg13 phosphorylation by immunoblotting in wildtype and mutant cells, both before and after nitrogen starvation or with rapamycin treatment, and quantified the resulting signals. In wildtype, *vps501*Δ*or sea1*Δ cells, Atg13 is clearly phosphorylated as indicated by a smear of the Atg13 band during vegetative growth, demonstrating that TORC1 is active (Figure 9C-D). Likewise, during autophagy-inducing conditions TORC1 is inactive, and the Atg13 band collapses in wildtype, *vps501*Δ*or sea1*Δ cells indicating that the majority of Atg13 is not phosphorylated (Figure 9C-D). Interestingly, while nitrogen starvation and rapamycin treatment both trigger TORC1 inactivation, they do so by different mechanisms. Under starvation conditions, low amino acid levels are communicated to TORC1 via the Gtr1/Gtr2 complex, part of a highly conserved family of Rag GTPases, which assembles as heterodimeric complexes on vacuolar membranes and are regulated by their guanine nucleotide loading status to active TORC1 via the SEA Complex (45). However, rapamycin acts by binding rapamycin binding protein, Fpr1 in yeast and the Fpr1-rapamycin complex directly binds to TORC1 to inactivate it, thereby bypassing any SEA complex inhibition (46) (47). Surprisingly, Atg13 remained phosphorylated in *vps501*Δ*sea1*Δ cells, regardless of nitrogen starvation or rapamycin treatment, indicating autophagy induction is defective in these mutants, (Figure 9C-D). Moreover, this suggests the vacuolar pool of TORC1 is not accessible to the Fpr1-rapamycin inhibition in *vps501*Δ*sea1*Δ cells, likely resulting in a broad TORC1 signaling defect independent of autophagy induction.

To test this hypothesis, we visualized two additional vacuolar membrane proteins to determine if their distribution is also affected in *vps501*Δ*or sea1*Δ cells. Atg27 is an autophagy-related transmembrane protein and was chosen for investigation as a potential mechanistic link because of its characterized vacuolar-endosomal trafficking itinerary (48). In wild-type cells, Atg27-2XGFP cycles between the vacuolar membrane, Golgi/endosome and autophagic compartments. In *vps501*Δ*sea1*Δ cells, we found that Atg27-2XGFP is significantly depleted from the vacuolar membrane, indicating TORC1 signaling maybe responsible for maintaining Atg27 at the vacuolar membrane (Figure 10). To assess non-autophagy related TORC1 pathway integrity, we also imaged Ypt7 in the mutant backgrounds of interest. Ypt7 is a Rab family GTPase that is required for endosome-endosome fusion and localizes the vacuolar membrane (49). Ypt7-mCherry was also notably depleted from the vacuolar membrane when Vps501 and Sea1 are ablated singly or together, suggesting aberrant TORC1 hyperactivity is also affecting Ypt7-dependent cellular pathways (Figure 10). However, it is not yet clear whether this mechanism is mediated by a direct or indirect interaction with Vps501 and the SEA complex or is an overall consequence of a broad TORC1 misregulation.

3.5 Discussion

In this study, we report the identification of a novel vacuolar membrane SNX-BAR protein, Vps501. While phylogenetically, Vps501 is most related to Vps5, an essential component of the yeast retromer complex, protein sequence analysis shows residue variations acquired during its divergence (Figure 1, Figure 2). In this study, we demonstrate how divergence from Vps501 and Vps5 has resulted in unique functional differences. Vps501 exclusively resides on the vacuolar membrane, a unique feature amongst the SNX-BAR protein family. We speculate Vps501 likely possesses lipid specificity beyond PI3P as was discovered in other sorting nexins (50). Future studies will help us understand the novel ways in which Vps501 recognizes vacuolar lipids and how this recognition influences its function and regulation.

Multiple lines of evidence support a role for Vps501 in TORC1 signaling during autophagy induction. Firstly, using a co-immunoprecipitation mass spectrometry approach, we identified subunits of the evolutionary conserved SEA complex (Sea1, Seh1) and TORC1 subunit Kog1 (Figure 3). Each of these identified proteins resides on the vacuolar membrane and colocalizes with Vps501. It is also worth noting that the previous studies in which mass spectrometry-based proteomics were used to discover the eight components of the SEA complex all utilized an individual band excision-based proteomic approach focusing on the most enriched bands (37). This design excluded low abundant or low affinity interactions and may account for why Vps501 was not detected in their screens.

Secondly, we found that Vps501 works together with the SEA complex to mediate GFP-Atg8 autophagic flux. We found that cells lacking Vps501 display a severe deficiency in autophagy only when SEA complex subunits were deleted in combination (Figure 4, Figure

5). A recent study came to similar conclusions, showing that loss of Sea2, Sea3 or Sea4 did not trigger major defects unless combined with *sea1*Δ (28, 37, 38). This led us to believe that Vps501 and the SEA complex cooperate within a synergistic pathway during autophagy induction.

Lastly, we have defined the role of Vps501 as a co-regulator of autophagy that promotes SEACIT inhibition of TORC1 during autophagy induction. We found the SEACIT subunits Npr2 and Npr3 are severely destabilized in *vps501*Δ*sea1*Δ cells. Npr2, Npr3, and Sea1 act as a GTPase-activating complex to Gtr1 and Gtr2 which in turn mediates TORC1 activation at the vacuolar membrane (45). Previous studies have demonstrated that deletion of Sea1 alone resulted in partial mislocalization of Npr2 and Npr3, which causes hyperactivation of TORC1 (29, 51). In our experiments, Npr2 and Npr3 are severely (>90%) destabilized in *vps501*Δ*sea1*Δ cells, more so than any single deletion alone (Figure 7). Therefore, Gtr1 and Gtr2 are unable to regulate their guanine nucleotide loading and TORC1 remains hyperactive in *vps501*Δ*sea1*Δ cells. Recently, it has also been documented that TORC1 initiates microautophagy which downregulates vacuole surface proteins (20-22). We investigated the possibility of this phenomenon by looking at two other vacuolar membrane proteins Atg27 and Ypt7 and indeed found both are destabilized from the vacuolar membrane in *vps501*Δ*sea1*Δ cells (Figure 10). This result suggested a TORC1 signaling defect beyond autophagy may also be present, which led us to hypothesize a broad TORC1 hyperactivation may be causing these phenotypes.

The yeast Rag GTPase-TORC1 complex is found in two spatially and functionally distinct pools, on both the vacuolar and endosomal membranes (42, 43). Vacuolar TORC1 promotes protein synthesis through its proximal effector Sch9, while endosomal TORC1

controls autophagy induction through phosphorylation of Atg13, preventing Atg1 complex formation at the pre-autophagosomal structure. Interestingly, *vps501*Δ*sea1*Δ cells show depletion of the Kog1-2XGFP subunit of TORC1 from the vacuolar membrane and enrichment in dot-like structures by nearly 2-fold (Figure 9). Likewise, the endosome-specific TORC1 substrate Atg13 is hyperphosphorylated in *vps501*Δ*sea1*Δ cells (Figure 9). In addition, the autophagy defects observed in *vps501*Δ*sea1*Δcells could not be bypassed by rapamycin treatment (Figure 6, Figure 9). This was surprising, given rapamycin is a potent lipophilic macrolide antifungal drug that blocks TORC1 signaling via a direct TOR1 inhibition that is independent of SEA complex regulation (52, 53). This result, combined with Kog1 mislocalization (Figure 9A, B), suggests an unregulated pool of TORC1 is causing broad TORC1 signaling dysfunction and likely the underlying defect in *vps501*Δ*sea1*Δ cells.

3.6 Figures

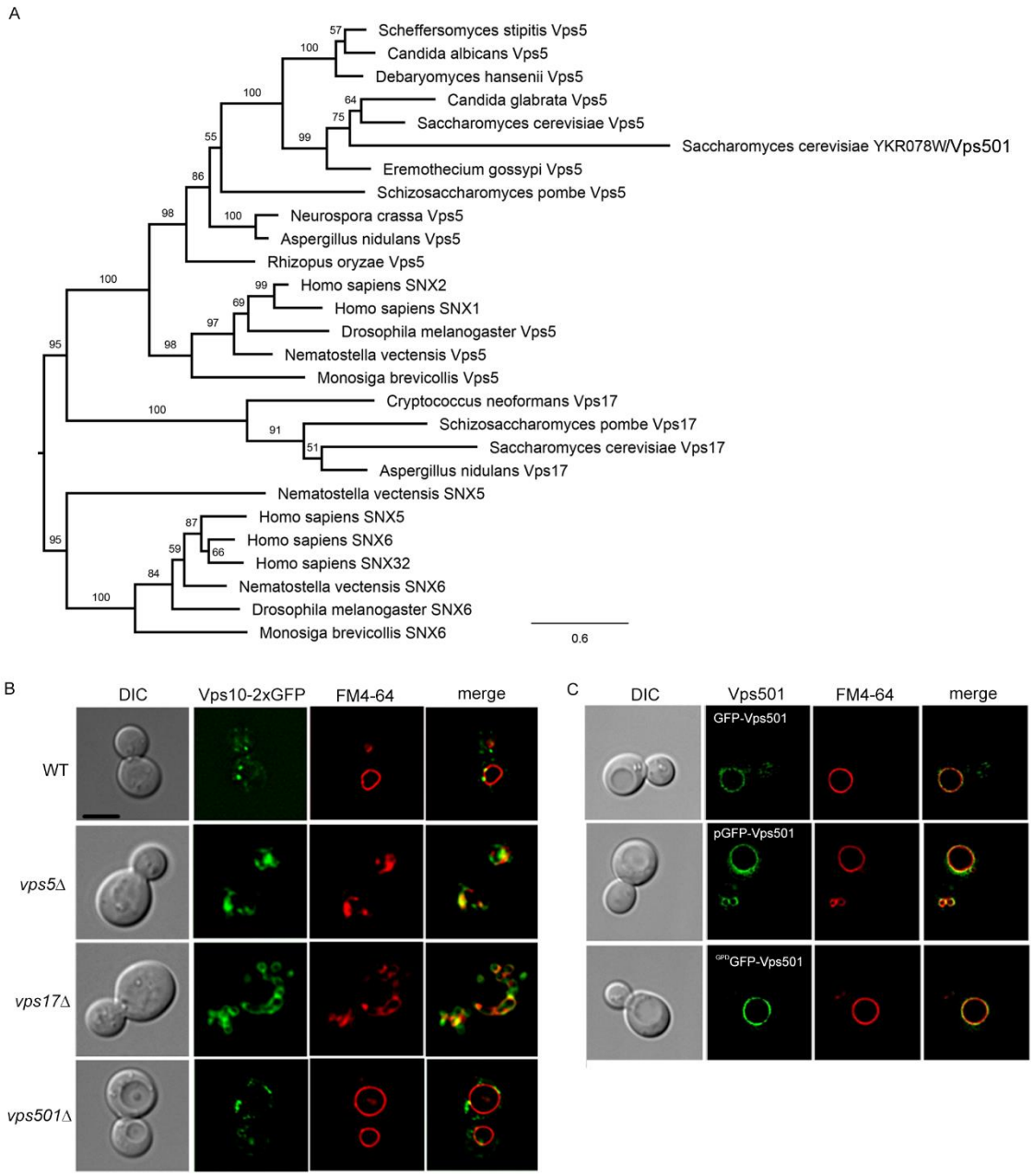

Figure 7. YKR078W/Vps501 is a paralog of Vps5 and resides on the vacuolar membrane. (A) Phylogenetic analysis of Vps5-like SNX-BAR proteins in selected animals, choanoflagellate, and fungi, including other species in the family Saccharomycetaceae indicates the presence of a Vps5-like protein (YKR078W) in *Saccharomyces cerevisiae*, referred to here as Vps501. (B) Micrographs of Vps10-2XGFP in wildtype and indicated mutant cells. Vps501 does not have a role in Vps10 trafficking, despite the phylogenetic

similarities with retromer SNX-BARs. (C) Vps501 localizes to the vacuolar membrane as a N-terminal GFP fusion protein. GFP-Vps501 expression is shown as locus integrations using native promoter (top), GPD promoter (bottom) or ectopically expressed as a 2-micron plasmid (middle). C-terminal fusions were found to be non-functional, not shown. Vacuolar membranes are shown using FM4-64 dye. The scale bar indicates 5 μm.

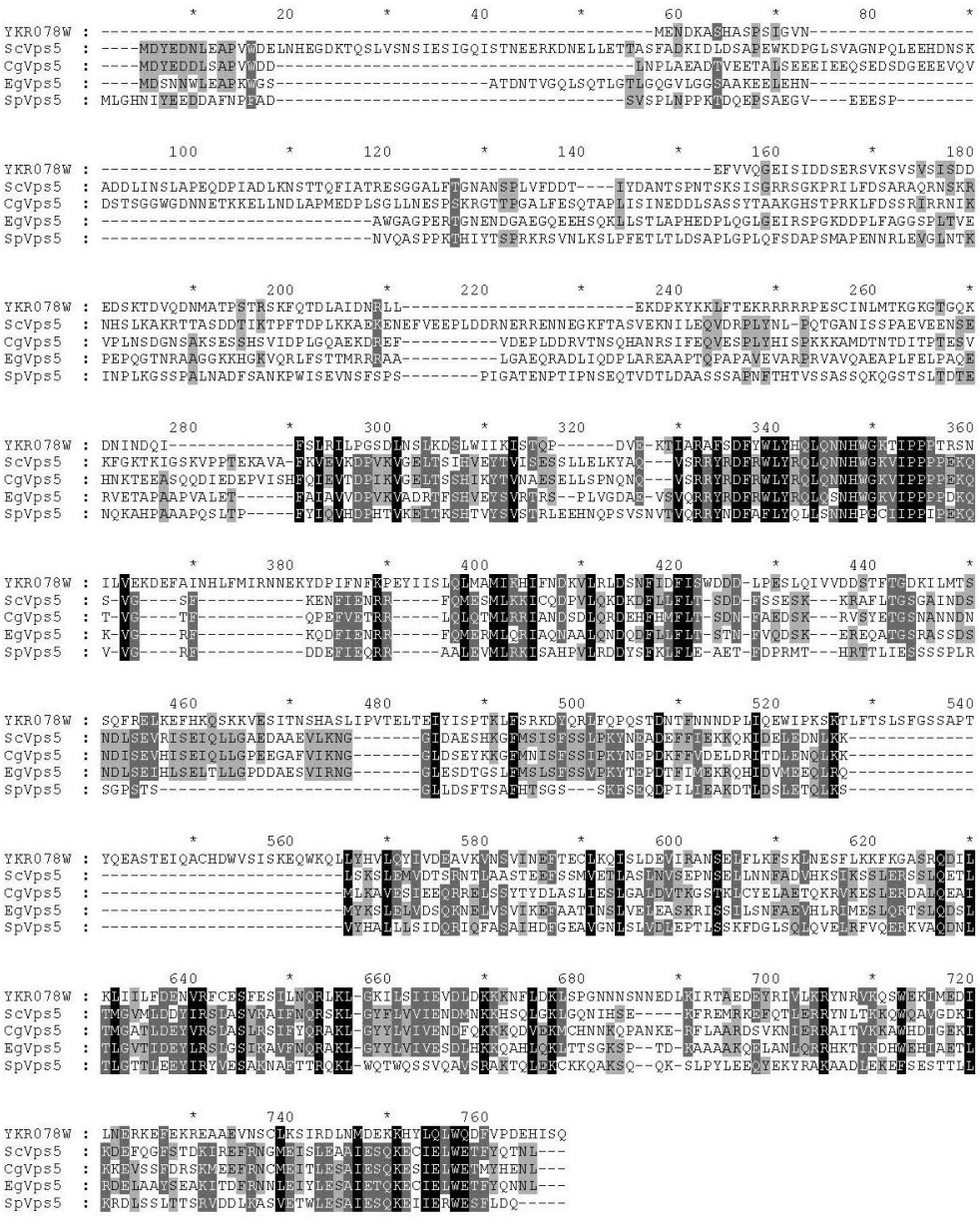

Figure 8. Sequence alignment of YKR078W/VPS501 to Vps5 proteins from other yeast taxa. Full-length sequences for all taxa for each gene family were aligned with Muscle 3.6 (54) and edited manually in the case of clear errors. Maximum likelihood analyses were conducted with RAxML v.8.2.4 (55) using a LG+G matrix model determined by ProtTest v.3 (56) and a trimmed alignment containing the conserved PX-BAR domains. Sc, *S. cerevisiae*, Cg, *C. glabrata*, Eg, *E. gossypi*, Sp, *S. pombe*.

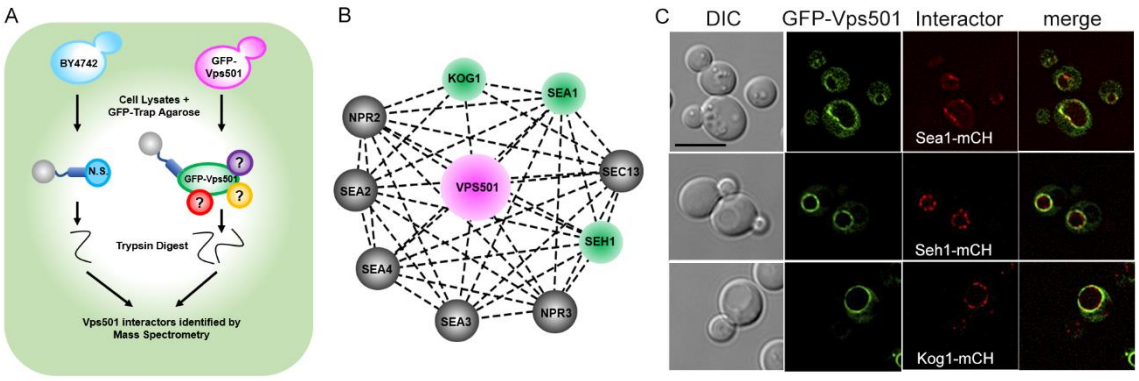

Figure 9. Vps501 interacts with subunits of TORC1 and the SEA complex. (A) Mass spectrometry experimental design to identify Vps501 interactors. GFP-Vps501 and interactors were purified by GFP-Trap affinity purification and SDS-PAGE, followed by in-gel trypsin digestion. Resulting peptides were analyzed and identified by LC–MS/MS according to their relative enrichment. (B) Mass spectrometry analysis using STRING software identified strong interactions with Kog1, a subunit of the TORC1 complex and Sea1 and Seh1, subunits of the SEA complex. Subunits of the SEA complex and TORC1 are represented as nodes in the graphical network. Proteins colored in green (Sea1, Seh1 and Kog1) are those detected by this proteomic study. Lines connecting the nodes represent previously reported interactions. (C) Micrographs show GFP-Vps501 colocalizes with Sea1-mCherry, Kog1-mCherry, Seh1-mCherry at the vacuolar membrane. The scale bar indicates 5 µm.

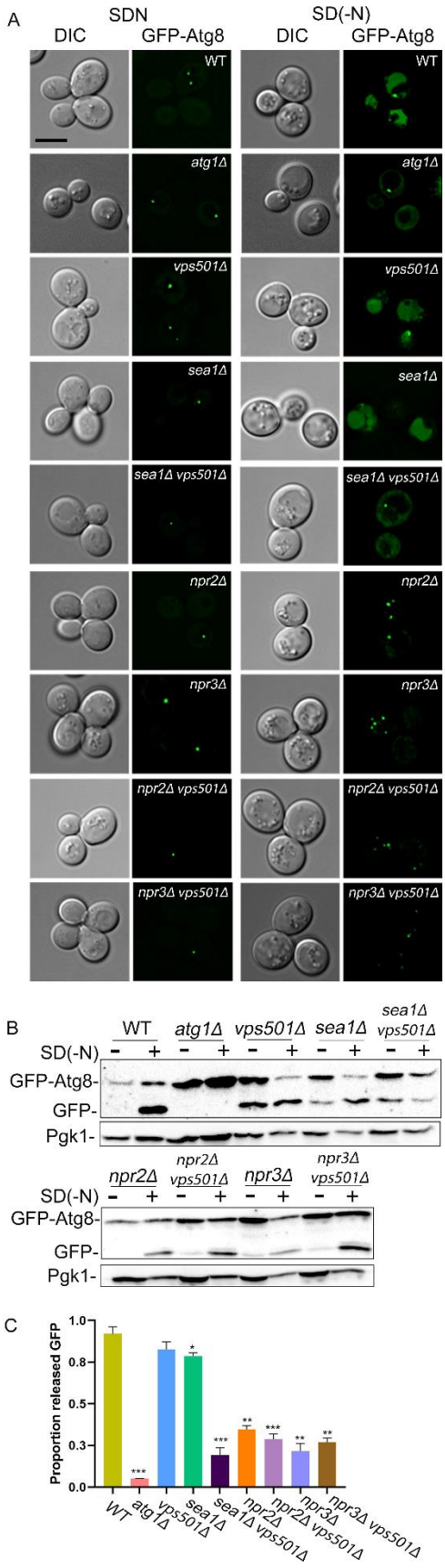
A
SDN
SD(-N)
DIC
GFP-Atg8
DIC
GFP-Atg8
WT
atg1Δ
vps501Δ
sea1Δ
sea1Δ vps501Δ
npr2Δ
npr3Δ
npr2Δ vps501Δ
npr3Δ vps501Δ
B
WT
atg1Δ
vps501Δ
sea1Δ
sea1Δ vps501Δ
SD(-N)
GFP-Atg8-
GFP-
Pgk1-
npr2Δ
npr2Δ vps501Δ
npr3Δ
npr3Δ vps501Δ
C
Proportion released GFP
1.0
0.8
0.5
0.3
0.0
WT
atg1Δ
vps501Δ
sea1Δ
sea1Δ vps501Δ
npr2Δ
npr2Δ vps501Δ
npr3Δ
npr3Δ vps501Δ

Figure 10. *vps501*Δ*sea1*Δ cells display a synthetic autophagy defect. (A) Maximum projection micrographs of cells expressing GFP-Atg8 in wildtype and indicated mutant cells before and after nitrogen starvation. GFP-Atg8 is found in the vacuole lumen (VL) in wildtype cells after nitrogen starvation, indicating successful autophagic flux has occurred. In *atg1*Δ cells, autophagy induction is inhibited and GFP-Atg8 is absent in the VL. A similar phenotype is also seen only when cells are ablated for both Vps501 and Sea1, indicating a synthetic genetic interaction between Vps501 and Sea1 is critical for autophagy. Note, cells ablated for Npr2 and Npr3 also show major autophagy defects as single knockouts and likely mask any synthetic phenotypes combined with Vps501 ablation. The scale bar indicates 5μm. (B) Quantitative immunoblotting was used to detect the amount of GFP-Atg8 flux before and after autophagy induction. There is a 3-fold decrease in GFP-Atg8 flux in *vps501*Δ*sea1*Δ cells, compared to single deletions, whereas there was no significant difference detected in Npr2 or Npr3 knockout cells. A representative immunoblot is shown. Anti-Pgk1 was used as a loading control. (C) Graph of quantification of GFP-Atg8 processing. The results are from three experiments and averaged using the standard error of the mean. Indicated significance is a comparison of wildtype to single deletions or double mutants. *$p<0.05$, ** $p<0.01$, ***$p<0.001$ indicates significance as calculated by Student's t-test.

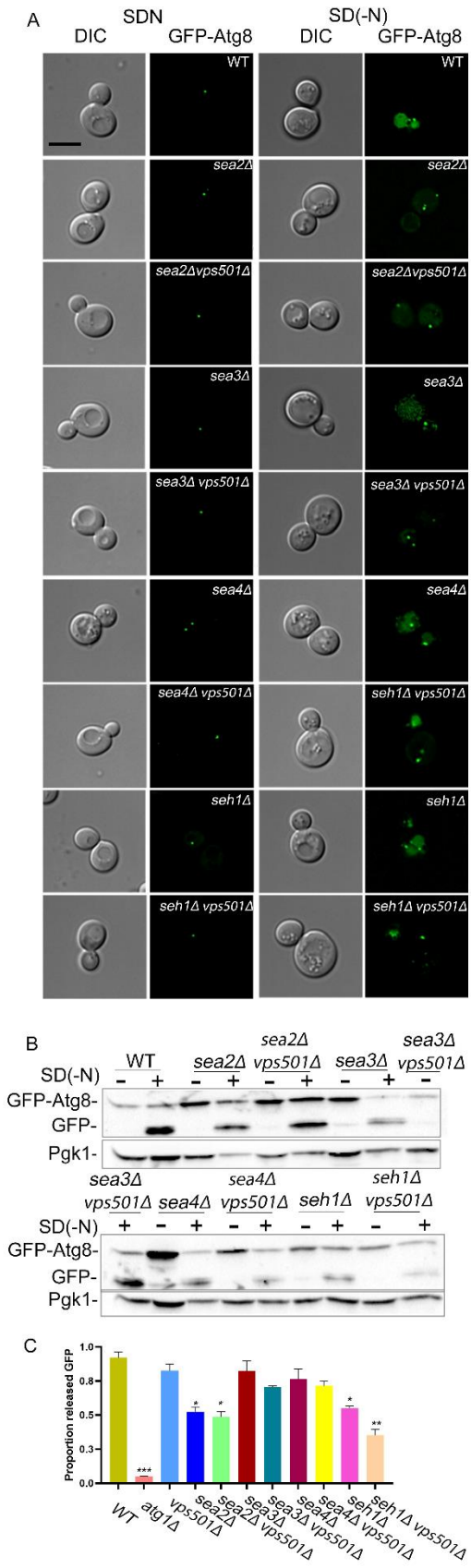
A
SDN
SD(-N)
DIC
GFP-Atg8
DIC
GFP-Atg8
WT
sea2Δ
sea2Δvps501Δ
sea3Δ
sea3Δ vps501Δ
sea4Δ
sea4Δ vps501Δ
seh1Δ
seh1Δ vps501Δ
B
WT
sea2Δ
sea2Δ vps501Δ
sea3Δ
sea3Δ vps501Δ
SD(-N)
GFP-Atg8-
GFP-
Pgk1-
sea3Δ vps501Δ
sea4Δ
sea4Δ vps501Δ
seh1Δ
seh1Δ vps501Δ
C
Proportion released GFP
1.0
0.8
0.5
0.3
0.0
WT
atg1Δ
vps501Δ
sea2Δ
sea2Δ vps501Δ
sea3Δ
sea3Δ vps501Δ
sea4Δ
sea4Δ vps501Δ
seh1Δ
seh1Δ vps501Δ

Figure 11. Vps501 interactions with the SEACAT complex during autophagy. (A) Maximum projection micrographs of cells expressing GFP-Atg8 in wildtype and indicated mutant cells before and after nitrogen starvation. The scale bar indicates 5μm. (B) Quantitative immunoblotting was used to assess GFP-Atg8 flux before and after autophagy induction. A partial reduction in GFP-Atg8 flux is seen when Vps501 is ablated in combination with each of the SEACAT subunits with the most significant defect occurring in *seh1*Δ*vps501*Δ cells. A representative immunoblot is shown. Anti-Pgk1 was used as a loading control. (C) Graph of quantification of GFP-Atg8 processing. The results are from three experiments and averaged using the standard error of the mean. Indicated significance is a comparison of wildtype to single deletions or double mutants. *$p<0.05$, ** $p<0.01$, ***$p<0.001$ indicates significance as calculated by Student's t-test.

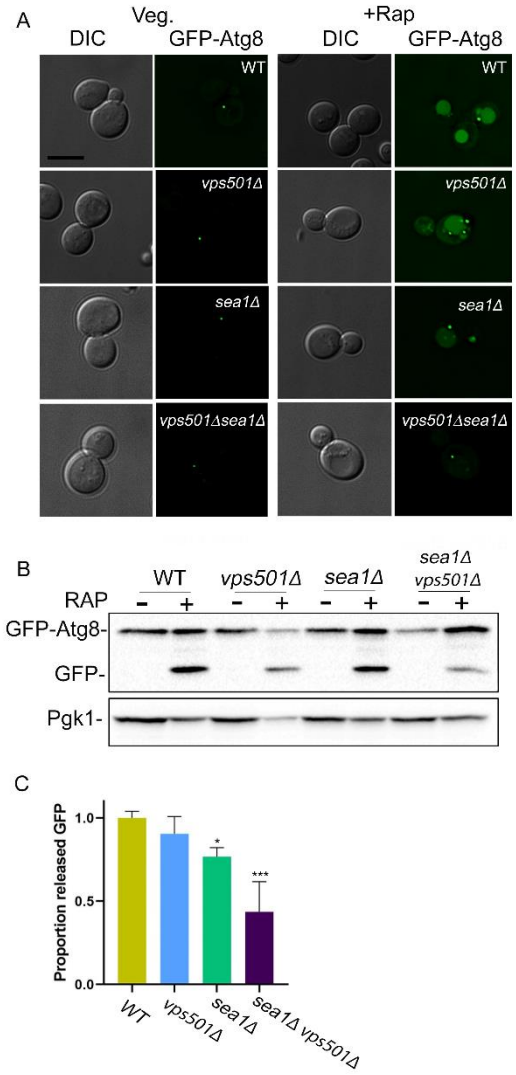

Figure 12. Autophagy influx is defective in *vps501Δsea1Δ* cells during rapamycin treatment. (A) Maximum projection micrographs of cells expressing GFP-Atg8 in wildtype and indicated mutant cells before and after rapamycin treatment. The scale bar indicates 5µm. (B) Quantitative immunoblotting was used to assess GFP-Atg8 flux before and after autophagy induction by rapamycin. A significant reduction in GFP-Atg8 flux is seen when Vps501 is ablated in combination with Sea1. A representative immunoblot is shown. Anti-Pgk1 was used as a loading control. (C) Graph of quantification of GFP-Atg8 processing. The results are from three experiments and averaged using the standard error of the mean. Indicated significance is a comparison of wildtype to single deletions or double mutants. *p<0.05, ** p<0.01, ***p<0.001 indicates significance as calculated by Student's t-test.

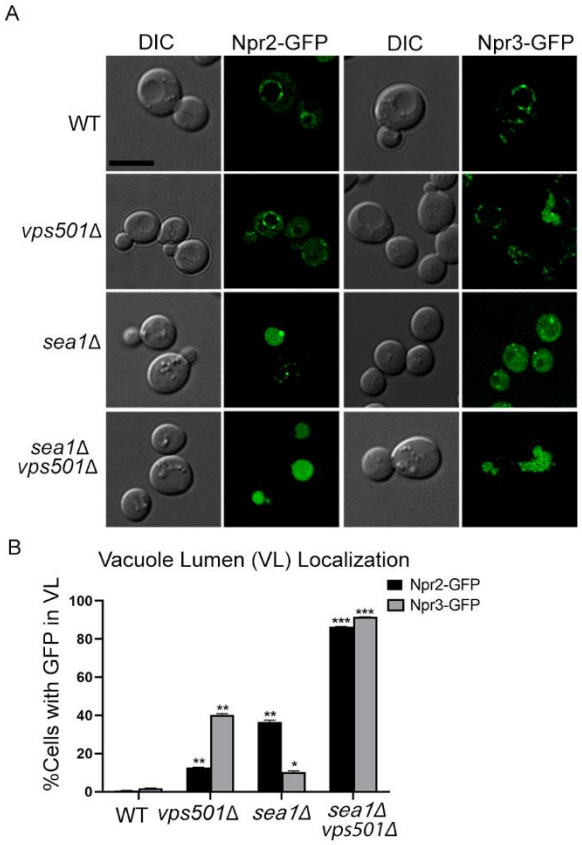

Figure 13 SEACIT subunits, Npr2 and Npr3 require Vps501 and Sea1 for vacuolar localization. (A) Npr2-GFP and Npr3-GFP localize to the vacuolar membrane in wildtype cells. In *vps501*Δ or *sea1*Δ cells, Npr2-GFP and Npr3-GFP are mislocalized to the vacuole lumen (VL) in 10-40% of cells. In *vps501*Δ*sea1*Δ cells, Npr2-GFP and Npr3-GFP are mislocalized to the VL in 85% of cells. (B) Graph represents vacuole lumen localization (VL) in wildtype cells or mutants, defined by visually scoring the presence of GFP in the vacuole lumen. The results are from three experiments and averaged using the standard error of the mean. Indicated significance is a comparison of wildtype to single deletions or double mutants. *p<0.05, ** p<0.01, ***p<0.001 indicates significance as calculated by Student's t-test.

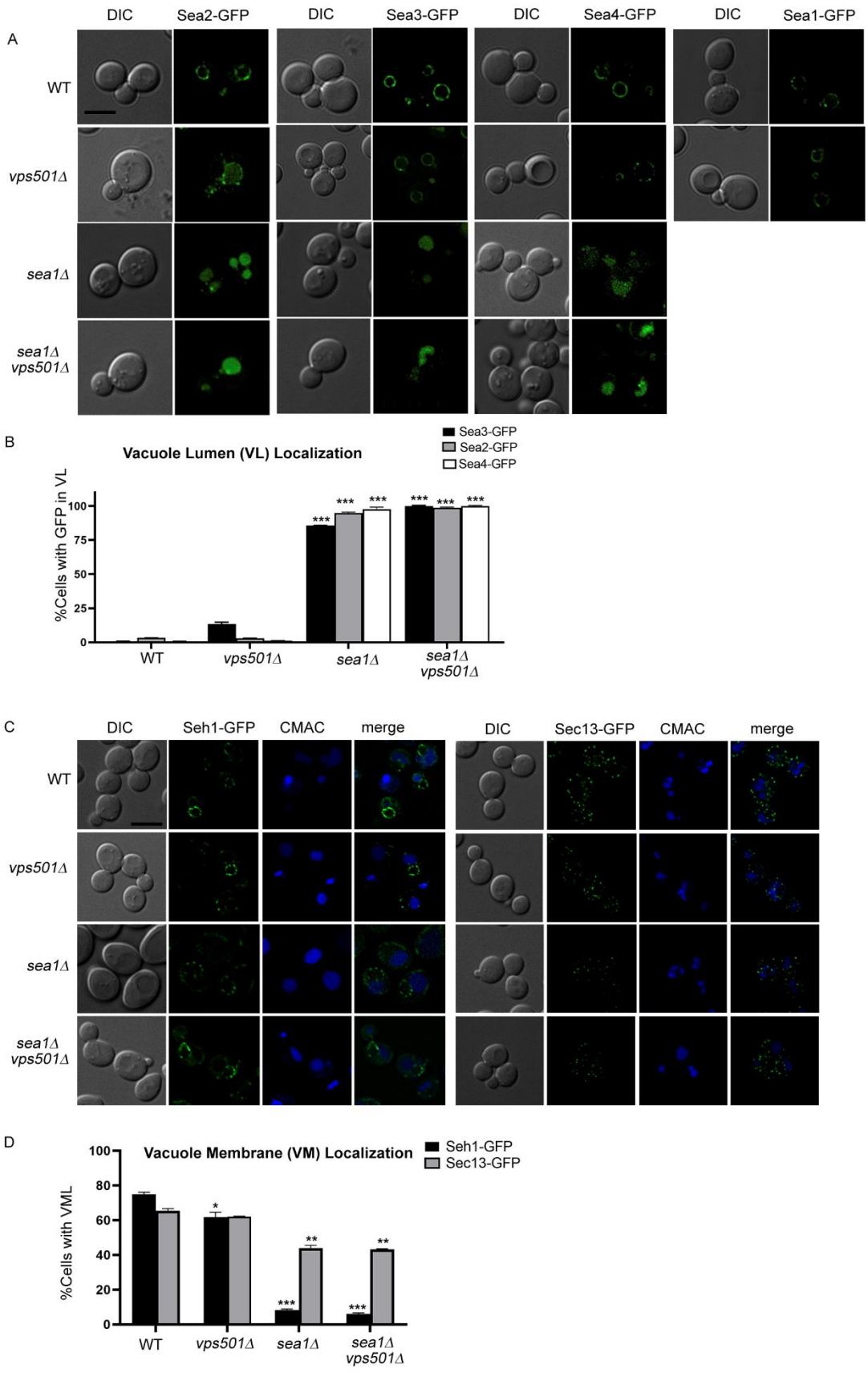
A
DIC
Sea2-GFP
DIC
Sea3-GFP
DIC
Sea4-GFP
DIC
Sea1-GFP
WT
vps501Δ
sea1Δ
sea1Δ vps501Δ
B
Vacuole Lumen (VL) Localization
Sea3-GFP
Sea2-GFP
Sea4-GFP
%Cells with GFP in VL
100
75
50
25
0
***
WT
vps501Δ
sea1Δ
sea1Δ vps501Δ
C
DIC
Seh1-GFP
CMAC
merge
DIC
Sec13-GFP
CMAC
merge
WT
vps501Δ
sea1Δ
sea1Δ vps501Δ
D
Vacuole Membrane (VM) Localization
Seh1-GFP
Sec13-GFP
%Cells with VML
100
80
60
40
20
0
*
**
***
WT
vps501Δ
sea1Δ
sea1Δ vps501Δ

Figure 14. SEACAT subunits, Sea2-GFP, Sea3-GFP, Sea4-GFP, Seh1-GFP and Sec13-GFP are partially mislocalized in *vps501*Δ*sea1*Δ cells. (A) Sea2-GFP, Sea3-GFP, Sea4-GFP and Sea1-GFP reside on the vacuolar membrane in wildtype and *vps501*Δ cells, but localize to the vacuolar lumen (VL) in *sea1*Δ cells and *vps501*Δ*sea1*Δ cells. Note, *sea1*Δ cells appear to mask any effects of VPS501. (B) VL localization is defined by visually scoring the presence of GFP in the VL. C) SEACAT subunits, Seh1-GFP and Sec13-GFP localize to the vacuolar membrane in wildtype and *vps501*Δ cells, but are enriched in non-vacuolar compartments in *sea1*Δ cells and *vps501*Δ*sea1*Δ cells. Seh1 and Sec13 have previously-reported nuclear and ER roles, respectively, and are likely enriched on these structures when vacuolar membrane localization is compromised. (B) VL localization as determined by calculating the percentage of cells with GFP signal on the vacuole using CMAC as a visual maker to determine vacuole boundaries. The results are from three experiments and averaged using the standard error of the mean. Indicated significance is a comparison of wildtype to single deletions or double mutants. *$p<0.05$, ** $p<0.01$, ***$p<0.001$ indicates significance as calculated by Student's t-test.

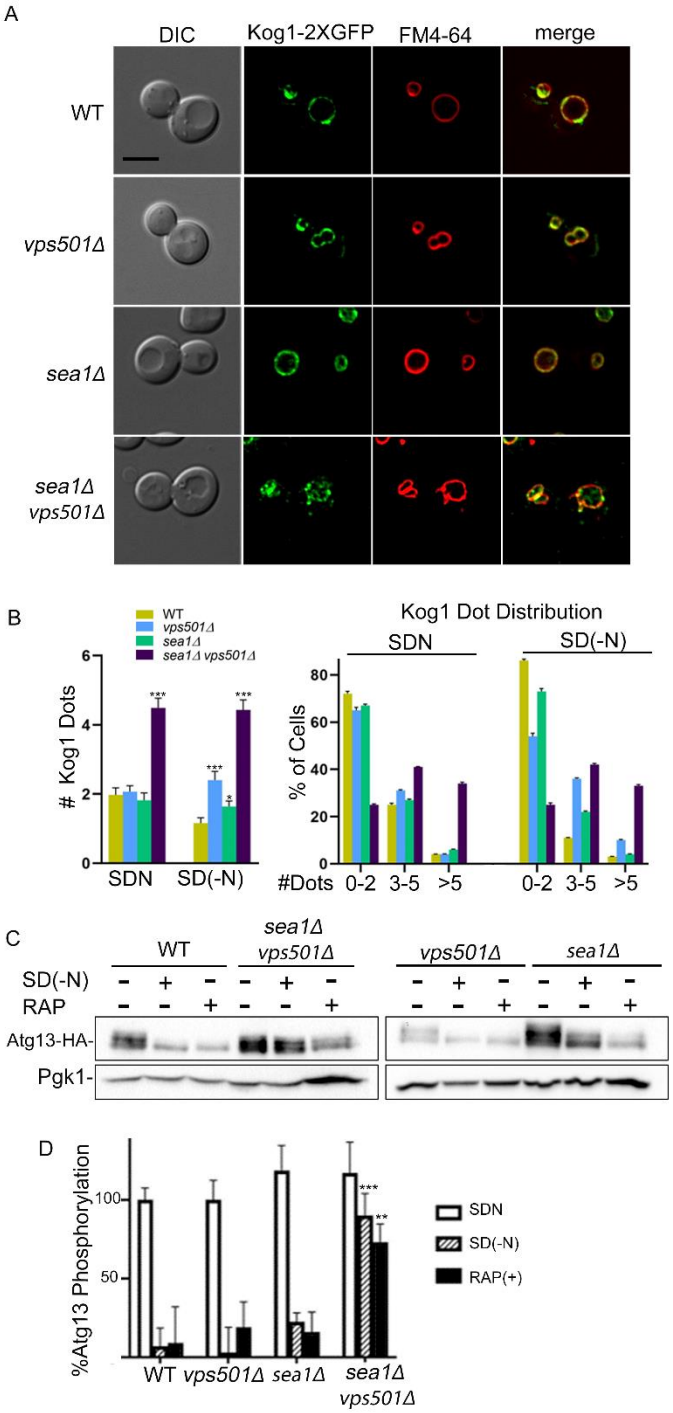

Figure 15. TORC1 and autophagy induction is defective in *vps501*Δ*sea1*Δ cells. (A) Micrographs of Kog1-2XGFP localization in wildtype and indicated mutant cells during vegetative growth. Kog1 a subunit of TORC1, typically localizes to the vacuolar membrane and in dot-like structures juxtaposed the vacuolar membrane, known as signaling endosomes. In *vps501*Δ*sea1*Δ cells, these dot-like structures accumulate indicating the pool of signaling endosomes are enriched, while the vacuole TORC1 pool appears reduced. Vacuolar

membranes are shown using FM4-64 dye. (B) The number of Kog1 dot-like structures were quantified in wildtype and indicated mutant cells before and after nitrogen starvation as described in the text. Regardless of starvation conditions, there was a 2-fold increase in dot-like structures in *vps501*Δ*sea1*Δ cells as compared to single mutants or wildtype cells (left graph). 3 or more dot-like structures were found in 80% of *vps501*Δ*sea1*Δ cells, while single mutants or wildtype cells typically had 0-2 dots (right graph). *$p<0.05$, ** $p<0.01$, ***$p<0.001$ indicates significance as calculated by a one-way ANOVA from three biological replicates. (C) Quantitative immunoblot analysis of Atg13 in wildtype and indicated mutant cells before and after nitrogen starvation or rapamycin treatment. In wildtype, *vps501*Δ*or sea1*Δ cells, Atg13 is phosphorylated as indicated by Atg13 band smear during vegetative growth, indicating TORC1 is active. In autophagy induction conditions, TORC1 is inactivated and Atg13 is not phosphorylated indicated by the loss of Atg13 band smear. In *vps501*Δ*sea1*Δ cells, Atg13 remains phosphorylated indicating autophagy induction is defective in these mutants, regardless of nitrogen starvation or rapamycin (see text for details). (D) Percentage of Atg13 phosphorylation was quantified by determining the proportion of Atg13 to total protein using densitometry. A representative immunoblot is shown. Anti-Pgk1 was used as a loading control. Indicated significance is a comparison of wildtype to single deletions or double mutants. *$p<0.05$, ** $p<0.01$, ***$p<0.001$ indicates significance as calculated by Student's t-test from three biological replicates.

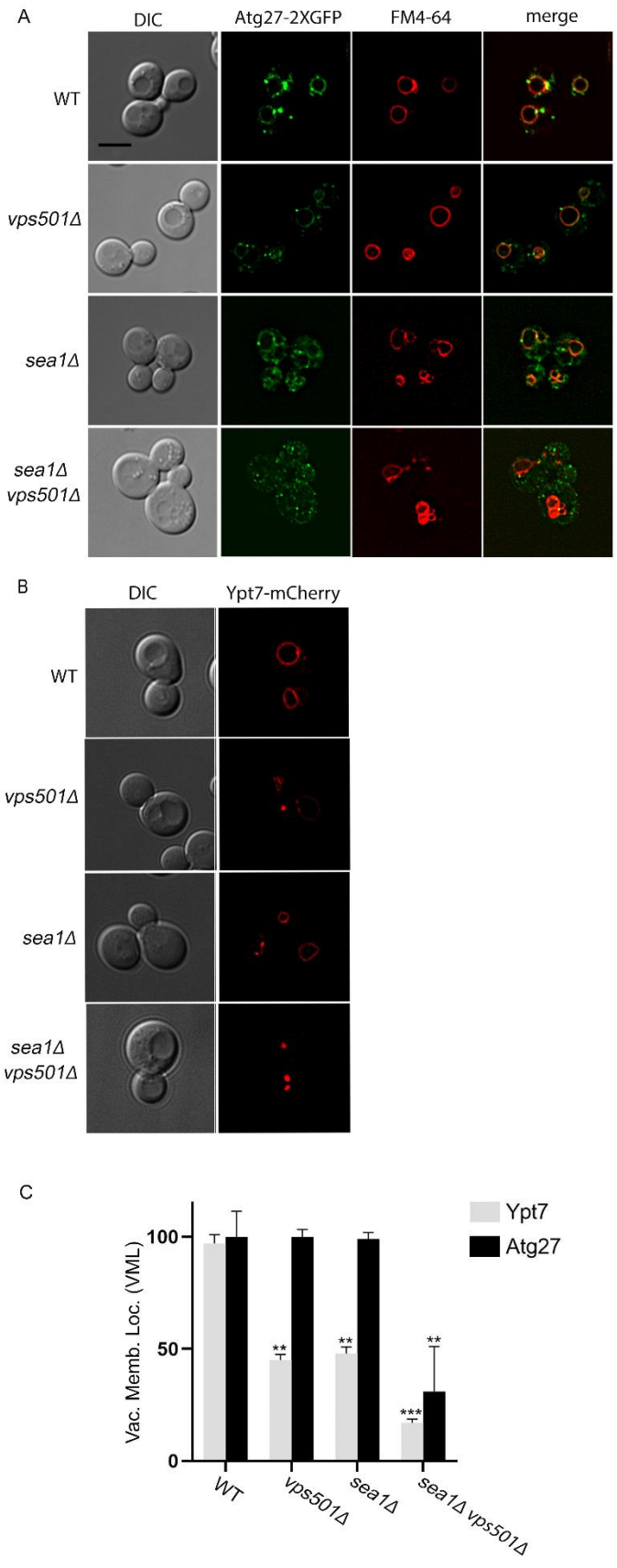
A
DIC
Atg27-2XGFP
FM4-64
merge
WT
vps501Δ
sea1Δ
sea1Δ vps501Δ
B
DIC
Ypt7-mCherry
WT
vps501Δ
sea1Δ
sea1Δ vps501Δ
C
Ypt7
Atg27
Vac. Memb. Loc. (VML)
100
50
0
**
**
**
***
WT
vps501Δ
sea1Δ
sea1Δ vps501Δ

Figure 16. Other vacuolar membrane proteins are mislocalized in *vps501*Δ*sea1*Δ cells. (A) Micrographs of Atg27-2XGFP in wildtype and indicated mutant cells. Atg27-2XGFP is typically localized to the vacuolar membrane, the Golgi and endosomal compartments. In *atg1*Δ cells, Atg27-2XGFP cycling is less abundant on the vacuolar membrane. In *vps501*Δ*sea1*Δ cells, Atg27-2XGFP is significantly depleted from the vacuolar membrane, indicating Atg27 cycling to and from the vacuolar membrane is dependent on Vps501 and Sea1 function during autophagy induction. (B) Micrographs of Ypt7-mCherry in wildtype and indicated mutant cells. Ypt7 is typically localized to the vacuolar membrane. In *vps501*Δ*sea1*Δ cells, Ypt7-mCherry is significantly depleted from the vacuolar membrane (C) Graph of the quantification of Atg27-2XGFP and Ypt7-mCherry vacuolar localization as described in the text. Percentage of cells with Atg27 vacuolar localization is between 85-95% in wildtype cells or in cells ablated for only Vps501 or Sea1 and is reduced ~20% *atg1*Δ cells and ~75% in *vps501*Δ*sea1*Δ cells. Percentage of cells with Ypt7 vacuolar localization is between 95-100%in wildtype cells, ~50% in single deletions and less than 30% in double deletion of *sea1*Δ *vps501*Δ The results are from three experiments and averaged using the standard error of the mean. Indicated significance is a comparison of wildtype to single deletions or double mutants. *$p<0.05$, ** $p<0.01$, ***$p<0.001$ indicates significance as calculated by Student's t-test. The scale bar indicates 5μm.

3.7 References

1. Gallon M, Cullen PJ. Retromer and sorting nexins in endosomal sorting. Biochem Soc Trans. 2015;43(1):33-47.
2. Chi RJ, Harrison MS, Burd CG. Biogenesis of endosome-derived transport carriers. Cell Mol Life Sci. 2015;72(18):3441-55.
3. Teasdale RD, Collins BM. Insights into the PX (phox-homology) domain and SNX (sorting nexin) protein families: structures, functions and roles in disease. Biochem J. 2012;441(1):39-59.
4. van Weering JR, Verkade P, Cullen PJ. SNX-BAR proteins in phosphoinositide-mediated, tubular-based endosomal sorting. Semin Cell Dev Biol. 2010;21(4):371-80.
5. Chi RJ, Liu J, West M, Wang J, Odorizzi G, Burd CG. Fission of SNX-BAR-coated endosomal retrograde transport carriers is promoted by the dynamin-related protein Vps1. J Cell Biol. 2014;204(5):793-806.
6. van Weering JR, Sessions RB, Traer CJ, Kloer DP, Bhatia VK, Stamou D, et al. Molecular basis for SNX-BAR-mediated assembly of distinct endosomal sorting tubules. EMBO J. 2012;31(23):4466-80.
7. Anton Z, Betin VMS, Simonetti B, Traer CJ, Attar N, Cullen PJ, et al. A heterodimeric SNX4--SNX7 SNX-BAR autophagy complex coordinates ATG9A trafficking for efficient autophagosome assembly. J Cell Sci. 2020;133(14).
8. Burd C, Cullen PJ. Retromer: a master conductor of endosome sorting. Cold Spring Harb Perspect Biol. 2014;6(2).
9. Ma M, Burd CG, Chi RJ. Distinct complexes of yeast Snx4 family SNX-BARs mediate retrograde trafficking of Snc1 and Atg27. Traffic. 2017;18(2):134-44.
10. Ma M, Kumar S, Purushothaman L, Babst M, Ungermann C, Chi RJ, et al. Lipid trafficking by yeast Snx4 family SNX-BAR proteins promotes autophagy and vacuole membrane fusion. Mol Biol Cell. 2018;29(18):2190-200.
11. Nemec AA, Howell LA, Peterson AK, Murray MA, Tomko RJ, Jr. Autophagic clearance of proteasomes in yeast requires the conserved sorting nexin Snx4. J Biol Chem. 2017;292(52):21466-80.
12. Su MY, Peng WH, Ho MR, Su SC, Chang YC, Chen GC, et al. Structure of yeast Ape1 and its role in autophagic vesicle formation. Autophagy. 2015;11(9):1580-93.
13. Yang Z, Klionsky DJ. Mammalian autophagy: core molecular machinery and signaling regulation. Curr Opin Cell Biol. 2010;22(2):124-31.
14. Nakatogawa H. Mechanisms governing autophagosome biogenesis. Nat Rev Mol Cell Biol. 2020;21(8):439-58.
15. Goyal S, R. Robinson M, A. Segarra V, J. Chi R. Intracellular Lipid Homeostasis and Trafficking in Autophagy. Cell Growth2020.
16. Albert V, Hall MN. mTOR signaling in cellular and organismal energetics. Curr Opin Cell Biol. 2015;33:55-66.
17. Eltschinger S, Loewith R. TOR Complexes and the Maintenance of Cellular Homeostasis. Trends Cell Biol. 2016;26(2):148-59.
18. Saxton RA, Sabatini DM. mTOR Signaling in Growth, Metabolism, and Disease. Cell. 2017;169(2):361-71.

19. Alfatah M, Wong JH, Krishnan VG, Lee YC, Sin QF, Goh CJH, et al. TORC1 regulates the transcriptional response to glucose and developmental cycle via the Tap42-Sit4-Rrd1/2 pathway in Saccharomyces cerevisiae. BMC Biol. 2021;19(1):95.
20. Oku M, Maeda Y, Kagohashi Y, Kondo T, Yamada M, Fujimoto T, et al. Evidence for ESCRT- and clathrin-dependent microautophagy. J Cell Biol. 2017;216(10):3263-74.
21. Rahman MA, Terasawa M, Mostofa MG, Ushimaru T. The TORC1-Nem1/Spo7-Pah1/lipin axis regulates microautophagy induction in budding yeast. Biochem Biophys Res Commun. 2018;504(2):505-12.
22. Zhu L, Jorgensen JR, Li M, Chuang YS, Emr SD. ESCRTs function directly on the lysosome membrane to downregulate ubiquitinated lysosomal membrane proteins. Elife. 2017;6.
23. Dauner K, Eid W, Raghupathy R, Presley JF, Zha X. mTOR complex 1 activity is required to maintain the canonical endocytic recycling pathway against lysosomal delivery. J Biol Chem. 2017;292(14):5737-47.
24. Dobzinski N, Chuartzman SG, Kama R, Schuldiner M, Gerst JE. Starvation-Dependent Regulation of Golgi Quality Control Links the TOR Signaling and Vacuolar Protein Sorting Pathways. Cell Rep. 2015;12(11):1876-86.
25. Jones CB, Ott EM, Keener JM, Curtiss M, Sandrin V, Babst M. Regulation of membrane protein degradation by starvation-response pathways. Traffic. 2012;13(3):468-82.
26. MacGurn JA, Hsu PC, Smolka MB, Emr SD. TORC1 regulates endocytosis via Npr1-mediated phosphoinhibition of a ubiquitin ligase adaptor. Cell. 2011;147(5):1104-17.
27. Binda M, Peli-Gulli MP, Bonfils G, Panchaud N, Urban J, Sturgill TW, et al. The Vam6 GEF controls TORC1 by activating the EGO complex. Mol Cell. 2009;35(5):563-73.
28. Algret R, Fernandez-Martinez J, Shi Y, Kim SJ, Pellarin R, Cimermancic P, et al. Molecular architecture and function of the SEA complex, a modulator of the TORC1 pathway. Mol Cell Proteomics. 2014;13(11):2855-70.
29. Panchaud N, Peli-Gulli MP, De Virgilio C. SEACing the GAP that nEGOCiates TORC1 activation: evolutionary conservation of Rag GTPase regulation. Cell Cycle. 2013;12(18):2948-52.
30. Dokudovskaya S, Rout MP. SEA you later alli-GATOR--a dynamic regulator of the TORC1 stress response pathway. J Cell Sci. 2015;128(12):2219-28.
31. Yen WL, Legakis JE, Nair U, Klionsky DJ. Atg27 is required for autophagy-dependent cycling of Atg9. Mol Biol Cell. 2007;18(2):581-93.
32. Koumandou VL, Klute MJ, Herman EK, Nunez-Miguel R, Dacks JB, Field MC. Evolutionary reconstruction of the retromer complex and its function in Trypanosoma brucei. J Cell Sci. 2011;124(Pt 9):1496-509.
33. Horazdovsky BF, Davies BA, Seaman MN, McLaughlin SA, Yoon S, Emr SD. A sorting nexin-1 homologue, Vps5p, forms a complex with Vps17p and is required for recycling the vacuolar protein-sorting receptor. Mol Biol Cell. 1997;8(8):1529-41.
34. Nothwehr SF, Hindes AE. The yeast VPS5/GRD2 gene encodes a sorting nexin-1-like protein required for localizing membrane proteins to the late Golgi. J Cell Sci. 1997;110 (Pt 9):1063-72.

35. Seaman MN, Marcusson EG, Cereghino JL, Emr SD. Endosome to Golgi retrieval of the vacuolar protein sorting receptor, Vps10p, requires the function of the VPS29, VPS30, and VPS35 gene products. J Cell Biol. 1997;137(1):79-92.
36. Huh WK, Falvo JV, Gerke LC, Carroll AS, Howson RW, Weissman JS, et al. Global analysis of protein localization in budding yeast. Nature. 2003;425(6959):686-91.
37. Dokudovskaya S, Rout MP. A novel coatomer-related SEA complex dynamically associates with the vacuole in yeast and is implicated in the response to nitrogen starvation. Autophagy. 2011;7(11):1392-3.
38. Dokudovskaya S, Waharte F, Schlessinger A, Pieper U, Devos DP, Cristea IM, et al. A conserved coatomer-related complex containing Sec13 and Seh1 dynamically associates with the vacuole in Saccharomyces cerevisiae. Mol Cell Proteomics. 2011;10(6):M110 006478.
39. Henkel V, Schurmanns L, Brunner M, Hamann A, Osiewacz HD. Role of sorting nexin PaATG24 in autophagy, aging and development of Podospora anserina. Mech Ageing Dev. 2020;186:111211.
40. Dong X, Yang Y, Zou Z, Zhao Y, Ci B, Zhong L, et al. Sorting nexin 5 mediates virus-induced autophagy and immunity. Nature. 2021;589(7842):456-61.
41. Hanley SE, Willis SD, Cooper KF. Snx4-assisted vacuolar targeting of transcription factors defines a new autophagy pathway for controlling ATG expression. Autophagy. 2021:1-19.
42. Chen Z, Malia PC, Hatakeyama R, Nicastro R, Hu Z, Peli-Gulli MP, et al. TORC1 Determines Fab1 Lipid Kinase Function at Signaling Endosomes and Vacuoles. Curr Biol. 2021;31(2):297-309 e8.
43. Hatakeyama R, Peli-Gulli MP, Hu Z, Jaquenoud M, Garcia Osuna GM, Sardu A, et al. Spatially Distinct Pools of TORC1 Balance Protein Homeostasis. Mol Cell. 2019;73(2):325-38 e8.
44. Kamada Y, Funakoshi T, Shintani T, Nagano K, Ohsumi M, Ohsumi Y. Tor-mediated induction of autophagy via an Apg1 protein kinase complex. J Cell Biol. 2000;150(6):1507-13.
45. Powis K, De Virgilio C. Conserved regulators of Rag GTPases orchestrate amino acid-dependent TORC1 signaling. Cell Discov. 2016;2:15049.
46. Inoue Y, Nomura W. TOR Signaling in Budding Yeast. The Yeast Role in Medical Applications2018.
47. Heitman J, Movva NR, Hiestand PC, Hall MN. FK 506-binding protein proline rotamase is a target for the immunosuppressive agent FK 506 in Saccharomyces cerevisiae. Proc Natl Acad Sci U S A. 1991;88(5):1948-52.
48. Segarra VA, Boettner DR, Lemmon SK. Atg27 tyrosine sorting motif is important for its trafficking and Atg9 localization. Traffic. 2015;16(4):365-78.
49. Haas A, Scheglmann D, Lazar T, Gallwitz D, Wickner W. The GTPase Ypt7p of Saccharomyces cerevisiae is required on both partner vacuoles for the homotypic fusion step of vacuole inheritance. EMBO J. 1995;14(21):5258-70.
50. Chandra M, Chin YK, Mas C, Feathers JR, Paul B, Datta S, et al. Classification of the human phox homology (PX) domains based on their phosphoinositide binding specificities. Nat Commun. 2019;10(1):1528.

51. Kira S, Tabata K, Shirahama-Noda K, Nozoe A, Yoshimori T, Noda T. Reciprocal conversion of Gtr1 and Gtr2 nucleotide-binding states by Npr2-Npr3 inactivates TORC1 and induces autophagy. Autophagy. 2014;10(9):1565-78.
52. Barbet NC, Schneider U, Helliwell SB, Stansfield I, Tuite MF, Hall MN. TOR controls translation initiation and early G1 progression in yeast. Mol Biol Cell. 1996;7(1):25-42.
53. Rohde J, Heitman J, Cardenas ME. The TOR kinases link nutrient sensing to cell growth. J Biol Chem. 2001;276(13):9583-6.
54. Edgar RC. MUSCLE: multiple sequence alignment with high accuracy and high throughput. Nucleic Acids Res. 2004;32(5):1792-7.
55. Stamatakis A. RAxML version 8: a tool for phylogenetic analysis and post-analysis of large phylogenies. Bioinformatics. 2014;30(9):1312-3.
56. Darriba D, Taboada GL, Doallo R, Posada D. ProtTest 3: fast selection of best-fit models of protein evolution. Bioinformatics. 2011;27(8):1164-5.
57. Longtine MS, McKenzie A, 3rd, Demarini DJ, Shah NG, Wach A, Brachat A, et al. Additional modules for versatile and economical PCR-based gene deletion and modification in Saccharomyces cerevisiae. Yeast. 1998;14(10):953-61.
58. Vida TA, Emr SD. A new vital stain for visualizing vacuolar membrane dynamics and endocytosis in yeast. J Cell Biol. 1995;128(5):779-92.
59. Shintani T, Huang WP, Stromhaug PE, Klionsky DJ. Mechanism of cargo selection in the cytoplasm to vacuole targeting pathway. Developmental cell. 2002;3(6):825-37.
60. Kamada Y. Novel tRNA function in amino acid sensing of yeast Tor complex1. Genes Cells. 2017;22(2):135-47.
61. Alberti S, Gitler AD, Lindquist S. A suite of Gateway cloning vectors for high-throughput genetic analysis in Saccharomyces cerevisiae. Yeast. 2007;24(10):913-9.
62. Deutsch EW, Csordas A, Sun Z, Jarnuczak A, Perez-Riverol Y, Ternent T, et al. The ProteomeXchange consortium in 2017: supporting the cultural change in proteomics public data deposition. Nucleic Acids Res. 2017;45(D1):D1100-D6.
63. Vizcaino JA, Cote RG, Csordas A, Dianes JA, Fabregat A, Foster JM, et al. The PRoteomics IDEntifications (PRIDE) database and associated tools: status in 2013. Nucleic Acids Res. 2013;41(Database issue):D1063-9.
64. Vizcaino JA, Csordas A, del-Toro N, Dianes JA, Griss J, Lavidas I, et al. 2016 update of the PRIDE database and its related tools. Nucleic Acids Res. 2016;44(D1):D447-56.

CHAPTER 4: VPS501 IS OLIGOMERIC AND REQUIRES LIPID AND PROTEIN INTERACTIONS FOR VACUOLAR MEMBRANE LOCALIZATION AND FUNCTION

Abstract

The SNX-BAR proteins have well-characterized biochemical and biophysical properties that promote membrane remodeling via their highly conserved Phox-homology (PX) and BAR (Bin/Amphiphysin/Rvs) domains. The PX domain is known to bind to lipid species such as phosphatidylinositol 3-phosphate (PI3P) through the formation of homodimers or heterodimers and contribute to the formation of tubule structures and vesicles on various membrane organelles. In vitro binding studies using recombinant SNX-BAR proteins on synthetic liposomes have long been utilized by researchers to reveal the precise makeup of lipids needed to drive membrane remodeling, thus revealing their mechanism of action. In our previous study, we identified Vps501 as the newest member of the yeast SNX-BAR protein family and found Vps501 uniquely localizes to the vacuolar membrane and interacts with the SEA complex to regulate TORC1 inactivation. In this study, we demonstrate Vps501 is recruited by Sea1 and uses a non-canonical PX domain to bind vacuolar lipids that is also required for its function. Furthermore, we discovered Vps501 purifies as large oligomers, which we hypothesize contributes to the regulation and function at the vacuolar membrane.

4.1. Introduction

The sorting nexin (SNX) family is an evolutionarily conserved class of proteins that have been found to be critical for many vesicle transport reactions in the cell (1, 2). Sorting nexins are recruited to the endosome membrane and aid in cargo capture via their characteristic phox homology (PX) domain, which binds phosphatidylinositol-3-monophosphate (PI3P), a lipid enriched on the endosome membrane. Mammalians encode thirty-three SNX proteins, which can be further divided into multiple subfamilies, according to the presence of other domains. (3). Most notably, the SNX-BAR subfamily is the largest subfamily consisting of twelve in human, while in budding yeast, *Saccharomyces cerevisiae*, the subfamily is reduced to just seven SNX-BARs. SNX-BAR proteins have both a PX domain and a Bin-Amphiphysin-Rvs (BAR) domain, which potentiates the local pools of lipids and bind avidly to membranes with high positive curvature. Therefore, the SNX-BAR family can accumulate on PI3P rich organelles such as the endosome and deform their membranes to form membrane tubules.

SNX-BAR proteins have intrinsic PI3P affinity through their canonical binding motif (ψPxxPxK) in a region known as the PPK loop in the PX domain that is thought to drive association to the outer leaflet of organelles. Yet despite the 90% conserved structural properties of all PX domains, many SNX-BARs have been found to bind a variety of phosphoinositide besides PI3P or not at all (4-6). Recently, a secondary noncanonical phosphoinositide binding motif was discovered in a subset of PX domains, characterized by a His/Tyr-basic motif that is found upstream of the canonical binding motif which is thought to aid in alternative lipid binding.

Apart from the PX domain, SNX-BAR proteins have also been characterized by the presence of a membrane-remodeling or curvature-sensing BAR domain. Various in vitro binding assays and structural studies have demonstrated that SNX-BAR proteins form homodimers or heterodimers and oligomerize on membrane surfaces via tip-to-tip interactions of the BAR domains (5), thereby generating regular arrays that wrap a membrane tubule. When present in sufficient concentration, some SNX-BAR proteins can drive a topological transition of synthetic liposomes into a narrow, coated tubule, suggesting that oligomerization of these SNX-BARs on the membrane could aid in the formation and scission of a tubular transport carrier (5, 6). In principle, each potential SNX-BAR oligomer could confer a cargo-specific trafficking pathway, but the extent to which this is the case is yet to be determined. In addition, a recent study solved the structure of full length SNX-BAR protein, Mvp1 using cryoelectron microscopy. It was reported that full length Mvp1 exists in an autoinhibited tetrameric complex mediated by the BAR domain as well as its unstructured N-terminal region (7).

A recent study from our group characterized Vps501, a novel yeast SNX-BAR protein and found GFP-Vps501 uniquely resides on the vacuole membrane. Furthermore, Vps501 was found to have strong physical and genetic interactions with Sea1, a subunit of the SEACIT complex, an evolutionarily conserved negative regulator of TORC1. The mechanism that recruits Vps501 to the vacuole membrane and whether vacuolar localization is required for function is not known. The vacuolar membrane is unique from other cellular membranes in that it has very low levels of ergosterol and sphingolipids and the major phosphoinositide

species on the vacuolar membrane is phosphatidylinositol 3,5-bisphosphate (PI(3,5)P2), which is generated from PI3P by the Fab1 kinase (8). PI(3,5)P2 is critical for maintaining vacuolar identity since PI(3,5)P2 effectors are required for protein sorting and retrograde trafficking from the vacuole to the endosome (8). This combined with Vps501 physical interactions with Sea1 led us to hypothesize an overall mechanism of recruitment to the vacuolar membrane that is driven by protein and vacuolar membrane lipid specificity.

4.2. Material and Methods

Yeast Strains and Culture Conditions

Yeast strains were grown using standard media and conditions (Guthrie and Fink, 1991) unless indicated. Yeast strains were constructed in BY4742 (*MATα his3-1, leu2-0, met15-0,* and *ura3-0)* by homologous recombination of gene-targeted, polymerase chain reaction (PCR)-generated DNAs using the method of (9) and/or derived from the EUROSCARF KANMX deletion collection (Open Biosystems/Thermo Scientific, Waltham, MA) or produced by replacement of the complete reading frame with the *HIS3MX6* or *URA3* cassette. Gene deletions were confirmed by PCR amplification of the deleted locus. Cells were grown in standard synthetic complete medium lacking nutrients required to maintain selection for auxotrophic markers and/or plasmid, unless indicated otherwise. To induce bulk or non-selective autophagy, cells were grown to log phase, harvested, and transferred to SD(-N) medium for nitrogen starvation (2% dextrose, 0.17% Yeast Nitrogen Base without amino acids and without ammonium sulfate) for 16 hours or resuspended in standard synthetic complete medium containing 0.2 μg/mL of rapamycin (R-5000, LC laboratories) for 2-4hrs at 30°C. For the construction of an integrated N terminal GFP-Vps501 yeast strain under a GPD promoter, we PCR amplified pGFP-^{GPD}Vps501 (described below) using the following primers that included 50 bp flanking the *VPS501* locus;

ATCAGAACTGCAACCCTACAGATTAGATATGGAGAACGACAAGGCGTCACGT GAGCAAGGGCGAGGAGCTGTTCA and GCTTTTTCAGTAGTAAATTATCTTCTTTAATTACGTTATTATGTACATATTTGG CTTATGTGCTCATCTGGTACA. PCR products were subsequently transformed into

cells ablated for *VPS501* (by replacement with a URA marker) and allowed to homologously recombine into the *VPS501* locus. Resulting clones were selected on F.O.A 5-Fluoroorotic Acid (5-FOA) and confirmed by PCR.

Light Microscopy and Image Analysis

Yeast cells from cultures grown to $OD_{600} \approx 0.5$ were mounted in growth medium, and 3D image stacks were collected at 0.3-µm z increments on a DeltaVision elite workstation (Cytiva) based on an inverted microscope (IX-70; Olympus) using a 100×1.4NA oil immersion lens. Images were captured at 24°C with a 12-bit charge-coupled device camera (CoolSnap HQ; Photometrics) and deconvolved using the iterative-constrained algorithm and the measured point spread function. To visualize the vacuolar membrane, FM4-64 (32nM) was added to cell cultures for 20 min at 30°C. Cells were then washed, resuspended in fresh medium, and then incubated for 60 minutes to allow FM4-64 to accumulate in the vacuolar membrane (10). Image analysis and preparation was done using Softworx 6.5 (Cytiva) and ImageJ v1.50d (Rasband). Vacuolar membrane localization analyses for GFP-Vps501 and GFP-Vps501^{YKAA} was determined using a manual method implemented using ImageJ v1.53c (Rasband). A region of interest (ROI) was selected to contain a single cell and the total sum of GFP fluorescence was calculated (TF). Next, we used the Mask macro to delineate the vacuole ROI defined by FM4-64 and overlayed onto the GFP channel to define the vacuole fluorescence (VF). To calculate cytosol fluorescence intensity (CF), the vacuole mask was inverted so that all pixels outside of the mask were assigned a maximum value and the regions corresponding the vacuole signal were assigned

a value of zero. A ratio of the VF to TF is presented in the graphs. A minimum of 100 cells was used in all experimental conditions and performed in biological triplicate.

GFP-Atg8 Processing and Immunoblotting

For quantitative immunoblot analysis of GFP-Atg8, cells were grown under standard vegetative or autophagy inducing conditions to $OD_{600} \approx 0.5$, as described above. Typically, 3.0×10^7 cells were harvested by centrifugation and lysed by glass bead agitation in SDS-PAGE sample buffer. 10% polyacrylamide gels were loaded with 5.0×10^7 cell equivalents and transferred onto standard 0.45 μm nitrocellulose. Anti-GFP primary mouse monoclonal antibody (1814460, Roche) was diluted 1:2500 and Santa Cruz (sc-2055) goat anti-mouse HRP-conjugated antibody was used at 1:10000. Anti-Pgk1 at 1:5000 (Life Technologies) was used as loading controls. Centromeric GFP-Atg8 (11) plasmids were used in the processing assays. All enhanced chemiluminescence *(ECL)* blots were development on a Chemidoc-MP (Bio-Rad) and band intensities were quantified using Quantity One 1D analysis software (Bio-Rad) and all statistical analysis done using GraphPad Prism 8.

Plasmids

pGFP-^{GPD}Vps501 was constructed using Gateway cloning. Plasmid insert was made using PCR amplified wild-type genomic *VPS501* locus with the following primers: GGGGACAAGTTTGTACAAAAAAGCAGGCTTAGAGAACGACAAGGCGTCACA

T and

GGGGACCACTTTGTACAAGAAAGCTGGGTTTCATTGGCTTATGTGCTCATCTG

GT and cloned using a BP recombination reaction into pDONR221. Resulting DONOR vector was recombined with pAG425GPD-EGFP-ccDB (12) in a final LR recombination reaction to generate the pAG415GPD-eGFP-Vps501 expression clone (pGFP-^{GPD}Vps501). pGFP-Vps501^{YKAA} was made commercially using site-directed mutagenesis (GenScript, Piscataway, NJ), introducing alanine mutations into following positions Y160A and K170A of pGFP-^{GPD}Vps501. pVps501^{YKAA} was derived from pGFP-Vps501^{YKAA} using Gateway cloning as described above.

Vps501 and Vps501^{YKAA} expression and purification from E. coli

His-tag fusion vector of Vps501 was made by synthesizing the Vps501 ORF as a NdeI and HindIII fragment (Genscript). The gene synthesis product was cloned in-frame into NdeI and HindIII sites of vector pET-30a(+) (Novagen), and the resulting plasmid was sequenced. The plasmid was transformed into *E. coli* BL21 and expressed by IPTG. Briefly, plasmids were transformed into BL21(DE3) competent cells and grown in LB containing the appropriate antibiotics in baffled flasks filled to 20% of the total volume. IPTG solution was added to a final concentration of 0.1 mM and cultures were grown at 37°C for 4 hours, then shifted to 15°C for 20 hours. Recombinant Vps501 contained a N-terminal His-tag and was purified using an ÄKTA START fast protein liquid chromatography (FPLC) system (Cytivia) equipped with a 1 ml His-Trap HP column followed by buffer exchange into assay buffer. 6XHIS-Vps501^{YKAA}, was created by site-directed mutagenesis and purified as described above with an additional step of size-exclusion chromatography (HiPREP16/60 Sephacryl S-300 HR, Cytivia) to remove

additional impurities. Snx4-Atg20 were purified as previously described (13). All purified protein concentrations were quantified by Brafford assay (Pierce).

Relative molecular weights were determined by concentrating peak FPLC fractions of Vps501 and Vps501^{YKAA} to ~10mg/ml. 1mL of concentrated protein was loaded onto a HiPrep 16/60 Sephacryl S300 HR gel filtration column equilibrated with TN50(20 mM TRIS/Cl pH 7.5, 250 mM NaCl, and 1.93 mM β-mercaptoethanol) and collected at 1 ml/min. Vps501 and Vps501^{YKAA} elution profiles were comparted to high molecular weight standards (Cytivia) Thyroglobulin(669 kDa), Ferritin (440 kDa), Aldolase (158 kDa) and Conalbumin (75 kDa). The calibration curve was plotted using the gel-phase distribution coefficient (Kav) versus logarithm of the molecular weight (Log Mw), $K_{av} = (V_e - V_o) / (V_c - V_o)$, where V_o = column void volume, V_e = elution volume, and V_c = geometric column volume. (20 mL). 38 mL void volume was calculated as the elution volume of blue dextran.

Liposome sedimentation assays

Liposomes were prepared as previously described in (13). Briefly, specified lipids compositions (See Table 1) of dehydrated lipids were resuspended by vortexing in Tris pH 7.4, 300 mM NaCl, 1 mM MgCl2 to make a final liposome concentration of 2.5mM. Liposomes were then extruded through 200-nm pore-size filters using a mini-extruder (Avanti Polar Lipids, Inc.) and used for binding assays within 3 days. Liposome binding assays were carried out as previously described (6). To test binding to PI containing liposomes, liposome compositions were (2.5 mM lipid) 0% or 11% PtdIns(3)P; 0% or 18%

PtdIns(3,5)P2; with PC adjusted to 100%. To test PS binding, liposomes (0% or 30% PS; 1% PtdIns(3)P; 20% ergosterol; with PC adjusted to 100%) were incubated with 4 μM Snx4-Atg20, Vps501-Vps501 or $Vps501^{YKAA}$ -$Vps501^{YKAA}$ for 30 min at 30°C and sedimented at 100,000xg for 20 minutes. Pellet (P) and supernatant (S) fractions were loaded onto 10% polyacrylamide gels and visualized using Coomassie Brilliant Blue stain. Band intensities were quantified using Quantity One 1D analysis software (Bio-rad) and proportion of SNX-BAR proteins in pellet fraction was quantified. Student's t-test was used to determine statistical significance (GraphPad Prism 7.01).

4.3. Results

Vps501 requires Sea1 for vacuolar membrane localization

During our initial characterization of Vps501, we found N-terminally tagged Vps501 localized to the vacuolar membrane and interacted with other vacuolar proteins such as Sea1. Due to Vps501's unique vacuolar localization and apparent interactions with vacuolar proteins, we hypothesized that direct recruitment via the SEA complex is critical for Vps501 vacuolar localization. Indeed, we found that ablation of Sea1 causes mislocalization of GFP-Vps501 to the cytoplasm (Figure 1). Interestingly, deletion of any other SEA complex subunit failed to trigger mislocalization of GFP-Vps501 from the vacuole, suggesting that an interaction with Sea1 specifically mediates Vps501 recruitment to the vacuolar membrane.

Vps501 requires a non-canonical PX domain for vacuolar membrane localization and function

During our initial characterization of Vps501 we also found both fluorescence microscopy and immunoblot analysis of *sea1*Δ*vps501*Δ cells showed a striking loss of autophagic flux in GFP-Atg8, indicating that Vps501 and the SEA complex function synergistically during autophagy. We next aimed to determine whether the vacuolar membrane localization of Vps501 is required for its autophagic function. In order to generate a mutant Vps501 protein that is unable to localize to the vacuolar membrane, we sought to first identify the domain responsible for this localization. We began by examining the lipid-binding PX domain that might mediate this localization through recognition of a specific lipid composition. Although the canonical lipid-binding motif in the PX domain of Vps501 is

missing key motif residues that would be required for PI3P lipid binding, we discovered a predicted secondary noncanonical binding motif (Figure 2A).

We used site-directed mutagenesis of the pGFP-Vps501 plasmid to disrupt the noncanonical lipid binding motif to determine its effect on localization of Vps501 to the vacuole. We substituted alanine for the key conserved tyrosine and lysine residues in the noncanonical lipid binding motif of Vps501, generating a mutant protein referred to here as GFP-Vps501^{YKAA}. Colocalization studies of pGFP-Vps501^{YKAA} and the vacuolar membrane marker FM4-64, indicated that GFP-Vps501^{YKAA} recruitment to the vacuolar membrane is reduced by 70% relative to the GFP-Vps501 control (Figure 2B, C). This 70% reduction in the vacuolar membrane recruitment of pGFP-Vps501^{YKAA} was seen in both *vps501*Δ and *sea1*Δ cells, and combination of pGFP-Vps501^{YKAA} with *vps501*Δ*sea1*Δ led to a near total loss of Vps501 vacuolar localization (Figure 2B, C).

This indicated that both protein-protein interaction with Sea1 and lipid recognition by the lipid-binding motif are important for Vps501 localization to the vacuolar membrane (Figure 2B, C). We next ectopically expressed *VPS501^{YKAA}* from a 2-micron plasmid and found that the mutant fails to complement *vps501*Δ*sea1*Δ cells in GFP-Atg8 processing assays (Figure 3A, B). Taken together with the severe defect in *sea1*Δ cell autophagic flux associated with the *VPS501^{YKAA}* mutant relative to the wild-type control (Figure 3A, B), the combination of Sea1 interaction and lipid-binding appears to be required not only for Vps501 recruitment to the vacuolar membrane but also for its role in autophagy and TORC1 signaling.

Vps501 purification and lipid binding specificity

Next, we tested whether Vps501 preferentially binds PI3P or PI(3,5)P2, the prevalent phosphoinositides (PI) on the vacuolar membrane. To do this we performed liposomes sedimentation studies using liposomes empirically derived from vacuole lipid composition or control liposomes devoid of PI3P or PI(3,5)P2 (14, 15). We tested recombinantly expressed Vps501^{WT} and the Vps501^{YKAA} PX mutant, and found strong binding affinities to liposomes enriched with PI3P when using Vps501^{WT} but a 9-fold reduction in binding for the Vps501^{YKAA} PX mutant (Figure 4A, B). We also observed some minor binding enhancements when PI(3,5)P2 was present alone or in combination with PI3P as compared to control liposomes (Figure 4A, B). However, Vps501^{WT} binding was 2-fold lower as compared to liposomes with only 11% PI3P, suggesting PI(3,5)P2 may have an inhibitory effect on Vps501 binding. Recently, we discovered other yeast SNX-BARs Snx4 and Atg20 heterodimerize and preferentially bind PS-containing membranes, however this was not the case for the Vps5-Vps17 retromer SNX-BARs, or for Mvp1, a homodimeric SNX-BAR that functions on the retromer pathway (16). Given the reported presence of phosphatidylserine (PS) on the vacuolar membrane we sought to determine if Vps501 possessed similar PS binding preferences (15). Indeed, we found Vps501^{WT} strongly binds to liposomes containing 30% PS, similar to Snx4-Atg20, whereas Vps501^{YKAA} PX mutant binding was reduced 2-fold (Figure 4C, D). Taken together, we conclude Vps501 vacuolar membrane binding is likely driven by strong binding preferences to PI3P and PS, but overall vacuole recruitment maybe regulated or transiently affected by PI(3,5)P2.

Vps501 forms large oligomeric structures

Existing crystal structures of SNX-BAR proteins reported to date are dimeric, with dimerization occurring via an extensive BAR-BAR interface that is conserved in all BAR domain-containing proteins. SNX-BAR dimers are then thought to oligomerize on membrane surfaces via tip-to-tip interactions of the BAR domains (5), in order to generate regular arrays that wrap a membrane tubule. However, more recent studies have begun to demonstrate some SNX-BAR proteins such a Mvp1 can also form tetrameric configurations that participate in regulatory roles. To determine if Vps501 formed homogenous homodimers or formed larger molecular arrays in vitro, we eluted Vps501 on Sephacryl S-300HR 16/60 size exclusion chromatography which is optimized to resolve 10-1500 kDa. Interestingly, we found Vps501 with an expected 70 kDa eluted just before thyroglobulin (660 kDa) at 40.40 ml, suggesting Vps501 purifies as an oligomer (Figure 5A). We further calculated relative molecular weight by plotting the column void volume and four high molecular weight standards versus the elution profile of Vps501, and found Vps501 natively purifies at 10-fold larger than the predicted 70 kDa molecular weight (Figure 5B). We observed a similar elution profile when purifying Vps501^{YKAA} suggesting Vps501 PX domain does not participate in oligomerization (Figure 5A, B).

4.4. Discussion

In this study, we provide a mechanistic insight into the functional requirements of Vps501 to localize and function at the vacuole membrane. Current models indicate that an evolutionarily conserved Phox-homology (PX) domain, a feature common in all sorting nexins, binds specifically to PI3P, the major phospholipid of the endosome. However, Vps501 has no canonical PI3P binding motif, as it is missing key motif residues. We performed a multiple sequence alignment of PX domains from Vps501 and Vps5, Snx1 and Snx2 that indicated Vps501's canonical motif is mutated at every key residue in the canonical binding site. However, the alternative noncanonical is completely intact and is likely responsible for lipid binding (Figure 2A). Vps501 also exclusively resides on the vacuolar membrane, a unique feature amongst the SNX-BAR protein family. We speculated Vps501 likely possesses lipid specificity beyond PI3P as was discovered in other sorting nexins (17). This notion was supported by the GFP-Vps501^{YKAA} mutant mislocalizing to the cytosol, leaving only a small percentage remaining on the vacuolar membrane, like GFP-Vps501^{WT} in *sea1*Δ cells (Figure 2B, C). Furthermore, Sea1 was found to be critical for Vps501 localization, indicating a physical recruitment to the vacuolar membrane (Figure 1). Interestingly, in *sea1*Δ *vps501^{YKAA}* cells, the cytoplasmic mislocalization of the Vps501^{YKAA} mutant was completely blocked from the vacuolar membrane and inhibited autophagy influx, suggesting Vps501 localization requires both the vacuolar membrane lipids and resident vacuolar proteins for its function (Figure 2 and Figure 3). Whether these two binding requirements are universal or specialized to each SNX-BAR protein is not known.

In this study, we hypothesized the unique lipid profile of the vacuolar membrane mediates Vps501 lipid binding. Unlike many other cellular compartments, the vacuole has very low levels of ergosterol and sphingolipids and the major phosphoinositide species on the vacuolar membrane is phosphatidylinositol 3,5-bisphosphate (PI(3,5)P2), which is generated from PI3P by the Fab1 kinase (8). PI(3,5)P2 is critical for maintaining vacuolar identity since PI(3,5)P2 effectors are required for protein sorting and retrograde trafficking from the vacuole to the endosome (8). However, in our sedimentation assays, we found Vps501 possesses more lipid specificity to PI3P and phosphatidylserine (PS), while the presence of PI(3,5)P2 appeared to decrease overall affinity, suggesting a possible mechanism of regulation (Figure 4) . Future studies will help us understand the novel ways in which Vps501 recognizes vacuolar lipids and how this recognition influences its function and regulation. An additional form of regulation for Vps501 may also come from its unique ability to oligomerize into decamers *in vitro* (Figure 5). A recent study highlighted the role of unstructured regions in the N-termini of SNX-BAR protein Mvp1, in promoting an autoinhibiting tetrameric configuration (7). The tetrameric structure of Mvp1 suggests a novel mechanism of regulation via protein-protein interaction or post-translational modification. Vps501 also contains an unstructured N-terminal region and it would be interesting to see if Vps501 can also organize into autoinhibitory structures and regulate its activity through conformational change, post-translational modifications or protein-protein interactions.

4.5. Figures and Tables

Table 3. Liposome compositions as indicated. The table includes a typical formulation for 400 microliters of liposome with a final concentration to 1 mol of lipid.

Lipid	0% PI3P 0% PI(3,5)P2		30% PS 1% PI3P 0% PI(3,5)P2		11% PI3P 0% PI(3,5)P2		0% PI3P 18% PI(3,5)P2		11% PI3P 18% PI(3,5)P2	
	Mol Frac	Volume to RXN (µl)	Mol Frac	Volume to RXN (µl)	Mol Frac	Volume to RXN (µl)	Mol Frac	Volume to RXN (µl)	Mol Frac	Volume to RXN (µl)
DOPC Avanti 850375	100	31	49	15.2	89	27.8	82	26	71	22
DOPS Avanti 840035	0	0	30	25	0	0	0	0	0	0
Ergosterol Sigma 47130-U	0	0	20	8	0	0	0	0	0	0
PI(3)P Avanti 850150P	0	0	1	10	11	110	0	0	11	110
PI(3,5)P2 Avanti 850154P	0	0	0	0	0	0	18	180	18	180

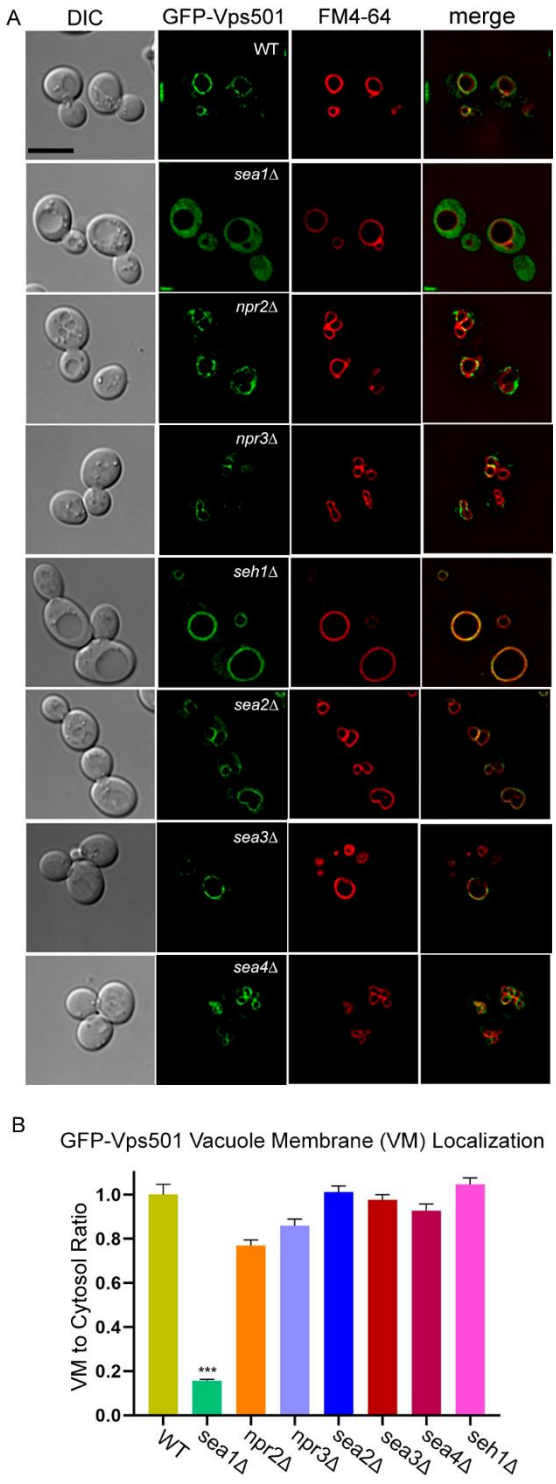

Figure 17. Vps501 requires Sea1 for vacuolar localization. (A) Micrographs of GFP-Vps501 in wildtype and SEA complex mutant cells. GFP-Vps501 is significantly mislocalized

in SEACIT mutant cells but not in SEACAT mutant cells. Note, *sec13*Δ cells are nonviable. (B) Vacuolar membrane localization was quantified by comparing GFP-Vps501 VML/cytosol ratios in wildtype versus SEA complex mutants. A minimum of 100 cells were measured in triplicate; standard error of the mean was calculated. *$p<0.05$, ** $p<0.01$, ***$p<0.001$ indicates significance as calculated by Student's t-test.

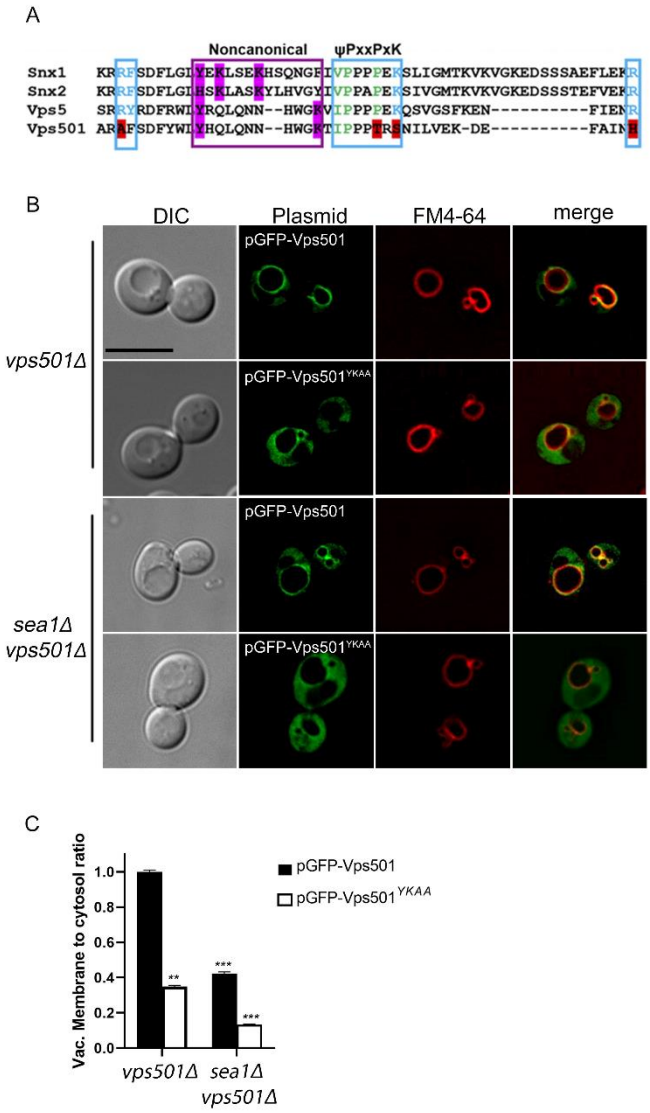

Figure 18. Vps501 non-canonical PX domain is required for localization. (A) Sequence alignments of human SNX1, SNX2 and yeast homologs VPS5 and VPS501 PX domains are shown. Blue indicates residues in the canonical PI3P motif. Magenta indicates key secondary lipid binding site residues. Vps501 canonical PI3P motif is not conserved, however, the non-canonical His/Tyr motif is conserved. (B) Alanine mutations to His/Tyr residues in the non-canonical motif resulted in GFP-Vps501^{YKAA} mislocalized to the cytosol in *vps501*Δ, and *vps501*Δ*sea1*Δ cells, indicating Vps501's recruitment to the vacuolar membrane is dependent on both PI3P recognition and Sea1 binding. The scale bar indicates 5μm (D) Top Graph, quantification of Vps501 localization was defined by vacuolar membrane to cytosol ratios as described in material and methods. GFP-Vps501^{YKAA} recruitment to the vacuolar membrane is reduced by ~60% in *vps501*Δ cells. When combined with ablation of Sea1 vacuolar membrane localization is reduced by ~90%. Indicated significance is a comparison of wildtype to single

deletions or double mutants. *$p<0.05$, ** $p<0.01$, ***$p<0.001$ indicates significance as calculated by Student's t-test.

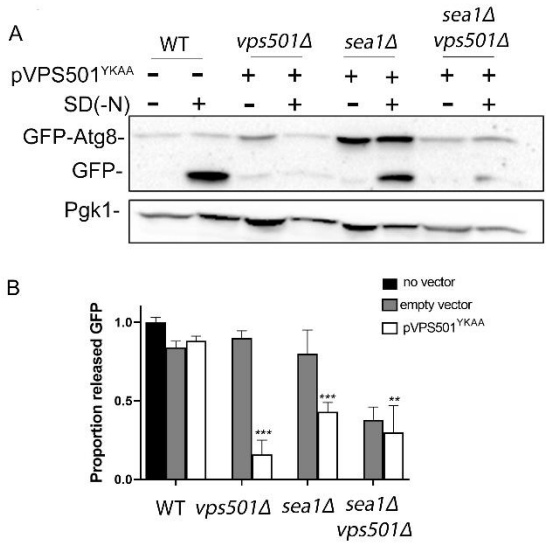

Figure 19. Vacuolar localization is required for Vps501 function. (A) Ectopic expression of Vps501^{YKAA} failed to complement *vps501*Δ*sea1*Δ cells in GFP-Atg8 processing assays and severely impairs autophagy flux when expressed in *sea1*Δ cells. (B) Graph of quantification of GFP-Atg8 processing when Vps501^{YKAA} is ectopically expressed in wildtype, *vps501*Δ, or *vps501*Δ*sea1*Δ cells. The results are from three experiments and averaged (standard deviation). *p<0.05, ** p<0.01, ***p<0.001 indicates significance as calculated by Student's t-test.

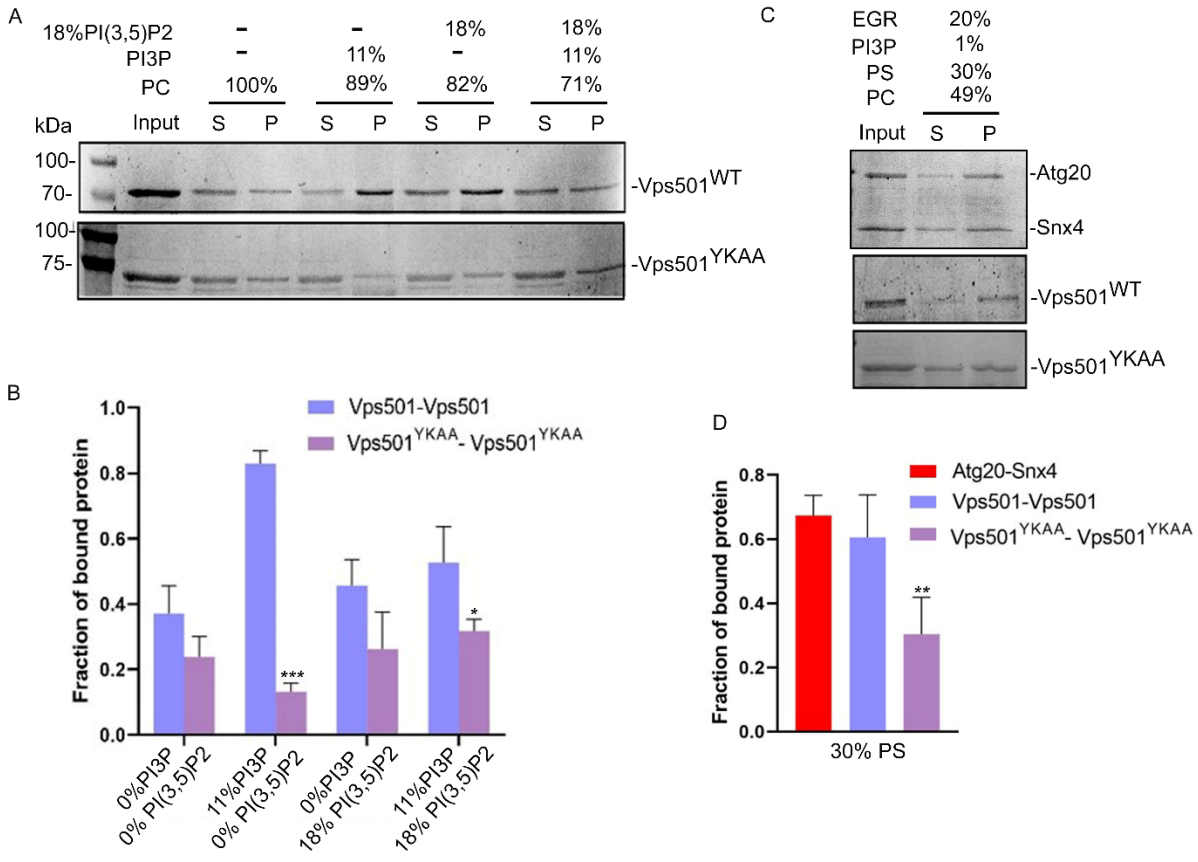

Figure 20. Vps501 lipid specificity. (A-B) PI liposome sedimentation assays and quantification. Query proteins and lipids are indicated on the figure. Vps501^{WT} bound to liposomes enriched with PI3P or PI(3,5)P. Binding was reduced when PI3P and PI(3,5)P lipids were combined on liposomes. (C-D) PS liposome sedimentation assays and quantification. Yeast SNX-BARs heterodimer Snx4-Atg20 has previously been shown to preferentially bind PS-containing membranes. Vps501^{WT} also strongly binds to liposomes containing 30% PS, similar to Snx4-Atg20, whereas Vps501^{YKAA} PX mutant binding was reduced 2-fold. Indicated significance is a comparison of wildtype to single deletions or double mutants.

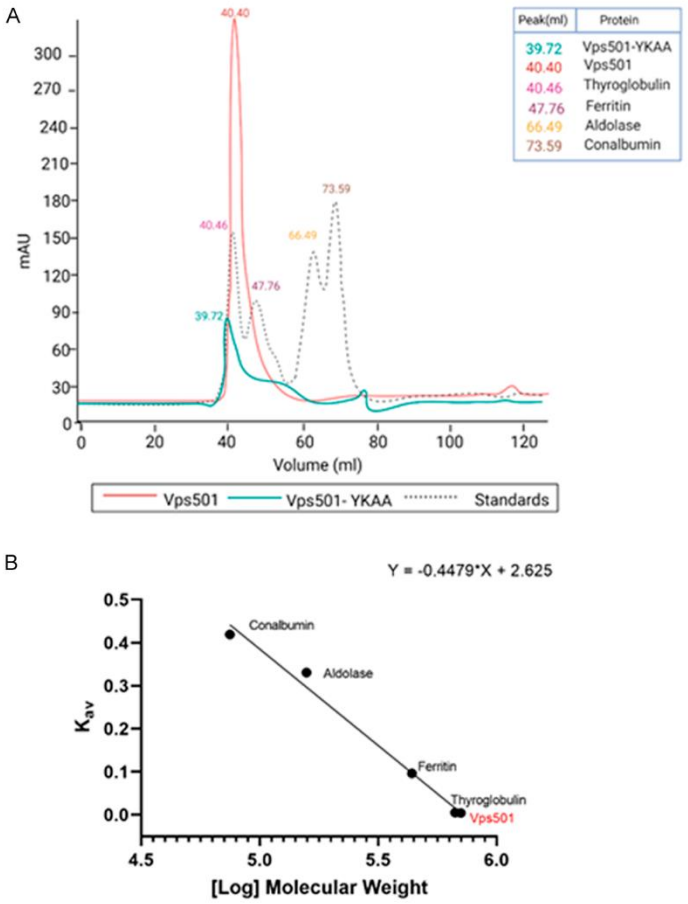

Figure 21. Vps501 purifies as large oligomers. (A) Elution profiles of indicated proteins. Elution volumes (Ve) are found at maximum peak height for each protein. (B) Calibration curve used to estimate the molecular weight of Vps501. HiPrep 16/60 Sephacryl S 300HR was calibrated using Thyroglobulin(669 kDa), Ferritin (440 kDa), Aldolase (158 kDa) and Conalbumin (75 kDa). Molecular weight of Vps501 was estimated to be 707317.6 Da as calculated from the equation Y=-0.4479*X+2.625 as described in material and methods.

4.6. References

1. Chi RJ, Harrison MS, Burd CG. Biogenesis of endosome-derived transport carriers. Cell Mol Life Sci. 2015;72(18):3441-55.
2. Burd C, Cullen PJ. Retromer: a master conductor of endosome sorting. Cold Spring Harb Perspect Biol. 2014;6(2).
3. Teasdale RD, Collins BM. Insights into the PX (phox-homology) domain and SNX (sorting nexin) protein families: structures, functions and roles in disease. Biochem J. 2012;441(1):39-59.
4. Wang J, Fedoseienko A, Chen B, Burstein E, Jia D, Billadeau DD. Endosomal receptor trafficking: Retromer and beyond. Traffic. 2018;19(8):578-90.
5. van Weering JR, Sessions RB, Traer CJ, Kloer DP, Bhatia VK, Stamou D, et al. Molecular basis for SNX-BAR-mediated assembly of distinct endosomal sorting tubules. EMBO J. 2012;31(23):4466-80.
6. Chi RJ, Liu J, West M, Wang J, Odorizzi G, Burd CG. Fission of SNX-BAR-coated endosomal retrograde transport carriers is promoted by the dynamin-related protein Vps1. J Cell Biol. 2014;204(5):793-806.
7. Sun D, Varlakhanova NV, Tornabene BA, Ramachandran R, Zhang P, Ford MGJ. The cryo-EM structure of the SNX-BAR Mvp1 tetramer. Nat Commun. 2020;11(1):1506.
8. Strahl T, Thorner J. Synthesis and function of membrane phosphoinositides in budding yeast, Saccharomyces cerevisiae. Biochim Biophys Acta. 2007;1771(3):353-404.
9. Longtine MS, McKenzie A, 3rd, Demarini DJ, Shah NG, Wach A, Brachat A, et al. Additional modules for versatile and economical PCR-based gene deletion and modification in Saccharomyces cerevisiae. Yeast. 1998;14(10):953-61.
10. Vida TA, Emr SD. A new vital stain for visualizing vacuolar membrane dynamics and endocytosis in yeast. J Cell Biol. 1995;128(5):779-92.
11. Shintani T, Huang WP, Stromhaug PE, Klionsky DJ. Mechanism of cargo selection in the cytoplasm to vacuole targeting pathway. Developmental cell. 2002;3(6):825-37.
12. Alberti S, Gitler AD, Lindquist S. A suite of Gateway cloning vectors for high-throughput genetic analysis in Saccharomyces cerevisiae. Yeast. 2007;24(10):913-9.
13. Ma M, Goyal S, Burd CG, Chi RJ. Expression, Purification, and Liposome Binding of Budding Yeast SNX-BAR Heterodimers. J Vis Exp. 2019(154).
14. Li SC, Kane PM. The yeast lysosome-like vacuole: endpoint and crossroads. Biochim Biophys Acta. 2009;1793(4):650-63.
15. Zinser E, Sperka-Gottlieb CD, Fasch EV, Kohlwein SD, Paltauf F, Daum G. Phospholipid synthesis and lipid composition of subcellular membranes in the unicellular eukaryote Saccharomyces cerevisiae. J Bacteriol. 1991;173(6):2026-34.
16. Ma M, Kumar S, Purushothaman L, Babst M, Ungermann C, Chi RJ, et al. Lipid trafficking by yeast Snx4 family SNX-BAR proteins promotes autophagy and vacuole membrane fusion. Mol Biol Cell. 2018;29(18):2190-200.
17. Chandra M, Chin YK, Mas C, Feathers JR, Paul B, Datta S, et al. Classification of the human phox homology (PX) domains based on their phosphoinositide binding specificities. Nat Commun. 2019;10(1):1528.

CHAPTER 5: CONCLUSION

In this thesis, we have found Vps501 uniquely localizes to the vacuolar membrane and interacts with the SEA complex to regulate TORC1 inactivation during autophagy induction. Collectively, these findings lead us to propose a new model for Vps501 function at the vacuolar membrane (Figure 1). When wildtype cells are deprived of nitrogen, the SEA complex acts through effector molecules such as the Gtr1-Gtr2/EGO complex to inhibit TORC1 and facilitate autophagic induction. We believe Vps501 acts as a structural stabilizer and tethers the SEA complex to the vacuolar membrane, using multiple interactions within the SEA complex (Sea1 and others) along with lipid specificity from its non-canonical PX domain to facilitate TORC1 inactivation, thereby inducing autophagy and promoting maintenance of vacuole proteins such as Atg27 and Ypt7. In contrast, *vps501*Δ*sea1*Δ cells exhibit destabilization of the SEA complex, resulting in the loss of the vacuolar pool of TORC1 and a concomitant increase to signaling endosomes resulting in TORC1 signaling hyperactivity. This results in broad TORC1 dysfunction in processes such as micro- or macroautophagy.

Future directions will be aimed at further testing this working model. In particular, we are interested in determining if the broad TORC1 signaling defect is specific to a particular type of autophagy (micro-, selective-), since many of these processes are not well understood, any additional information could provide a significant advancement in their respective fields. We are also interested in understanding the significance of the Vps501 oligomers that we see during protein purification and the negative effects of PI(3,5)P2 on lipid binding . We speculate these two features will be key to understanding the

mechanisms of Vps501 at the vacuolar membrane, however, substantial molecular and biophysical approaches will be needed to confirm this speculative model.

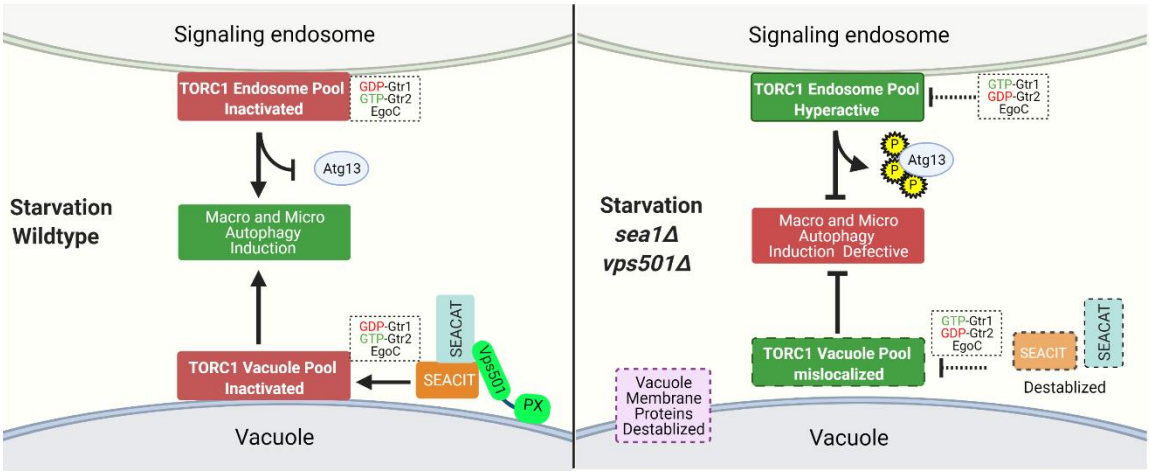

Figure 22. Vps501 cooperates with the SEA complex to inactivate TORC1. Under starvation conditions, Vps501 acts as a stabilizer for the SEA complex to the vacuole membrane using a non-canonical PX domain and a direct interaction within the SEA Complex. This interaction promotes SEACIT inactivation of the vacuole and endosomal pools TORC1 via the GTR1/GTR2/EGO complex, resulting in the induction macro and microautophagy. In vps501Δ sea1Δ cells, the SEA complex is destabilized and the vacuole pool of TORC1 is mislocalized. TORC1 endosomal pools are enriched and hyperactive, resulting in aberrant Atg13 phosphorylation and defective macro and microautophagy which can lead to the overall destabilization of other vacuole membrane proteins.

APPENDIX

Table 1: Novel interactors of Vps501 found from the mass-spectrometry (MS) study.

Gene names	Protein names	Log2 Norm Ratio (VE/BE)*
YKR078W	Uncharacterized protein YKR078W	VE Only
LEU2	3-isopropylmalate dehydrogenase	VE Only
GPH1	Glycogen phosphorylase	VE Only
ATG4	Cysteine protease ATG4	VE Only
NMD3	60S ribosomal export protein NMD3	VE Only
YEF1	ATP-NADH kinase YEF1	VE Only
ALF1	Tubulin-specific chaperone B	VE Only
CIS3	Cell wall mannoprotein CIS3;Cell wall protein PIR5;Cell wall mannoprotein PIR3;Cell wall mannoprotein PIR1;Cell wall mannoprotein HSP150	VE Only
HSP78	Heat shock protein 78, mitochondrial	VE Only
YML082W	Putative cystathionine gamma-synthase YML082W	VE Only
SMC1	Structural maintenance of chromosomes protein 1	VE Only
TY3B-I	Transposon Ty3-I Gag-Pol polyprotein;Capsid protein;Spacer peptide p3;Nucleocapsid protein p11;Ty3 protease;Spacer peptide J;Reverse transcriptase/ribonuclease H;Integrase p52;Integrase p49	VE Only
ATP3	ATP synthase subunit gamma, mitochondrial	VE Only
HHT1	Histone H3	VE Only
COR1	Cytochrome b-c1 complex subunit 1, mitochondrial	VE Only
GAD1	Glutamate decarboxylase	VE Only
YPK1	Serine/threonine-protein kinase YPK1	VE Only
YMR196W	Uncharacterized protein YMR196W	VE Only
YER156C	UPF0160 protein YER156C	VE Only
GRE3	NADPH-dependent aldose reductase GRE3	VE Only
MDH3	Malate dehydrogenase, peroxisomal	VE Only
DGA1	Diacylglycerol O-acyltransferase 1	VE Only
IML1	Vacuolar membrane-associated protein IML1	VE Only
SPB1	27S pre-rRNA (guanosine(2922)-2-O)-methyltransferase	VE Only
ARO10	Transaminated amino acid decarboxylase	VE Only
ITR1	Myo-inositol transporter 1	VE Only
ISW1	ISWI chromatin-remodeling complex ATPase ISW1	VE Only
PHA2	Putative prephenate dehydratase	VE Only

RFC3	Replication factor C subunit 3	VE Only
UTP20	U3 small nucleolar RNA-associated protein 20	VE Only
DCS1	m7GpppX diphosphatase	VE Only
MIC60	MICOS complex subunit MIC60	VE Only
YPP1	Cargo-transport protein YPP1	VE Only
MAK21	Ribosome biogenesis protein MAK21	VE Only
EMC2	ER membrane protein complex subunit 2	VE Only
STE23	A-factor-processing enzyme	VE Only
ALY2	Arrestin-related trafficking adapter 3	VE Only
VPS13	Vacuolar protein sorting-associated protein 13	VE Only
WSC3	Cell wall integrity and stress response component 3	VE Only
YOL024W	Putative uncharacterized protein YOL024W	VE Only
HCA4	ATP-dependent RNA helicase HCA4	VE Only
CMK2	Calcium/calmodulin-dependent protein kinase II	VE Only
STR3	Cystathionine beta-lyase	VE Only
ARO9	Aromatic amino acid aminotransferase 2	VE Only
YGP1	Protein YGP1	VE Only
HHO1	Histone H1	VE Only
MET10	Sulfite reductase (NADPH) flavoprotein component	VE Only
SRM1	Guanine nucleotide exchange factor SRM1	VE Only
MYO5	Myosin-5	VE Only
PAN5	2-dehydropantoate 2-reductase	VE Only
EHT1	Medium-chain fatty acid ethyl ester synthase/esterase 2	VE Only
KGD1	2-oxoglutarate dehydrogenase, mitochondrial	VE Only
ARG5,6	Protein ARG5,6, mitochondrial;N-acetyl-gamma-glutamyl-phosphate reductase;Acetylglutamate kinase	VE Only
RSC8	Chromatin structure-remodeling complex protein RSC8	VE Only
QRI1	UDP-N-acetylglucosamine pyrophosphorylase	VE Only
PCS60	Peroxisomal-coenzyme A synthetase	VE Only
SRP68	Signal recognition particle subunit SRP68	VE Only
MFT1	THO complex subunit MFT1	VE Only
PET112	Glutamyl-tRNA(Gln) amidotransferase subunit B, mitochondrial	VE Only
RDI1	Rho GDP-dissociation inhibitor	VE Only
SVF1	Survival factor 1	VE Only
ARI1	NADPH-dependent aldehyde reductase ARI1	VE Only
FAL1	ATP-dependent RNA helicase FAL1	VE Only
YDL086W	Putative carboxymethylenebutenolidase	VE Only

ACH1	Acetyl-CoA hydrolase	VE Only
MET3	Sulfate adenylyltransferase	VE Only
SEC17	Alpha-soluble NSF attachment protein	VE Only
NOP16	Nucleolar protein 16	VE Only
NSP1	Nucleoporin NSP1	VE Only
MEX67	mRNA export factor MEX67	VE Only
RNQ1	(PIN+) prion protein RNQ1	VE Only
CHS5	Chitin biosynthesis protein CHS5	VE Only
TSR1	Ribosome biogenesis protein TSR1	VE Only
LYS1	Saccharopine dehydrogenase (NAD(+), L-lysine-forming)	VE Only
YNL115C	Uncharacterized vacuolar membrane protein YNL115C	VE Only
TRM8	tRNA (guanine-N(7)-)-methyltransferase	VE Only
MRPS35	37S ribosomal protein S35, mitochondrial	VE Only
VPS4	Vacuolar protein sorting-associated protein 4	VE Only
UBP6	Ubiquitin carboxyl-terminal hydrolase 6	VE Only
CDC3	Cell division control protein 3	VE Only
MSC2	Probable zinc transporter MSC2	VE Only
KOG1	Target of rapamycin complex 1 subunit KOG1	VE Only
MUM3	Protein MUM3	VE Only
NAB6	RNA-binding protein NAB6	VE Only
RTN2	Reticulon-like protein 2	VE Only
TYR1	Prephenate dehydrogenase (NADP(+))	VE Only
VNX1	Low affinity vacuolar monovalent cation/H(+) antiporter	VE Only
MET13	Methylenetetrahydrofolate reductase 2	5.58234818
YMR315W	Uncharacterized protein YMR315W	5.19483388
VAC8	Vacuolar protein 8	4.54547709
PGM2	Phosphoglucomutase-2	3.92717723
GLT1	Glutamate synthase (NADH)	3.80721991
ARG4	Argininosuccinate lyase	3.68760965
VMA13	V-type proton ATPase subunit H	3.46755248
GPD1	Glycerol-3-phosphate dehydrogenase (NAD(+)) 1	3.22968309
YNL134C	Uncharacterized protein YNL134C	3.11171115
CPA2	Carbamoyl-phosphate synthase arginine-specific large chain	3.05876815
CIN1	Chromosome instability protein 1	3.02927826
NUP157	Nucleoporin NUP157	2.68738384
MET6	5-methyltetrahydropteroyltriglutamate--homocysteine methyltransferase	2.5688593

PDA1	Pyruvate dehydrogenase E1 component subunit alpha, mitochondrial	2.51017851
YCK1	Casein kinase I homolog 1	2.40887643
HIS4	Histidine biosynthesis trifunctional protein;Phosphoribosyl-AMP cyclohydrolase;Phosphoribosyl-ATP pyrophosphohydrolase;Histidinol dehydrogenase	2.24653594
ACO1	Aconitate hydratase, mitochondrial	2.16721438
HHF1	Histone H4	2.03417875
HXK1	Hexokinase-1	1.9623143
LPD1	Dihydrolipoyl dehydrogenase, mitochondrial	1.95046966
UFD4	Ubiquitin fusion degradation protein 4	1.86661593
MDH1	Malate dehydrogenase, mitochondrial	1.83960221
ALD4	Potassium-activated aldehyde dehydrogenase, mitochondrial	1.83935593
PBP1	PAB1-binding protein 1	1.74582463
ATP1	ATP synthase subunit alpha, mitochondrial	1.72508338
TDH1	Glyceraldehyde-3-phosphate dehydrogenase 1	1.72006378
RPL32	60S ribosomal protein L32	1.68395028
UBP12	Ubiquitin carboxyl-terminal hydrolase 12	1.66815052
ARA1	D-arabinose dehydrogenase (NAD(P)+) heavy chain	1.59304885
HTB2;HTB1	Histone H2B.2;Histone H2B.1	1.57901149
HSP82	ATP-dependent molecular chaperone HSP82	1.57273519
PGM1	Phosphoglucomutase-1	1.55558358
RPL6B	60S ribosomal protein L6-B	1.55503576
IDI1	Isopentenyl-diphosphate Delta-isomerase	1.44567406
LEU4	2-isopropylmalate synthase	1.42922382
FUS3	Mitogen-activated protein kinase FUS3	1.40005358
VPS1	Vacuolar protein sorting-associated protein 1	1.38745492
FAS1	Fatty acid synthase subunit beta;3-hydroxyacyl-(acyl-carrier-protein) dehydratase;Enoyl-(acyl-carrier-protein) reductase (NADH);(Acyl-carrier-protein) acetyltransferase;(Acyl-carrier-protein) malonyltransferase;S-acyl fatty acid synthase thioesterase	1.37233835
ACC1	Acetyl-CoA carboxylase;Biotin carboxylase	1.37158601
LAT1	Dihydrolipoyllysine-residue acetyltransferase component of pyruvate dehydrogenase complex, mitochondrial	1.37000729
FAS2	Fatty acid synthase subunit alpha;Acyl carrier;3-oxoacyl-(acyl-carrier-protein) reductase;3-oxoacyl-(acyl-carrier-protein) synthase	1.35029111

KGD2	Dihydrolipoyllysine-residue succinyltransferase component of 2-oxoglutarate dehydrogenase complex, mitochondrial	1.34135528
URA8	CTP synthase 2	1.33443695
ILV3	Dihydroxy-acid dehydratase, mitochondrial	1.3269094
LEU1	3-isopropylmalate dehydratase	1.32090663
POR1	Mitochondrial outer membrane protein porin 1	1.31629645
TPS1	Alpha,alpha-trehalose-phosphate synthase (UDP-forming) 56 kDa subunit	1.29742233
MET17	Protein MET17;O-acetylhomoserine sulfhydrylase;O-acetylserine sulfhydrylase	1.29561054
KAR2	78 kDa glucose-regulated protein homolog	1.27477296
GLK1	Glucokinase-1	1.23211208
RPL20B;RPL20A	60S ribosomal protein L20-B;60S ribosomal protein L20-A	1.22605401
OST1	Dolichyl-diphosphooligosaccharide--protein glycosyltransferase subunit 1	1.2178384
FAA1	Long-chain-fatty-acid--CoA ligase 1	1.21417911
YDL124W	NADPH-dependent alpha-keto amide reductase	1.21182063
TUB1	Tubulin alpha-1 chain	1.20084116
HSP42	Heat shock protein 42	1.19701541
CLC1	Clathrin light chain	1.18662212
RVB1	RuvB-like protein 1	1.1728459
SHM2	Serine hydroxymethyltransferase, cytosolic	1.15132951
BAT1	Branched-chain-amino-acid aminotransferase, mitochondrial	1.12431319
TUB2	Tubulin beta chain	1.12373802
SPT6	Transcription elongation factor SPT6	1.12122287
YMR018W	TPR repeat-containing protein YMR018W	1.10335308
CAM1	Elongation factor 1-gamma 1	1.09144211
LSP1	Sphingolipid long chain base-responsive protein LSP1	1.0796049
SSA1	Heat shock protein SSA1	1.07025342
ILV5	Ketol-acid reductoisomerase, mitochondrial	1.05041648
REB1	DNA-binding protein REB1	1.04673294
STE24	CAAX prenyl protease 1	1.03775519
XRN1	5-3 exoribonuclease 1	1.03045311
QNS1	Glutamine-dependent NAD(+) synthetase	1.01518117
DAK1	Dihydroxyacetone kinase 1	1.00838418
SPF1	Manganese-transporting ATPase 1	1.0056108
POB3	FACT complex subunit POB3	1.00534409
TSL1	Trehalose synthase complex regulatory subunit TSL1	0.98709835

RPL4B	60S ribosomal protein L4-B	0.9832823
SCP160	Protein SCP160	0.97871442
GDH1	NADP-specific glutamate dehydrogenase 1	0.97599748
ADH5	Alcohol dehydrogenase 5	0.97062108
RPL26A	60S ribosomal protein L26-B;60S ribosomal protein L26-A	0.94983636
HSP104	Heat shock protein 104	0.94374669
STI1	Heat shock protein STI1	0.90832196
PRP6	Pre-mRNA-splicing factor 6	0.88828846
PDB1	Pyruvate dehydrogenase E1 component subunit beta, mitochondrial	0.88814195
CDC48	Cell division control protein 48	0.88604178
PIL1	Sphingolipid long chain base-responsive protein PIL1	0.86984315
MAE1	NAD-dependent malic enzyme, mitochondrial	0.86709414
SSC1	Heat shock protein SSC1, mitochondrial	0.86057912
ILV1	Threonine dehydratase, mitochondrial	0.86053562
SAH1	Adenosylhomocysteinase	0.85393882
HSP60	Heat shock protein 60, mitochondrial	0.85369018
CBF5	H/ACA ribonucleoprotein complex subunit 4	0.84631089
VMA8	V-type proton ATPase subunit D	0.84152862
ADH6	NADP-dependent alcohol dehydrogenase 6	0.84088226
RPS7B	40S ribosomal protein S7-B	0.83987812
GLC7	Serine/threonine-protein phosphatase PP1-2	0.83435669
NOP12	Nucleolar protein 12	0.82910465
IDH2	Isocitrate dehydrogenase (NAD) subunit 2, mitochondrial	0.82880078
RVS167	Reduced viability upon starvation protein 167	0.82876519
SBE22	Protein SBE22	0.82371707
ATP2	ATP synthase subunit beta, mitochondrial	0.82295663
RNR4	Ribonucleoside-diphosphate reductase small chain 2	0.82011231
RRP3	ATP-dependent rRNA helicase RRP3	0.81861799
CCR4	Glucose-repressible alcohol dehydrogenase transcriptional effector	0.81861799
RPS16B;RPS16A	40S ribosomal protein S16-B;40S ribosomal protein S16-A	0.79284208
PRP43	Pre-mRNA-splicing factor ATP-dependent RNA helicase PRP43	0.78748037
RPL21B;RPL21A	60S ribosomal protein L21-B;60S ribosomal protein L21-A	0.76010572
PYC1	Pyruvate carboxylase 1	0.75309175
ADE4	Amidophosphoribosyltransferase	0.74569555

LSC1	Succinyl-CoA ligase (ADP-forming) subunit alpha, mitochondrial	0.7402177
TEF1	Elongation factor 1-alpha	0.7352211
TPA1	Prolyl 3,4-dihydroxylase TPA1	0.73478051
SEH1	Nucleoporin SEH1	0.72454599
DIC1	Mitochondrial dicarboxylate transporter	0.72336012
SAC6	Fimbrin	0.72065339
ASP1	L-asparaginase 1	0.71484687
ACS2	Acetyl-coenzyme A synthetase 2	0.70403867
OLA1	Obg-like ATPase 1	0.69696014
RFA1	Replication factor A protein 1	0.69543406
RPL14B;RPL14A	60S ribosomal protein L14-B;60S ribosomal protein L14-A	0.67453042
SPT16	FACT complex subunit SPT16	0.67028156
FRA1	Putative Xaa-Pro aminopeptidase FRA1	0.6652456
VMA5	V-type proton ATPase subunit C	0.66389575
SHE9	Sensitive to high expression protein 9, mitochondrial	0.66007984
HSC82	ATP-dependent molecular chaperone HSC82	0.65463239
MNN11	Probable alpha-1,6-mannosyltransferase MNN11	0.6543789
PYK2	Pyruvate kinase 2	0.64869299
ALD6	Magnesium-activated aldehyde dehydrogenase, cytosolic	0.64835006
KRE33	UPF0202 protein KRE33	0.64718963
VBA4	Vacuolar basic amino acid transporter 4	0.64626868
CPR6	Peptidyl-prolyl cis-trans isomerase CPR6	0.64489313
TCB1	Tricalbin-1	0.63875012
SSE1	Heat shock protein homolog SSE1	0.63848262
RNR2	Ribonucleoside-diphosphate reductase small chain 1	0.63595959
PYC2	Pyruvate carboxylase 2	0.62958416
RPL10	60S ribosomal protein L10	0.62697558
EMI2	Putative glucokinase-2	0.62687163
RPL30	60S ribosomal protein L30	0.62126153
RPL8A	60S ribosomal protein L8-A	0.61868414
VPH1	V-type proton ATPase subunit a, vacuolar isoform	0.61415167
IDP1	Isocitrate dehydrogenase (NADP), mitochondrial	0.61217005
PDC6	Pyruvate decarboxylase isozyme 3	0.61216711
ADH3	Alcohol dehydrogenase 3, mitochondrial	0.60767652
IMD4	Inosine-5-monophosphate dehydrogenase 4	0.60741412
LYS12	Homoisocitrate dehydrogenase, mitochondrial	0.606908
BFR1	Nuclear segregation protein BFR1	0.6066029
RLI1	Translation initiation factor RLI1	0.60433585

YOL087C	Uncharacterized WD repeat-containing protein YOL087C	0.59840276
UTR1	NAD(+) kinase	0.59574813
SAP185	SIT4-associating protein SAP185	0.59328739
RPL3	60S ribosomal protein L3	0.58050623
PSA1	Mannose-1-phosphate guanyltransferase	0.57016855
GCD11	Eukaryotic translation initiation factor 2 subunit gamma	0.56996375
ASN1	Asparagine synthetase (glutamine-hydrolyzing) 1	0.569329
TRM1	tRNA (guanine(26)-N(2))-dimethyltransferase, mitochondrial	0.56271589
TRP5	Tryptophan synthase	0.56147304
RPN9	26S proteasome regulatory subunit RPN9	0.55416899
GFA1	Glutamine--fructose-6-phosphate aminotransferase (isomerizing)	0.54910257
ADH1	Alcohol dehydrogenase 1	0.54437772
TAL1	Transaldolase	0.53424716
PDI1	Protein disulfide-isomerase	0.53195218
SSA2	Heat shock protein SSA2	0.5291187
CDC60	Leucine--tRNA ligase, cytoplasmic	0.52755883
NDE1	External NADH-ubiquinone oxidoreductase 1, mitochondrial	0.52443024
SAM2	S-adenosylmethionine synthase 2	0.52092451
GLN1	Glutamine synthetase	0.51737987
WTM1	Transcriptional modulator WTM1	0.5149969
RPO21	DNA-directed RNA polymerase II subunit RPB1	0.5126763
ERG20	Farnesyl pyrophosphate synthase	0.50845117
ENO1	Enolase 1	0.50743945
GUS1	Glutamate--tRNA ligase, cytoplasmic	0.50596253
TIF4632	Eukaryotic initiation factor 4F subunit p130	0.50153621
RPL27B;RPL27A	60S ribosomal protein L27-B;60S ribosomal protein L27-A	0.50081975
CAR2	Ornithine aminotransferase	0.49784875
PET9	ADP,ATP carrier protein 2	0.49532245
CCS1	Superoxide dismutase 1 copper chaperone	0.48254361
RPN1	26S proteasome regulatory subunit RPN1	0.48173608
DOT6	Transcriptional regulatory protein DOT6	0.47960917
PDC5	Pyruvate decarboxylase isozyme 2	0.47466359
SUB2	ATP-dependent RNA helicase SUB2	0.47271828
RPL19B;RPL19A	60S ribosomal protein L19-B;60S ribosomal protein L19-A	0.47243913
HAS1	ATP-dependent RNA helicase HAS1	0.4700905

VMA1	V-type proton ATPase catalytic subunit A;Endonuclease PI-SceI	0.45854484
RVB2	RuvB-like protein 2	0.45520692
HRR25	Casein kinase I homolog HRR25	0.45486523
NOP1	rRNA 2-O-methyltransferase fibrillarin	0.45456003
UGP1	UTP--glucose-1-phosphate uridylyltransferase	0.44538125
CHC1	Clathrin heavy chain	0.43946958
PDC1	Pyruvate decarboxylase isozyme 1	0.43766104
ARO1	Pentafunctional AROM polypeptide;3-dehydroquinate synthase;3-phosphoshikimate 1-carboxyvinyltransferase;Shikimate kinase;3-dehydroquinate dehydratase;Shikimate dehydrogenase	0.43763063
HOM6	Homoserine dehydrogenase	0.4360066
YHR020W	Putative proline--tRNA ligase YHR020W	0.43330631
THS1	Threonine--tRNA ligase, cytoplasmic	0.43201562
ARB1	ABC transporter ATP-binding protein ARB1	0.43030337
MRH1	Protein MRH1	0.42849443
TIF4631	Eukaryotic initiation factor 4F subunit p150	0.42564105
PRS1	Ribose-phosphate pyrophosphokinase 1	0.42455915
RPS13	40S ribosomal protein S13	0.4178872
ILS1	Isoleucine--tRNA ligase, cytoplasmic	0.41340524
ETT1	Enhancer of translation termination 1	0.41116622
PUB1	Nuclear and cytoplasmic polyadenylated RNA-binding protein PUB1	0.41049095
TPS3	Trehalose synthase complex regulatory subunit TPS3	0.3978551
OAC1	Mitochondrial oxaloacetate transport protein	0.39616152
DLD3	D-lactate dehydrogenase (cytochrome) 3	0.39316308
DPS1	Aspartate--tRNA ligase, cytoplasmic	0.39291243
NOP58	Nucleolar protein 58	0.39122178
YGR012W	Putative cysteine synthase	0.38955492
ARC35	Actin-related protein 2/3 complex subunit 2	0.38782421
RPL18B;RPL18A	60S ribosomal protein L18-B;60S ribosomal protein L18-A	0.38230336
DED81	Asparagine--tRNA ligase, cytoplasmic	0.37994963
IPP1	Inorganic pyrophosphatase	0.37992385
ADH2	Alcohol dehydrogenase 2	0.37229826
RPL5	60S ribosomal protein L5	0.37022625
TUB3	Tubulin alpha-3 chain	0.36679043
RPL4A	60S ribosomal protein L4-A	0.36472768
RPS15	40S ribosomal protein S15	0.35832497

APE2	Aminopeptidase 2, mitochondrial	0.35808649
RPT4	26S protease subunit RPT4	0.35732106
YEF3	Elongation factor 3A	0.35708574
GRS1	Glycine--tRNA ligase 1, mitochondrial	0.35052379
DET1	Broad-range acid phosphatase DET1	0.34654552
TOM70	Mitochondrial import receptor subunit TOM70	0.34600645
HCR1	Eukaryotic translation initiation factor 3 subunit J	0.34600103
ACT1	Actin	0.34288913
PAB1	Polyadenylate-binding protein, cytoplasmic and nuclear	0.34150208
DHH1	ATP-dependent RNA helicase DHH1	0.33826184
SHM1	Serine hydroxymethyltransferase, mitochondrial	0.33310971
CYS4	Cystathionine beta-synthase	0.32972912
TUP1	General transcriptional corepressor TUP1	0.32835159
RPT2	26S protease regulatory subunit 4 homolog	0.32585803
ZWF1	Glucose-6-phosphate 1-dehydrogenase	0.32297978
HOM2	Aspartate-semialdehyde dehydrogenase	0.31933123
ASC1	Guanine nucleotide-binding protein subunit beta-like protein	0.31888102
EMP70	Transmembrane 9 superfamily member 1;Protein p24a	0.3182942
EFT1	Elongation factor 2	0.31665555
FKS1	1,3-beta-glucan synthase component FKS1	0.31610902
HMG2	3-hydroxy-3-methylglutaryl-coenzyme A reductase 2	0.31509753
FUN12	Eukaryotic translation initiation factor 5B	0.31235166
RPS18B;RPS18A	40S ribosomal protein S18-B;40S ribosomal protein S18-A	0.30361201
TOM40	Mitochondrial import receptor subunit TOM40	0.30171012
FBA1	Fructose-bisphosphate aldolase	0.29493663
CDC19	Pyruvate kinase 1	0.2913035
SUP45	Eukaryotic peptide chain release factor subunit 1	0.29081349
TKL1	Transketolase 1	0.2875785
RPT3	26S protease regulatory subunit 6B homolog	0.28180042
RPS4B;RPS4A	40S ribosomal protein S4-B;40S ribosomal protein S4-A	0.27780396
ASN2	Asparagine synthetase (glutamine-hydrolyzing) 2	0.27258905
FPR3	FK506-binding nuclear protein	0.27199792
PTC2	Protein phosphatase 2C homolog 2	0.26886711
SNZ1;SNZ2;SNZ3	Pyridoxine biosynthesis protein SNZ1;Probable pyridoxine biosynthesis protein SNZ2;Probable pyridoxine biosynthesis protein SNZ3	0.26495651
ECM33	Cell wall protein ECM33	0.25721254

APE3	Aminopeptidase Y	0.24940165
GCN1	Translational activator GCN1	0.24600959
GVP36	Protein GVP36	0.23690171
MNN9	Mannan polymerase complexes subunit MNN9	0.23365549
ERG24	Delta(14)-sterol reductase	0.23365549
SLA2	Protein SLA2	0.23365549
SDA1	Protein SDA1	0.23365549
RPL11B;RPL11A	60S ribosomal protein L11-B;60S ribosomal protein L11-A	0.23161699
PMT2	Dolichyl-phosphate-mannose--protein mannosyltransferase 2	0.22264508
NAP1	Nucleosome assembly protein	0.22001906
SSZ1	Ribosome-associated complex subunit SSZ1	0.21956433
ILV6	Acetolactate synthase small subunit, mitochondrial	0.20852597
NOP4	Nucleolar protein 4	0.20507211
MIR1	Mitochondrial phosphate carrier protein;Mitochondrial phosphate carrier protein, N-terminally processed	0.20381104
MCM4	DNA replication licensing factor MCM4	0.20280546
SSB1	Heat shock protein SSB1	0.20080632
ILV2	Acetolactate synthase catalytic subunit, mitochondrial	0.19748458
HXT3	Low-affinity glucose transporter HXT3	0.1947739
ADO1	Adenosine kinase	0.19354643
RPN6	26S proteasome regulatory subunit RPN6	0.19200761
STM1	Suppressor protein STM1	0.18955369
RPP0	60S acidic ribosomal protein P0	0.18751792
RPL28	60S ribosomal protein L28	0.18708795
ERG10	Acetyl-CoA acetyltransferase	0.18644218
SEC23	Protein transport protein SEC23	0.18576107
FRS2	Phenylalanine--tRNA ligase alpha subunit	0.18385953
SPN1	Transcription factor SPN1	0.18284543
SBP1	Single-stranded nucleic acid-binding protein	0.18051935
SST2	Protein SST2	0.17762471
AAT2	Aspartate aminotransferase, cytoplasmic	0.17275783
DED1	ATP-dependent RNA helicase DED1	0.17197704
GAS1	1,3-beta-glucanosyltransferase GAS1	0.16904508
ALA1	Alanine--tRNA ligase, mitochondrial	0.16639684
URA7	CTP synthase 1	0.16210897
SEC31	Protein transport protein SEC31	0.15986519
NUP84	Nucleoporin NUP84	0.15886306

DBP5	ATP-dependent RNA helicase DBP5	0.15469002
RPS14A;RPS14B	40S ribosomal protein S14-A;40S ribosomal protein S14-B	0.15418566
DUG1	Cys-Gly metallodipeptidase DUG1	0.15255516
ZUO1	Zuotin	0.15250563
YDR341C	Arginine--tRNA ligase, cytoplasmic	0.15077298
BEM2	GTPase-activating protein BEM2/IPL2	0.14933095
PEP4	Saccharopepsin	0.14785946
NOP56	Nucleolar protein 56	0.14119252
PGK1	Phosphoglycerate kinase	0.13788009
SIS1	Protein SIS1	0.13486493
RPS23B;RPS23A	40S ribosomal protein S23-B;40S ribosomal protein S23-A	0.13418161
YAP1	AP-1-like transcription factor YAP1	0.13059344
VMA2	V-type proton ATPase subunit B	0.13011232
SSO1;SSO2	Protein SSO1;Protein SSO2	0.12974512
KRS1	Lysine--tRNA ligase, cytoplasmic	0.12766983
TRR1	Thioredoxin reductase 1	0.12718528
SAM1	S-adenosylmethionine synthase 1	0.12083101
PMI40	Mannose-6-phosphate isomerase	0.10776817
DBP8	ATP-dependent RNA helicase DBP8	0.10722415
UTP5	U3 small nucleolar RNA-associated protein 5	0.10168732
GUA1	GMP synthase (glutamine-hydrolyzing)	0.09851189
PSK1	Serine/threonine-protein kinase PSK1	0.09540474
TY1B-ML1;TY1B-DR5;TY1B-PR2;TY1B-MR2;TY1B-OR	Transposon Ty1-ML1 Gag-Pol polyprotein;Capsid protein;Ty1 protease;Integrase;Reverse transcriptase/ribonuclease H;Transposon Ty1-DR5 Gag-Pol polyprotein;Capsid protein;Ty1 protease;Integrase;Reverse transcriptase/ribonuclease H;Transposon Ty1-PR2 Gag-Pol polyprotein;Capsid protein;Ty1 protease;Integrase;Reverse transcriptase/ribonuclease H;Transposon Ty1-MR2 Gag-Pol polyprotein;Capsid protein;Ty1 protease;Integrase;Reverse transcriptase/ribonuclease H;Transposon Ty1-OR Gag-Pol polyprotein;Capsid protein;Ty1 protease;Integrase;Reverse transcriptase/ribonuclease H	0.09229964
ARO8	Aromatic/aminoadipate aminotransferase 1	0.08947228
PMT4	Dolichyl-phosphate-mannose--protein mannosyltransferase 4	0.08862473
ENO2	Enolase 2	0.08739185
GLR1	Glutathione reductase	0.08728524

IKI3	Elongator complex protein 1	0.08321816
RPN5	26S proteasome regulatory subunit RPN5	0.08271979
SMI1	Cell wall assembly regulator SMI1	0.08169333
RPS7A	40S ribosomal protein S7-A	0.07929431
RPL36B;RPL36A	60S ribosomal protein L36-B;60S ribosomal protein L36-A	0.0710907
PGI1	Glucose-6-phosphate isomerase	0.07037585
GSC2	1,3-beta-glucan synthase component GSC2	0.07015675
RPG1	Eukaryotic translation initiation factor 3 subunit A	0.06725472
ABP1	Actin-binding protein	0.06279899
CRP1	Cruciform DNA-recognizing protein 1;CRP1 short N-terminal subpeptide;CRP1 short C-terminal subpeptide	0.06042902
FOL1	Folic acid synthesis protein FOL1;Dihydroneopterin aldolase;2-amino-4-hydroxy-6-hydroxymethyldihydropteridine pyrophosphokinase;Dihydropteroate synthase	0.05864421
TIF1	ATP-dependent RNA helicase eIF4A	0.05617098
RAS2	Ras-like protein 2	0.05604766
TDH3	Glyceraldehyde-3-phosphate dehydrogenase 3	0.05557016
RPS24B;RPS24A	40S ribosomal protein S24-B;40S ribosomal protein S24-A	0.05542102
PFK2	ATP-dependent 6-phosphofructokinase subunit beta	0.04894078
EBP2	rRNA-processing protein EBP2	0.03932851
GLN4	Glutamine--tRNA ligase	0.03706457
GCY1	Glycerol 2-dehydrogenase (NADP(+))	0.03689435
RPT1	26S protease regulatory subunit 7 homolog	0.02657897
CYS3	Cystathionine gamma-lyase	0.02402346
CDC39	General negative regulator of transcription subunit 1	0.02352011
IMD3	Inosine-5-monophosphate dehydrogenase 3	0.02094603
RPT5	26S protease regulatory subunit 6A	0.01819568
KAP123	Importin subunit beta-4	0.01012321
SER1	Phosphoserine aminotransferase	0.00719535
BMH1	Protein BMH1	0.00379911

* VE = Vps501 Only, BE= Beads Only